The Role of Flyby Interactions in Shaping Galaxy Evolution

By

Meagan Lang

Dissertation

Submitted to the Faculty of the

Graduate School of Vanderbilt University

in partial fulfillment of the requirements

for the degree of

DOCTOR OF PHILOSOPHY

in

Physics

August 2015

Nashville, Tennessee

Approved:

Prof. Kelly Holley-Bockelmann

Prof. Andreas Berlind

Prof. David A. Weintraub

Prof. Kirill Bolotin

I dedicate this thesis to

My Family,

For their endless support and encouragement,

and

My Friends,

For making me smile, giving me perspective, and making Nashville a home.

ACKNOWLEDGMENTS

This work was made possible by financial support from the Vanderbilt Provost Graduate Fellowship, National Science Foundation Graduate Research Fellowship, and Extreme Science and Engineering Discovery Environment computing allocation.

I am grateful to the Vanderbilt astronomy group for providing such a diverse and welcoming community, fostering my growth as both a scientist and a person. I want to thank Dr. Manodeep Sinha in particular for his patience and guidance. Our daily discussions challenged me to explore unfamiliar concepts and strengthen my research ideas. I would also like to thank my Dissertation Committee for their invaluable feedback. I am especially grateful to Dr. Kelly Holley-Bockelmann, my committee chairperson, for her contribution to my professional development as my advisor and mentor. She encouraged me to pursue new lines of research and instilled in me the need to always be aware of the larger picture.

I also want to thank the friends I have made both inside and outside the astronomy community during my journey to this point. They have made me a better person, given me the strength to take on new challenges, and made me feel at home even when my family is far away. Finally, I wish to thank my parents for their unending love and support in every goal I set, even when it takes me hundreds or thousands of miles away from them.

TABLE OF CONTENTS

LIST OF TABLES

LIST OF FIGURES

Chapter I

INTRODUCTION

Galaxy interactions are integral to our current understanding of how galaxies grow and evolve; however, while there exist extensive theoretical and observational studies of mergers, wherein two galaxies coalesce into one, few investigations exist of flyby interactions, during which the galaxies' halos interpenetrate but later detach. Given that galaxy flybys are theorized to occur just as often as mergers for some redshifts (Sinha & Holley-Bockelmann 2012), the lack of research on flybys presents a significant oversight in our understanding of galaxy evolution. This thesis is a first step in exploring the role that flybys play in galaxy transformation. In addition to my flyby work, this thesis will also explore potential imprints of interactions (specifically a minor merger) on our own Milky Way Galaxy, as well as a new technique for more accurately describing dark matter halos that are assembled through interactions.

1.1 Historical Context

Since the discovery of galaxies, astronomers have observed close pairs and multiple systems of galaxies with distorted shapes and odd kinematics, suggesting that they were interacting or dynamically coupled (Zwicky 1956, 1959). Initially it was believed that the gravitational tides generated by interacting galaxies alone would be insufficient to cause the observed features (Spitzer & Baade 1951; Gold & Hoyle 1959; Pikel'ner 1968). In fact, even after early simulations demonstrated interactions could be responsible for tidal tails and

bridges (Holmberg 1941; Pfleiderer & Siedentopf 1961; Pfleiderer 1963), their influence was largely dismissed based on statistical arguments. It wasn't until the 1970s, with increasing evidence from simulations, that galaxy interactions were an accepted dynamical process.

Early investigations of interactions using simulations focused on explaining observed features like tidal tails (Toomre & Toomre 1972; White 1978) and ring galaxies (Lynds & Toomre 1976; Theys & Spiegel 1977), with very little emphasis on the link between interactions and galaxy evolution itself (Toomre & Toomre 1972). In the mid 1970s to early 1980s, when theorists realized that a large static potential was required to stabilize simulated disks against relaxation and bar formation, Rubin et al. (1980) announced her findings that the velocity profiles of observed disks required a non-luminous mass component. The emergence of the dark matter halo had significant implications for estimates on merger rates (Aarseth & Fall 1980); because dark matter halos extend well beyond the visible galaxy, the galaxy-galaxy interaction cross-section is much larger than what it would be from the luminous components alone. This increases the expected merger rate and makes mergers a common event throughout the Universe (Lacey & Cole 1993; Maller et al. 2006).

Numerical simulations have been an instrumental tool for exploring interactions. Due to the high computational cost of directly computing the forces between all particles in a simulation ($\propto N^2$, where N is the number of particles), early numerical studies of galaxy interactions were limited to using massless test particles in simple potentials (Toomre & Toomre 1972) or a small number of particles, resulting in a low resolution (White 1978, $N \sim 200$). By instead estimating force contributions from distant particles as low-order multipole expansions (Barnes & Hut 1986), the computational cost decreased significantly ($\propto N \log N$). In conjunction with new methods for including gas (Negroponte 1982; Barnes

& Hernquist 1991) and sub-resolution physics like star formation (Noguchi & Ishibashi 1986), supernova, accretion onto a central black hole, as well as feedback from all these processes, simulations soon demonstrated that galaxy interactions can cause a vast zoo of features (e.g., Barnes & Hernquist 1991; Hernquist 1992; Mihos & Hernquist 1996; Miwa & Noguchi 1998; Jogee 2006; Hopkins et al. 2006; Dubinski & Chakrabarty 2009).

While galaxy mergers have been explored in great detail, little attention has been paid to the subtle influence of flybys. Like mergers in the 1950s, flybys have been ignored due to the belief that they are insignificant to galaxy evolution as a whole. However, recent studies have exposed this judgment to be hasty and misinformed. First, the cosmological simulations of Sinha & Holley-Bockelmann (2012) found that at low redshifts, flybys are actually more common than mergers for massive halos (See Fig. 1). Therefore, even if flybys have only a minor impact on galactic structure, it is possible for them to still dominate galaxy evolution at certain redshifts. Second, using linear perturbation theory, Vesperini & Weinberg (2000) concluded that even low mass halo flybys could induce long-lived asymmetries in the primary, and generally excite perturbations similar to minor mergers. This is further supported by D'Onghia et al. (2010) findings that the quasi-resonant interaction between stars in a spinning disk and a high-velocity perturber can cause tidal features like tails. Although the perturbations expected from flybys are smaller than those predicted for major mergers, even small perturbations can have a significant impact on a galaxy's evolution, particularly when resonances are excited (Weinberg 1998).

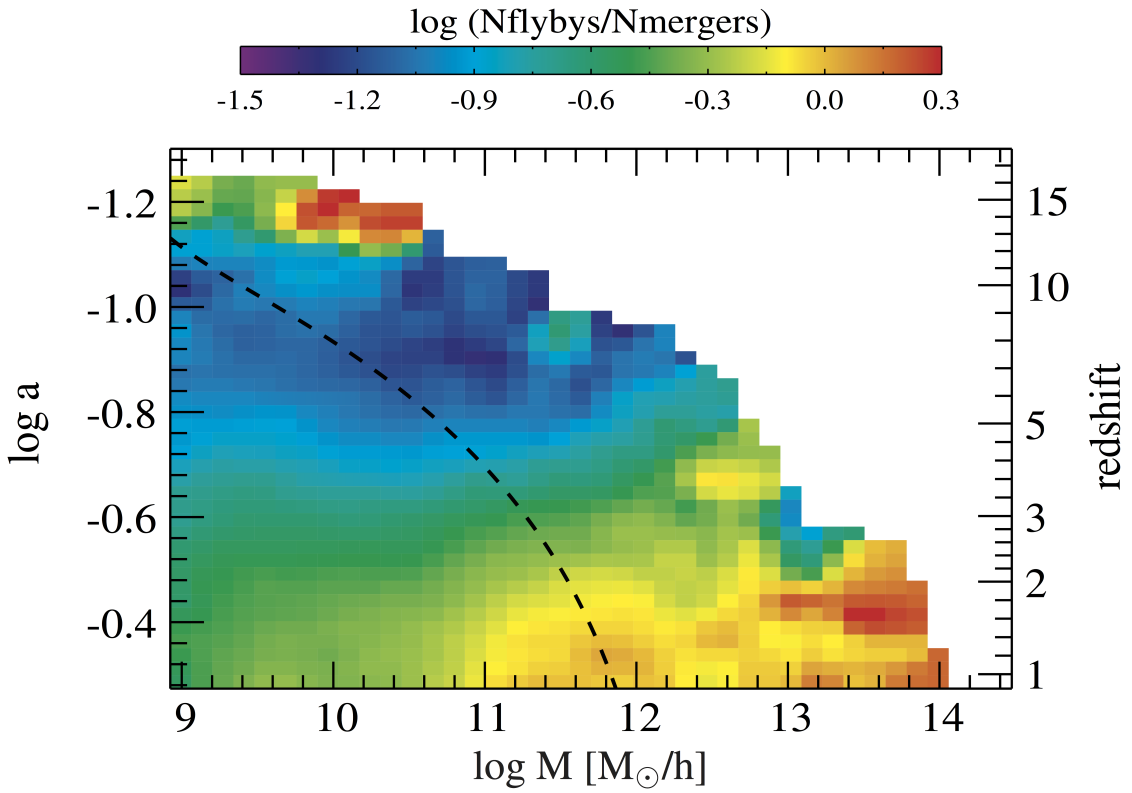

Fig. 1. Comparison of flyby vs. merger rates for different redshifts and halo masses from the cosmological simulations of Sinha & Holley-Bockelmann (2012). The dashed line indicates the track a Milky Way massed halo would take. Note that, above $\sim 10^{12}$M$_\odot$and for $z < 2$, flybys and mergers are comparable.

1.2 The Effects of Interactions on Galaxy Components

Tidal forces can leave a long-lasting imprint on the interacting galaxies in a number of ways, from exciting spiral arms and bars (Berentzen et al. 2004; Weinberg & Blitz 2006; Lokas et al. 2014) to triggering star formation (Hernquist & Mihos 1995; Kaviraj 2013) to fueling of active galactic nuclei (AGN; Hopkins & Quataert 2010; Kaviraj 2014).

1.2.1 Tidal Features

The first features associated with interactions were tidal tails (Toomre & Toomre 1972; White 1978). Simulations showed that the tidal forces between two galaxies in the process of interacting were strong enough to significantly disturb one or both galaxies. The size and mass enclosed within such tails depends upon the relative masses of the galaxies, the slope of the gravitational potentials, orbit parameters, and galaxy morphology (See Figure 2; Barnes 1988; Hibbard & Mihos 1995; Springel & White 1999).

While major mergers between disk galaxies ($M_1/M_2 < 10$, $M_1 > M_2$) can draw out long tidal tails from both galaxies, minor mergers will only do so for the smaller galaxy, which may be destroyed entirely if the forces are strong enough (Hernquist & Weinberg 1989; Weinberg 1998; Johnston et al. 1995; HolleyBockelmann & Richstone 1999). In this case, the effects of tidal forces on the primary will be more subtle, such as the excitation of spiral arms and bars (Berentzen et al. 2004; Weinberg & Blitz 2006; Lokas et al. 2014).

In addition to drawing out existing stars into long tidal tails, any gas within the galaxy will also be affected. If the tidal forces are strong enough and can compress the gas to sufficiently high densities, bursts of star formation will occur within over-dense knots

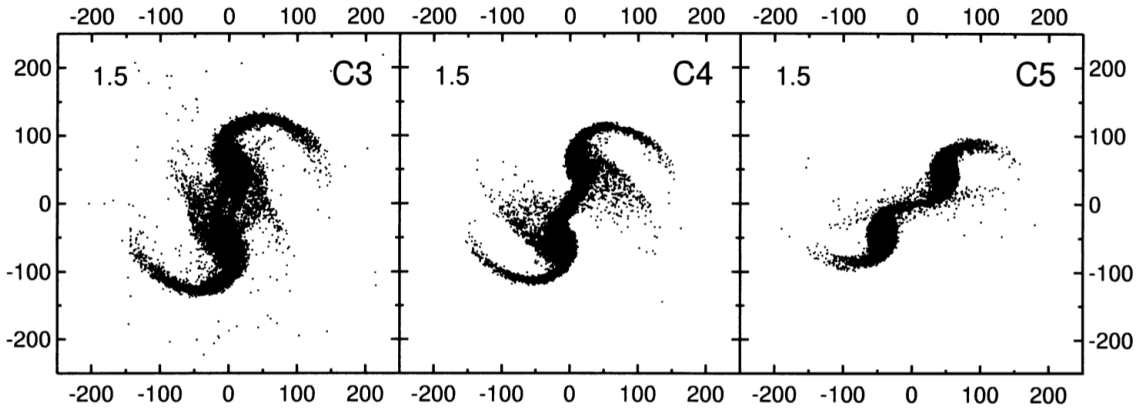

Fig. 2. Examples from Springel & White (1999) of the differences between the tidal tails formed during simulations of major mergers with different impact parameters (28, 56, and $112\,h^{-1}$kpc from left to right).

along the tidal tails and in the galaxies themselves. This is seen in both observations (van der Hulst 1979; Mirabel et al. 1991; Whitaker et al. 2014; Scudder et al. 2015) and simulations (Barnes & Hernquist 1991; Mihos & Hernquist 1996; Naab & Burkert 2001; Di Matteo et al. 2007). The tidal forces experienced during an interaction will also induce gravitational instabilities, removing angular momentum from the gas, and allowing gas inflow toward the centers of the interacting galaxies. Observations (Mundell & Shone 1999; Georgakakis et al. 2000) and simulations (Barnes & Hernquist 1991; Bekki 1995; Mihos & Hernquist 1996; Mayer et al. 2007) confirm that gas-rich galaxies that are experiencing or have recently experienced an interaction will have higher gas densities and enhanced central star formation. Such inflow may even help to fuel the growth of central supermassive black holes (SMBHs) and power AGN if enough angular momentum can be transported away from the gas (Hopkins et al. 2006; Jogee 2006; Mayer et al. 2007; Hopkins & Quataert 2010).

Tidal tails have also been used as tracers of the underlying dark matter potential. Since the slope of the more massive galaxy's gravitational potential determines how large tidal tails will be (i.e. steeper potentials produce larger tidal tails), the positions and motions of the streams of stars left behind by satellite galaxies as they fall into the dark matter halos of larger galaxies can be used to place better constraints on the mass and distribution of the dark matter (Dubinski et al. 1999; Mayer et al. 2002; Warnick et al. 2008).

1.2.2 Bars

Simulations show that dynamically cold disks are unstable against bar formation (Toomre 1964; Sparke & Sellwood 1987) and even disks stabilized by a higher velocity dispersion (Athanassoula & Sellwood 1986), massive dynamically warm dark matter halo (Ostriker & Peebles 1973), or central spheroid (Hasan & Norman 1990; Shen & Sellwood 2004) can form bars under sufficient perturbation (Dubinski et al. 2009). Once a perturbation in the smooth gravitational potential of the disk is sufficient to overcome the dispersion of the disk, it can grow in a runaway process to form a bar (Sellwood 1981). It is possible that even the small transient quadrupole produced by a flyby could produce a bar in galaxy's disk if it were sufficiently cold (Noguchi 1987; Gerin et al. 1990; Miwa & Noguchi 1998; Berentzen et al. 2004; Lokas et al. 2014; Lang et al. 2014). In addition, linear perturbation theory and N-body simulations predict that bars produced by external triggers like flybys may be larger than those produced by local instabilities (Weinberg & Katz 2002; Holley-Bockelmann et al. 2005). Although it is unclear how long bars typically survive, studies indicate that bars can be destroyed by mergers (Athanassoula 1996), growth of

a central stabilizing bulge (Hasan & Norman 1990; Shen & Sellwood 2004), or a triaxial halo (Berentzen et al. 2006). However, if bars die out on relatively long time scales, their influence on a galaxy's disk, bulge, SMBH, and dark matter halo could have long-lived consequences.

Due to its collisional nature, gas in a barred galaxy can pile up on the bar's leading edge while stars remain trapped on orbits within the potential of the bar. As the stellar component trails the gas, the negative torque it exerts can efficiently remove angular momentum from the gas and drive inflow toward the galactic center (See Figure 3; Athanassoula 2000; Hernquist & Mihos 1995; Hopkins & Quataert 2010). As gas falls into the central regions

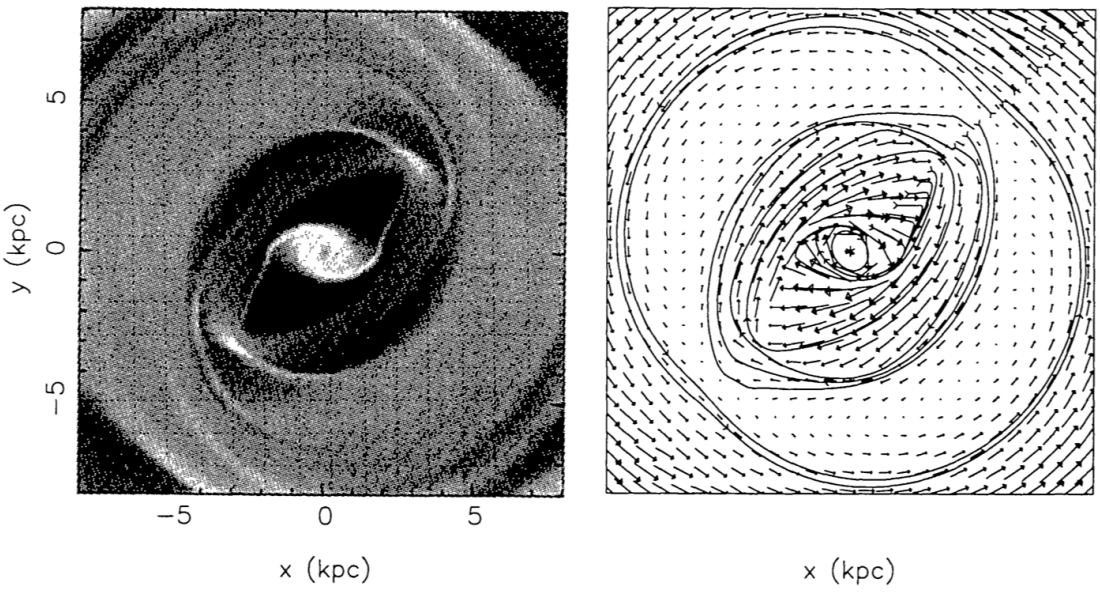

Fig. 3. Gas response in density (left) and trajectory (right) to a bar (Figure 1, Athanassoula 2000).

of a galaxy it can be compressed sufficiently by shocks to form stars, resulting in a central

concentration of young stars in a disk or bulge that may rotate due to the angular momentum of the inflowing gas (Barnes & Hernquist 1991, 1996). Although gas can become trapped at resonances (Athanassoula 2000), asymmetric features in the inner regions of a galaxy like nuclear bars or spiral features can remove additional angular momentum from the gas such that it may even reach a SMBH located at its center (Shlosman et al. 1989; Hopkins & Quataert 2010).

Simulations of feedback regulated SMBH and bulge growth due to merger induced gas inflow (Di Matteo et al. 2005; Robertson et al. 2006; Hopkins et al. 2007; Johansson et al. 2009) have successfully reproduced correlations observed between the mass of a galaxy's SMBH and properties of its bulge including velocity dispersion ($M_{\rm BH} - \sigma_{\rm b}$; Ferrarese & Merritt 2000; Gebhardt et al. 2000; Tremaine et al. 2002) and mass ($M_{\rm BH} - M_{\rm b}$; Kormendy & Richstone 1995; Magorrian et al. 1998; McLure & Dunlop 2002; Marconi & Hunt 2003; Häring & Rix 2004). However, observations indicate that SMBHs embedded in isolated barred galaxies follow a systematically offset (but still consistent) $M_{\rm BH} - \sigma_{\rm b}$ relation from that of merging galaxies (Hu 2008; Graham 2008). This finding is believed to result from differences in the bulges produced by different processes.

While bulges produced in both barred and merging systems may receive contributions from young stars formed out of inflowing gas, bulges produced in major mergers would also contain old stars scattered from the disk by the companion. The resulting dichotomy may be reflected in the emerging distinction between classical and pseudobulges in observations. pseudobulges, usually found in barred galaxies, are less concentrated and less spherical than classical bulges sometimes having disky shapes that often coincide with nuclear spiral or bar shaped structures (Kormendy & Kennicutt 2004; Fisher & Drory 2010). In addition,

$M_{\rm BH}$ does not correlate with $\sigma_{\rm b}$ for galaxies with pseudobulges (See Figure 4; Kormendy & Ho 2013). Such properties are consistent with bulges formed from gas inflow in simulations

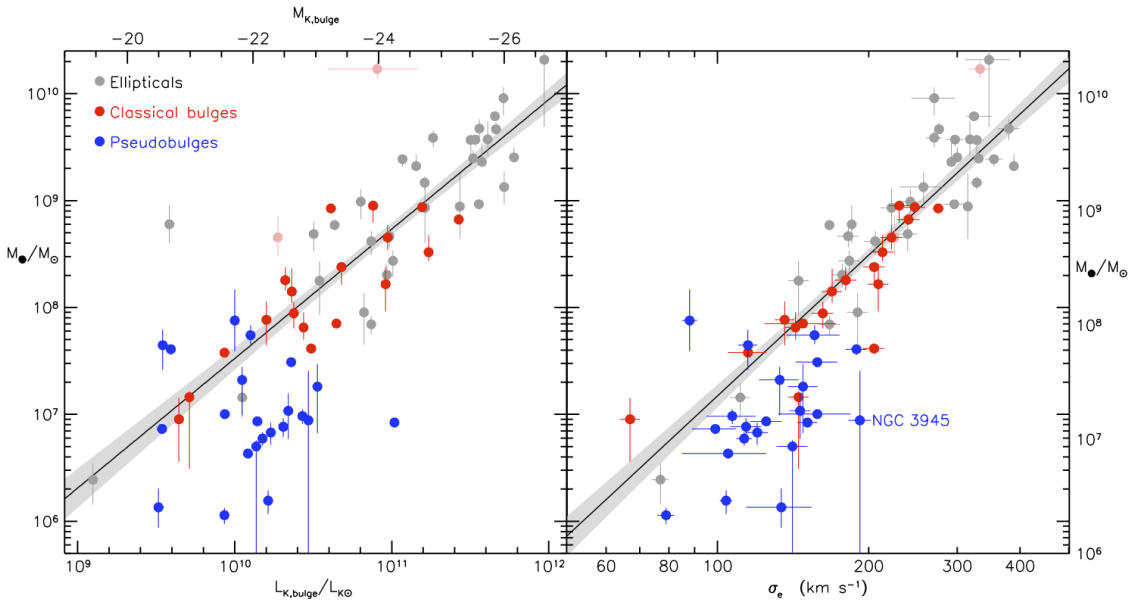

Fig. 4. Relationship between black hole mass and bulge luminosity (left) or velocity dispersion (right) for elliptical galaxies, classical bulges, and pseudobulges (Kormendy & Ho 2013).

by both bars (Younger et al. 2008) and minor mergers (Eliche-Moral et al. 2006).

Bars can also affect a galaxy's dark matter halo through angular momentum transfer between the bar, disk, and halo (Lynden-Bell & Kalnajs 1972; Tremaine & Weinberg 1984; Weinberg 1985; Athanassoula 2002). A number of N-body simulations have shown that a massive bar rotating in a spherical dark matter halo will form a core in the halo's mass distribution with larger bars generating larger cores (Holley-Bockelmann et al. 2005; Weinberg & Katz 2007b; Sellwood 2008; Klypin et al. 2009). The size of the core formed

in these simulations is in turn found to affect how large future bars will be (larger cores leading to larger bars and so on). Since larger bars are expected from external interactions over internal instabilities (Weinberg & Katz 2002), the size of observed cores could be used a method for identifying bars formed by flybys vs. secular evolution if internal instabilities form bars in nature (See Sellwood 2000). However, the exact relation is not clear as different simulations find different core sizes. Several studies argue that this result is very sensitive to both numerical effects, including particle number, force resolution, and time step, as well as the structure of the initial model, such as disk thickness and the mass ratio between the disk and dark matter (Dubinski et al. 2009; Klypin et al. 2009).

1.2.3 Disk Warping

Bars are not the only feature that interactions may excite in galaxies. If perturbing the dark matter halo causes an asymmetry in the halo, then it is possible that the disk could become warped in response to the asymmetry (Dubinski & Chakrabarty 2009). Warped disks have often been attributed to satellite interactions (Kalirai et al. 2006). In our own galaxy, tidal interactions with the Magellanic Clouds have been suggested as one way of explaining the warp observed in the Milky Way's disk (Garcia-Ruiz et al. 2002; Weinberg & Blitz 2006). While simulations by Vesperini & Weinberg (2000) find that this effect is small in the primary for unequal mass external flybys, perturbations induced by internal flybys can propagate to and persist in a disk for moderate mass ratios (See Figure 5; Kim et al. 2014). Similar features could be excited by tidal interactions during the early stages of mergers, but might also be accompanied by disk heating (Quinn et al. 1993; Walker et al. 1996; Velazquez & White 1999).

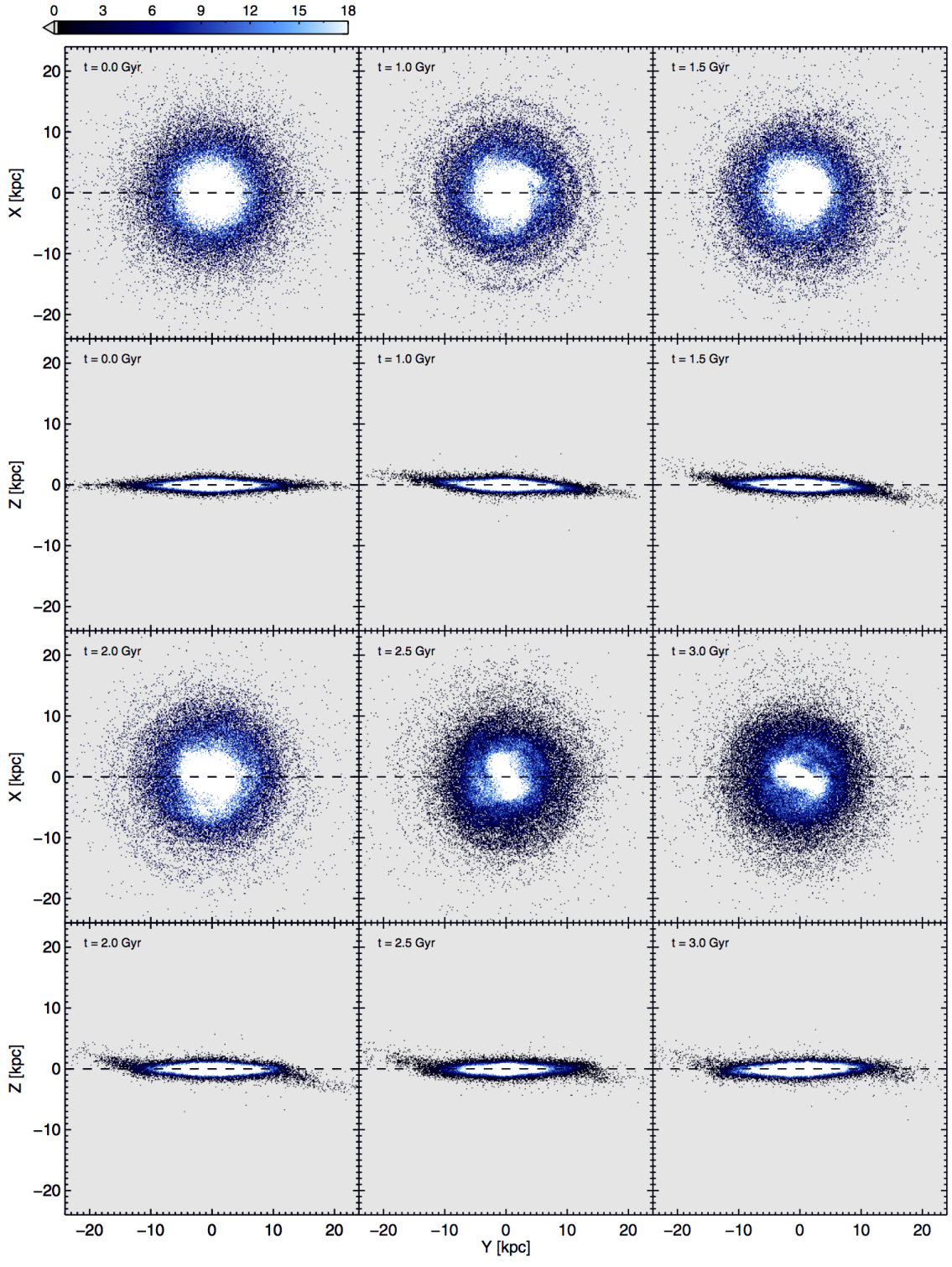

Fig. 5. Disk warping during a simulation of a flyby interaction with a dark matter halo (Kim et al. 2014).

1.2.4 Decoupled Cores

Astronomers have found that the centers of some elliptical galaxies rotate in a sense that is different and even opposite to the rest of the galaxy (See Figure 6; Efstathiou et al. 1982; Franx & Illingworth 1988; Bender & Surma 1992; Davies et al. 2001; Geha et al. 2005; Kleineberg et al. 2011). Since a different kinematic profile indicates a different origin for the core in comparison with the rest of the galaxy, kinematically decoupled cores (KDCs) are believed to result from an interaction with another galaxy that transfers mass or angular momentum (Bertola & Corsini 1999). Although they are generally attributed to mergers, both major (Hernquist & Barnes 1991) and minor (Kormendy 1984; Balcells & Quinn 1990), KDCs simply require tidal torquing of some sort, and a flyby could provide a strong torque as well (De Rijcke et al. 2004). Further, many of the observed KDCs cannot be adequately explained by a merger scenario due to their geometry. These include those whose angular momentum is perpendicular to that of the host galaxy (Balcells & Quinn 1990). KDCs recently found in spiral galaxies like NGC 4672 and NGC 4698 (Sarzi et al. 2000; Bertola & Corsini 1999) may also present problems for the merger scenario given that a merger could heat the disk (Walker et al. 1996; Velazquez & White 1999). Although simulations indicate that KDCs produced by fast interactions like flybys are larger than those observed in small elliptical galaxies (González-García et al. 2005), it is possible that some of these odd spiral KDCs are formed by such interactions (Hau & Thomson 1994; De Rijcke et al. 2004).

1.2.5 Dark Matter Halos

Interactions also leave an imprint on the dark matter halo. Theoretical models for the spherical collapse of overdensities in the early universe suggest that virialized halos

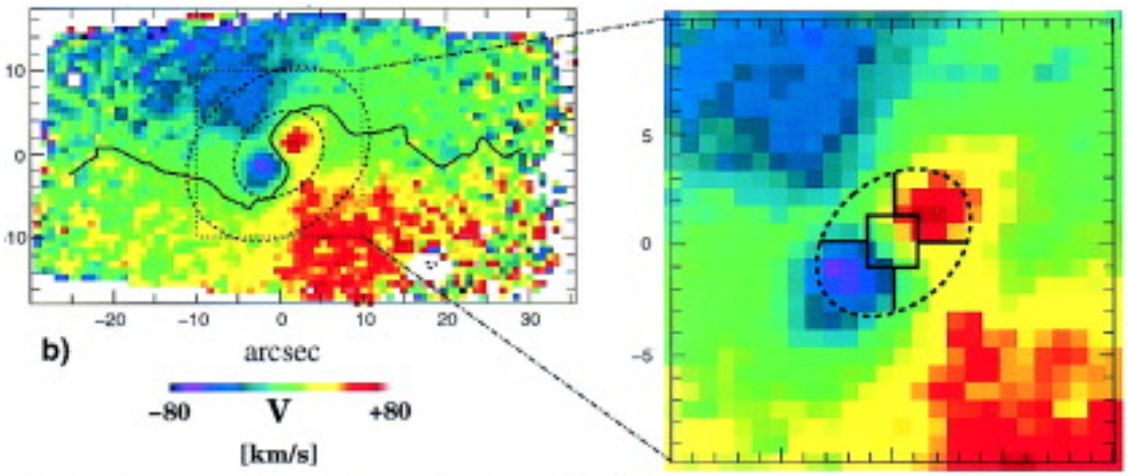

Fig. 6. Radial velocity map for NGC 4365, a galaxy hosting a KDC. Taken from Figure 1 of Davies et al. (2001).

should obey a specific density profile. The most common density profile is the NFW profile (Navarro et al. 1997),

$$\rho(r) = \frac{\rho_0}{\frac{r}{R_s}\left(1+\frac{r}{R_s}\right)^2}. \tag{1.1}$$

NFW profiles are typically characterized in terms of concentration $c = R_{\rm vir}/R_s$, where $R_{\rm vir}$ is the virial radius; a halo's concentration is expected to reflect the state of the universe at the time when it formed. As a result, studies find that smaller halos are more concentrated than larger halos and halos of the same mass are more concentrated at lower redshifts (e.g., Bullock et al. 2001a; Neto et al. 2007; Klypin et al. 2011; Diemer & Kravtsov 2015). However, even virialized halos can be non-spherical or contain substructure, making the measurement of concentration difficult. A new technique for measuring concentration that allows for deviations from the theoretical profile is discussed in Chapter IV. This is particularly important for interacting halos.

Halos in cosmological simulations that have recently undergone major mergers are the least virialized, are not well fit by an NFW profile, and have properties (e.g., shape, concentration, spin) that deviate significantly from the average for systems at the same mass and redshift (See Figure 7, Jing 2000; Neto et al. 2007; Maccio et al. 2007; Power et al. 2012). Similar results are found for halos with different accretion histories overall (Zhao et al. 2009; Power et al. 2012; Ludlow et al. 2013). As a result, halos that occupy different environments and are experiencing interactions at different rates may also have different properties (Avila-Reese et al. 1999; Maccio et al. 2007; Hearin et al. 2015). Although it is not possible to directly observe how interactions impact the dark matter in nature, we can infer information from the dynamics of the visible components (Dubinski et al. 1999; Warnick et al. 2008; Loebman et al. 2014) as well as from gravitational lensing (Meneghetti et al. 2010; Giocoli et al. 2014).

Dark matter halos assemble from the accretion of smaller halos in a hierarchical manner. As small halos fall into these ever larger halos, they orbit within the parent halos as substructure until they are tidally disrupted. This process results in halos that are embedded with substructure and appear quite clumpy, as seen in Figure 7. Subhalos tend to be more triaxial (Kuhlen et al. 2007), more concentrated (Diemand et al. 2007), and less dense (Diemand & Moore 2011) than isolated or parent halos (See Figure 8 for a comparison of parent and subhalo profiles). The tidal forces exerted by substructure can induce changes in the morphology of the central galaxies including enhanced star formation, ring-like structures, bars, and other asymmetries (Kazantzidis et al. 2008; Romano-Díaz et al. 2008). In addition, stellar halos are theorized to form from material tidally stripped from satellite galaxies hosted by infalling subhalos (Harding et al. 2001; Bullock et al. 2001b;

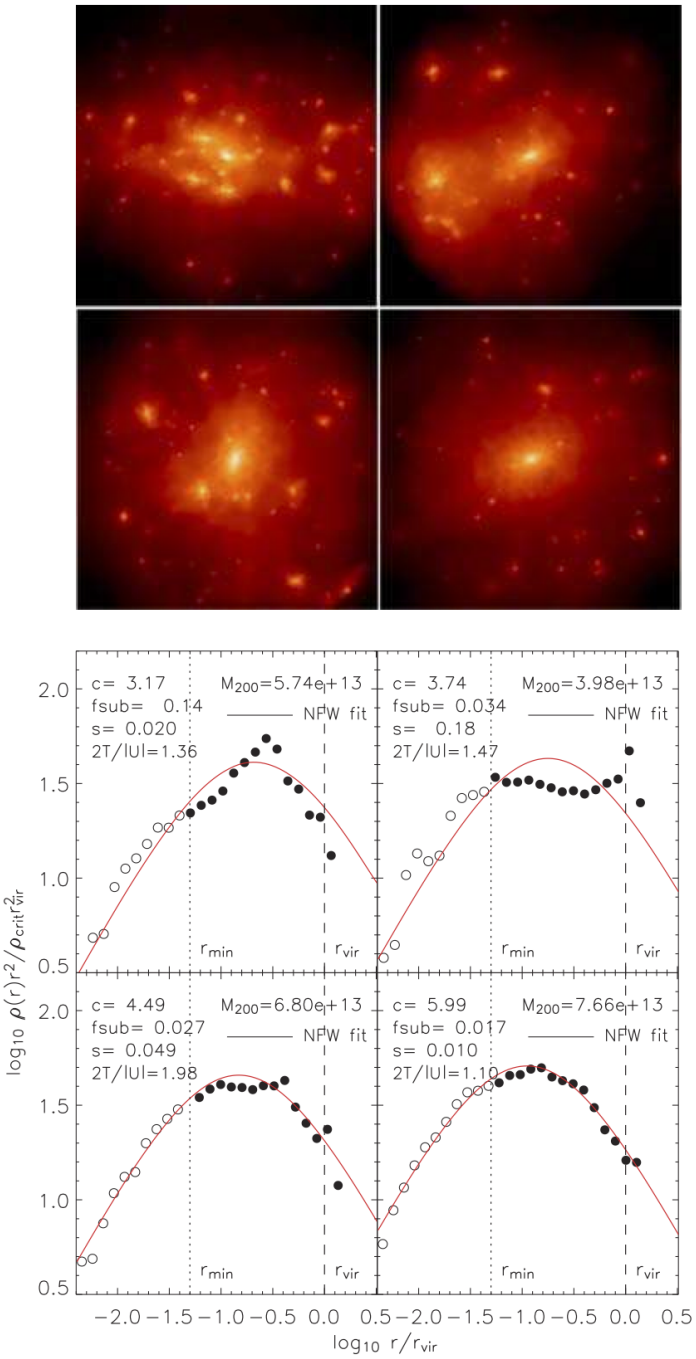

Fig. 7. Images (top) and spherically averaged density profiles (bottom) for halos from Neto et al. (2007). While the bottom right halo is well fit by an NFW profile (red line), the other three are not. The top left halo has a lot of substructure, the top right halo is undergoing a major merger, and the bottom left is not virialized.

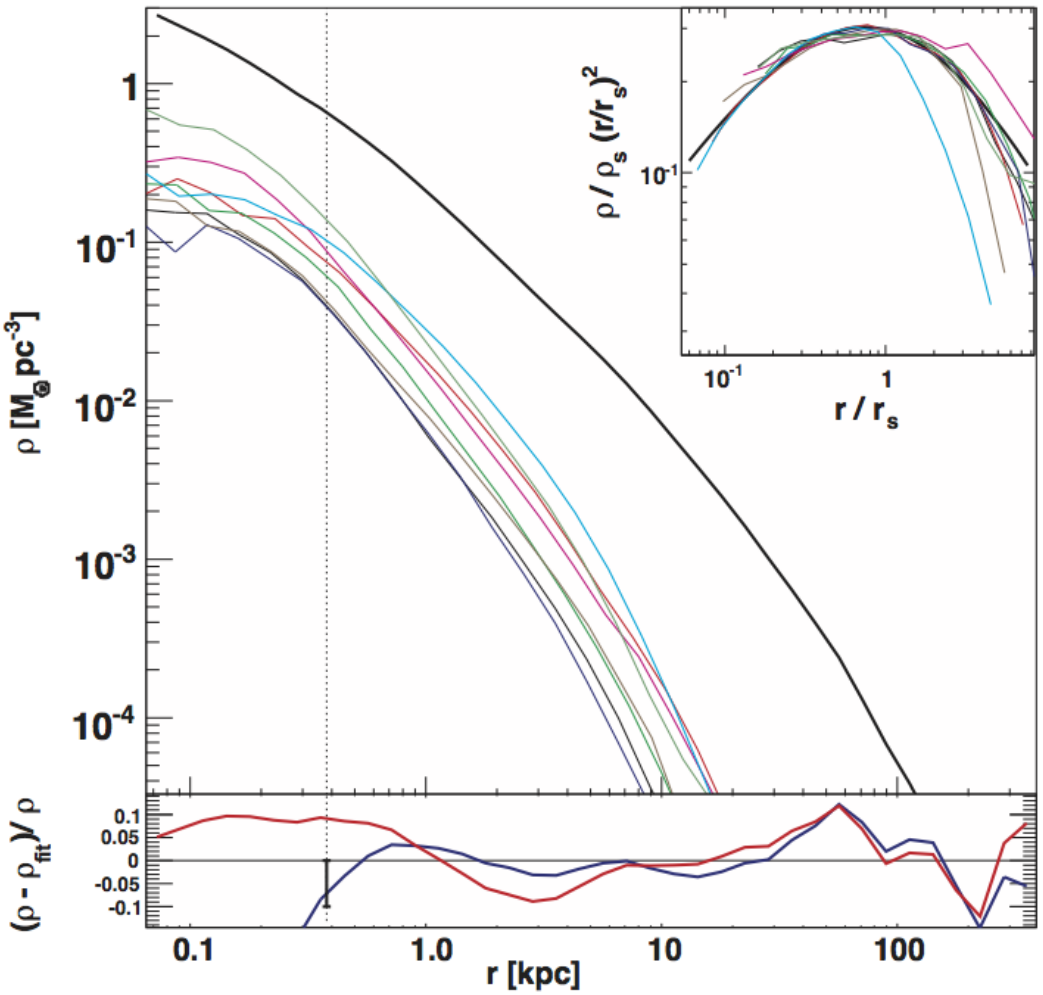

Fig. 8. The density profiles for the parent halo (black) and 8 most massive subhalos (colors) from the Via Lactea simulation (Diemand & Moore 2011) The bottom panel shows normalized residuals after fitting and the inset compares the profiles after they are normalized to the density at the scale radius.

Bullock & Johnston 2005; Warnick et al. 2008). In clusters where substructure is abundant, the cumulative effect of continuous tidal interactions between substructure and the central galaxy or even other substructure, referred to as 'galaxy harassment,' can enhanced the morphological evolution, tidal stripping, and disruption of satellite galaxies (Moore et al. 1996, 1998; Ghigna et al. 1998; Knebe et al. 2006).

1.3 Interactions in the Cosmological Context

Due to the vast influence interactions can have on galaxy evolution, understanding what types of interactions are common and how often they occur can provide insight into why the universe looks the way it does. This can be done by examining interactions between dark matter halos in cosmological simulations.

Given particle information describing the dark matter distribution at each redshift, overdensities can be identified and grouped into halos and subhalos based on some form of density contrast criterion. There exist a large variety of methods for identifying halos (See Knebe et al. 2013), but the majority use either inter-particle separations (Friends-of-Friends, e.g., Davis et al. 1985; Klypin et al. 1999; Springel et al. 2001a) or density estimates (e.g., Knollmann & Knebe 2009; Planelles & Quilis 2010).

Once halos and subhalos are identified, they can then be linked between snapshots at different redshifts with their corresponding progenitor and descendent halos in order to identify interactions and create histories for each halo. This has typically been used to track halo mergers (Wechsler et al. 2002; Boylan-Kolchin et al. 2009; Tweed et al. 2009; Wetzel et al. 2009), but has also been used to study halo flybys (See Figure 9, Sinha & Holley-Bockelmann 2012).

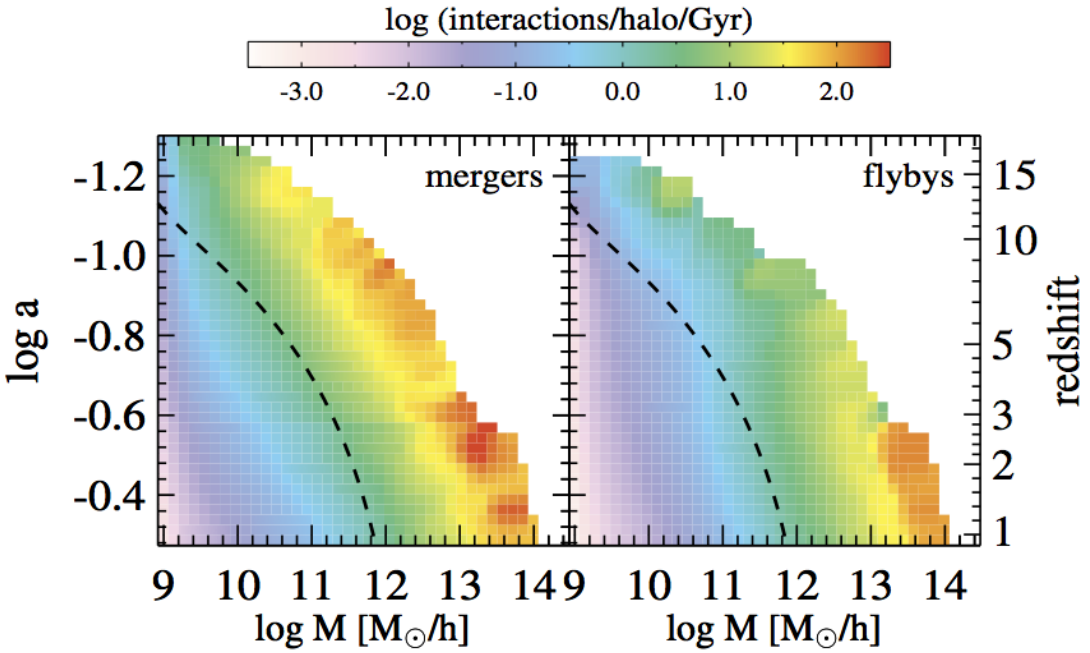

Fig. 9. Comparison of the merger (left) and flyby (right) interaction rates as a function of halo mass and redshift from Sinha & Holley-Bockelmann (2012). The dashed line shows the track a Milky Way mass halo would take.

Halo interaction rates are broadly consistent across different simulations, halo finders, and merger tree techniques (Hopkins et al. 2010b). These merger rates also agree with what is derived from the halo mass function predicted by the extended Press-Schechter (EPS; Press & Schechter 1974; Bower 1991) formalism (Lacey & Cole 1993; Neistein & Dekel 2008; Zhang et al. 2008), which is predicted as the assumption of linear evolution. These studies find that interactions are more common in dense environments, that minor interactions more common than major ones, that interaction rates are higher at earlier times, and that more massive halos interact more often than less massive halos (Gottlober

et al. 2001; Fakhouri & Ma 2008; Stewart et al. 2009; Genel et al. 2009; Wetzel et al. 2009; Fakhouri et al. 2010; Hopkins et al. 2010a; Sinha & Holley-Bockelmann 2012).

From the interaction rates for dark matter halos, galaxy interaction rates can be inferred by assigning galaxy masses to halo masses based on an assumed relationship (Guo & White 2008; Wetzel et al. 2009; Behroozi et al. 2010). These galaxy merger rates can then be compared to rates derived from the fraction of observed galaxies with close pairs or morphological signs of an interactions (Le Fevre et al. 2000; Cassata et al. 2005; Bell et al. 2006; Berrier et al. 2006; Patton & Atfield 2008; Lotz et al. 2008; Conselice et al. 2008, 2009; de Ravel et al. 2009; Jogee et al. 2009; Lotz et al. 2011). However, while halo interactions rates between studies are consistent, different choices for how galaxies are assigned to halos can lead to galaxy interaction rates that can differ by a factor of ~ 2 between different studies (Hopkins et al. 2010b).

This thesis furthers our understanding of how interactions between galaxies influence galaxy evolution. The main thrust of this work explores flyby interactions. Bars are capable of driving significant galaxy evolution, but very little is known about flyby interactions and the role they could play in bar formation. To answer this question, Chapter II presents work exploring the role of flyby interactions in triggering the formation of stellar bars. In addition to this main thrust, work is also included which explores evidence for a recent minor merger within observations of the Milky Way Galactic Center (Chapter III) and a new technique for accurately characterizing dark matter halos that are disturbed by interactions (Chapter IV).

Chapter II

BAR FORMATION FROM GALAXY FLYBYS

The following work was published in the Astrophysical Journal Letters (Lang et al. 2014) and is reprinted below in its entirety.

Bar Formation from Galaxy Flybys

Meagan Lang[1], Kelly Holley-Bockelmann[1,2], & Manodeep Sinha[1]
[1]Department of Physics and Astronomy, Vanderbilt University, Nashville, TN
email: meagan.lang@vanderbilt.edu
[2]Fisk University, Department of Physics, Nashville, TN
email:k.holley@vanderbilt.edu

Abstract

Recently, both simulations and observations have revealed that flybys - fast, one-time interactions between two galaxy halos - are surprisingly common, nearing/comparable to galaxy mergers. Since these are rapid, transient events with the closest approach well outside the galaxy disk, it is unclear if flybys can transform the galaxy in a lasting way. We conduct collisionless N-body simulations of three co-planar flyby interactions between pure-disk galaxies to take a first look at the effects flybys have on disk structure, with particular focus on stellar bar formation. We find that some flybys are capable of inciting a bar with bars forming in both galaxies during our 1:1 interaction and in the secondary during our 10:1 interaction. The bars formed have ellipticities $\gtrsim 0.5$, sizes on the order of the host

disk's scale length, and persist to the end of our simulations, ∼5 Gyr after pericenter. The ability of flybys to incite bar formation implies that many processes associated with secular bar evolution may be more closely tied with interactions than previously though.
Key words: galaxies: interactions — galaxies: flybys — galaxies: bars

2.1 Introduction

While interacting galaxies bind together and eventually coalesce during a merger, more energetic encounters allow the two galaxies to disconnect and separate forever. These flybys generate a short, but intense, perturbation in both galaxies. Linear perturbation theory predicts that such an impulse should be similar in amplitude to that excited by a minor merger (Vesperini & Weinberg 2000) and therefore may transform galaxies in similar ways.

For example, numerical simulations have shown that, if a disk is kinematically cool enough, even a small perturbation can induce a stellar bar (Noguchi 1987; Gerin et al. 1990; Miwa & Noguchi 1998; Berentzen et al. 2004) and this is supported by bars triggered during simulations of minor mergers (Noguchi 1987; Steinmetz & Navarro 2002; Berentzen et al. 2004; Dubinski et al. 2008) and tidal interactions (Lokas et al. 2014). Almost at odds with this, simulations have shown that minor mergers can also destroy bars (Romano-Díaz et al. 2008). Therefore, the similar impulse induced by flybys could play a role in both the creation and destruction of bars.

Bars drive significant galaxy evolution in the form of angular momentum exchange (Lynden-Bell & Kalnajs 1972; Tremaine & Weinberg 1984; Weinberg 1985; Athanassoula 2002; Holley-Bockelmann et al. 2005), gas inflow and nuclear star formation (Hernquist

& Mihos 1995), and even super-massive black hole (SMBH) growth (Hopkins & Quataert 2010). If flybys can excite or destroy bars, we may observe large-scale evolution beyond what is expected through hierarchical growth. In particular, bar-induced gas inflow has been invoked as one possible explanation for disky pseudo-bulges (Kormendy & Kennicutt 2004; Laurikainen et al. 2007; Scannapieco et al. 2010) and the resulting deviations in the $M - \sigma$ relation (Hu 2008; Graham 2008).

Flyby induced impulses have also been suggested as mechanisms for forming kinematically decoupled cores (KDCs) (De Rijcke et al. 2004), tidal tails (D'Onghia et al. 2010) and spiral arms (Tutukov & Fedorova 2006), evolution from spiral to S0 Hubble type (Bekki & Couch 2011), disk warping (Dubinski & Chakrabarty 2009), and even increased lithium abundance due to tidal cosmic rays (Prodanović et al. 2012). Furthermore, ram pressure and tidal stripping during a flyby can quench star formation and lower a galaxy's mass-to-light (M/L) ratio. The result is a population of red galaxies obeying the halo occupation distribution for satellites, but classified as central galaxies (Wetzel et al. 2014).

Our aim is to investigate the ability of flybys to trigger bar formation. §2.2 discusses simulations and analysis techniques, §2.3 reports our findings, §2.4 discusses the results and their role in a larger context, and §2.5 summarizes our findings and outlines future research.

2.2 Methods

To assess the ability of flybys to excite bars, we launch three planar interactions – an equal mass prograde, an equal mass retrograde, and a minor prograde encounter, where the primary and intruder mass ratio is 10:1.

2.2.1 Galaxies

We constructed two-component galaxy models with an exponential stellar disk and Hernquist dark matter halo (Hernquist 1990) that is ~ 30 times more massive than the disk. One galaxy was Milky Way (MW)-sized, while the other is 10% as massive. See Table 1 for a complete description of the galaxy parameters.

Galaxy	MW1		MW10	
Component	Disk	Halo	Disk	Halo
Total Mass ($M_\odot$)	4.0×10^{10}	1.2×10^{12}	4.0×10^{9}	1.2×10^{11}
Scale Radius (kpc)	4.9	43	2.3	20
Scale Height (kpc)	0.49	n/a	0.23	n/a
# of Particles	5.0×10^{5}	9.4×10^{6}	5.0×10^{4}	9.4×10^{5}
Particle Mass m_p	8.0×10^{4}	1.3×10^{5}	8.0×10^{4}	1.3×10^{5}
Softening (kpc)	0.05	0.058	0.05	0.058

Table 1. Summary of component properties for each model galaxy.

We exclude a bulge from the models so any $m = 2$ perturbation has maximal impact on the disk. Bulges are thought to stabilize disks against bar formation (Shen & Sellwood 2004; Athanassoula et al. 2005) and are thus omitted from this initial simulation suite.

The gravitational softening is set by the inter-particle separation at the disk scale length. The halo softening length is scaled from this by $\sqrt{m_{\rm p,halo}/m_{\rm p,disk}}$.

The initial conditions were evolved in isolation for 3 Gyr using GADGET-2 (Springel et al. 2001b; Springel 2005) to ensure that the system was close to dynamical equilibrium and assess the perturbations induced by secular evolution. This is especially important because artificial halo truncation drives minor evolution of the system.

2.2.2 Interactions

We selected planar orbits with impact parameters equal to 10% of $R_{\rm vir,1} + R_{\rm vir,2}$. To explore the effect of mass ratio and inclination angle, we model 1:1 prograde, 10:1 prograde, and 1:1 retrograde interactions. Interactions start with a separation of $R_{\rm vir,1} + R_{\rm vir,2}$ and velocity such that $v_{\rm peri} = 2v_{\rm circ}$. Being at the energetic boundary of a merger and flyby, we consider the dynamical excitations produced here to be a lower limit for the typical flyby.

Although planar interactions are cosmologically rare, planar prograde and retrograde interactions maximally torque the disk. Since we are interested in maximizing the impact of the interactions, intermediate inclination angles are left for future study.

Interactions were evolved for a minimum of 5 Gyr using GADGET-2 (Springel et al. 2001b; Springel 2005) with snapshots every 0.05 Gyr, capturing pericenter and several dynamical times afterward to study the persistence of any perturbations.

2.2.3 Analysis

2.2.3.1 Spherical Harmonics

To assess bar strength, disk potentials are decomposed in spherical harmonics using a self-consistent field (SCF) approach (cf. Hernquist et al. 1995). As bars are traced by the $m = 2$ part of the potential ($\Phi_{m=2}$), the amplitude compared to the total potential ($\Phi_{\rm tot}$) defines an $m = 2$ amplitude ($A_{m=2} = \Phi_{m=2}/\Phi_{\rm tot}$) at any position. By projecting azimuthally averaged $A_{m=2}$ onto polar coordinates in the plane of the disk, we can identify borders of positive $m = 2$ regions signifying a bar, and define an overall bar amplitude as the maximum value of $A_{m=2}$ within these borders.

We define a bar as a region of positive $A_{m=2}$ with a constant position angle that does not change by greater than 10° along its length with amplitude $A_{m=2} \gtrsim 0.04$ (cf. Athanassoula et al. 2013). The radial extent of this region is a proxy for bar length ($l_{m=2}$).

2.2.3.2 Ellipse Fitting

As a cross-check, we use an observationally-based technique which fits ellipses to isophotes; the change in ellipses with radius defines the bar (See Jedrzejewski 1987). Here we fit ellipses to a proxy for surface brightness, the projected mass density of the face-on disk (I). For a given semi-major axis (a), an ellipse is characterized by a center ($X0$,$Y0$), ellipticity (ε), and position angle (ϕ) and is fit to the projected mass density as follows:

1. Find azimuthally averaged intensity at nE eccentric anomalies (E) along a trial ellipse and calculate residuals from the mean intensity along the ellipse.

2. Find dI/da via finite differencing between neighboring ellipses within *derwid* of the trial ellipse's semi-major axis, but with the same center, ellipticity, and position angle.

3. Express residuals as a 2^{nd} order Fourier expansion in E to obtain 4 harmonics (A_1, B_1, A_2, B_2) and the root-mean-square error (rms).

4. Ellipse parameters are accepted if:

   - a maximum number of iterations is exceeded ($maxIter$),
   - dI/da is less than $dertol * rms$
   - the largest harmonic is less than $errtol * rms$ and a minimum number of iterations ($minIter$) has been met

Otherwise....

5. Apply the largest harmonic as a correction factor to the corresponding ellipse parameter such that the harmonic is reduced to zero (See Jedrzejewski 1987), reducing the correction factor by 1% with each iteration to ensure convergence.

6. The process is then repeated for a new trial ellipse with a different a.

We set $nE = 100$, $derwid = 0.05$, $dertol = 0.5$, $errtol = 0.04$, $minIter = 8$, and $maxIter = 20$ and verified that results do not change for a 10% increase/decrease in each parameter. When iterations are ceased but error tolerance is not met, the set of parameters corresponding to the iteration with the smallest harmonic is selected.

For each snapshot, we extract bar parameters from the ellipse fits at 20 radii (See Marinova & Jogee 2007). With this technique, we define a bar as a region of nearly constant angle ($< 10^{\circ}$ along its length) with an ellipticity that rises with increasing radius to $\gtrsim 0.25$ and then decreases by $\gtrsim 0.1$ at the bar edge ($l_{\rm ell}$). Bars smaller than three image bins are excluded and maximum ellipticity ($e_{\rm max}$) is used as a proxy for bar strength.

2.2.3.3 Impact of Spiral Pattern

Regardless of technique, coincident spiral patterns make identifying and characterizing bars difficult. For one, both bars and two-armed spiral patterns reflect $m = 2$ modes. Since bars and spirals dominate in different regions, distinguishing the two contributions is relatively simple when they are misaligned. However, when the bar and spiral pattern speeds differ, periodic alignment prevents clean measurement of the bar contribution. This is seen as periodic variation in the bar amplitude due to confusion with the overlapping

spiral pattern (See Figures 10 & 12). Therefore, while large scale trends can be trusted, short duration features cannot.

Ellipse fits are also affected. While fits to strong bars are generally well-behaved and converge, harmonic expansion along an ellipse intercepting a spiral pattern will exhibit additional power in the harmonic corresponding to the number of arms. For example, an ellipse intercepting a two-armed spiral will have larger A_2 or B_2 harmonics and may not converge on a position angle or ellipticity if the spiral feature is not subtracted. However, since we are interested in fitting the inner disk where a bar would dominate, we ignore transient effects driven by the spiral.

2.3 Results

2.3.1 1:1 Prograde

Figure 10 shows the primary at various stages throughout the 1:1 prograde interaction. Both galaxies experience significant perturbation and both analysis techniques identify a bar (bottom row, Figure 10).

Prior to pericenter, neither method identifies a bar. $A_{m=2}$ remains below 0.01 and $e_{\max}$ varies widely. The disk features a transient three-armed spiral within ~ 4 kpc that is also present when evolved in isolation. In isolation, this feature is dominated by fluctuating $m = 1$ and $m = 3$ modes that never grow above 2% of the potential. These modes also appear intermittently throughout the prograde interaction, however the interaction induces a much stronger $m = 2$ mode reaching $> 10\%$ of the potential. Given that these odd modes

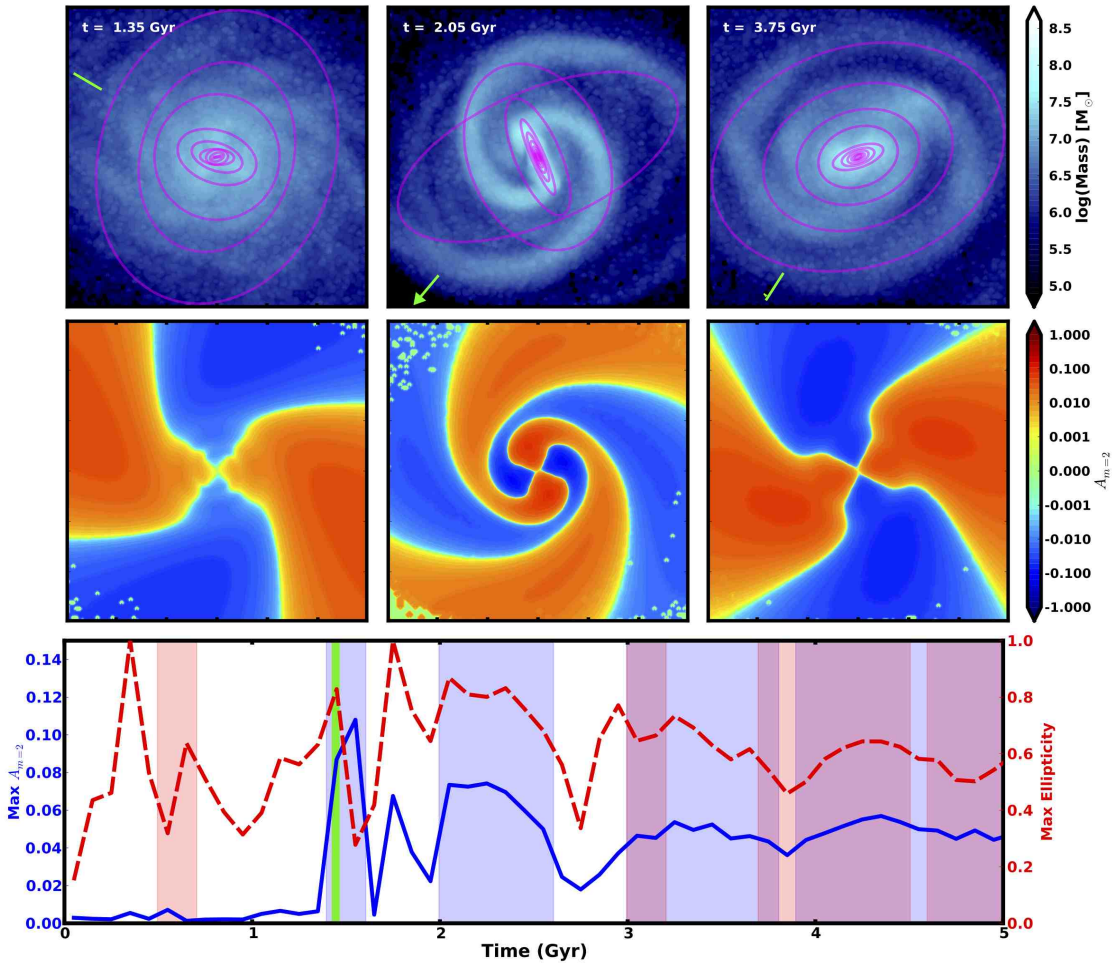

Fig. 10. 1:1 Prograde Primary. Row 1: Face-on projected mass distributions of the inner 30 kpc of the disk for three times during the interaction. Ellipse fits are in magenta, times are printed in each column, and the direction to the secondary is marked with a green arrow. Row 2: Projected $m = 2$ amplitude. Row 3: Time dependence of $A_{m=2}$ (left axis, blue solid line) and $e_{\rm max}$ (right axis, red dashed line). The blue and red regions meet requirements for positively identifying a bar using SCF and ellipse methods respectively. The solid green vertical line marks pericenter.

are transient and constitute a small fraction of the potential, we believe that our conclusions on the ability of flybys to form bars are robust.

$A_{m=2}$ rises to a peak of 0.11 just 0.1 Gyr after pericenter with intermittent bar identification. Although our ellipse fitting bar criteria is not satisfied during this period, we begin to see $e_{\max}$ trace $\sim$1 Gyr periodic variations in $A_{m=2}$.

At $\sim$ 3 Gyr, $A_{m=2}$ and $e_{\max}$ level out to 0.05 and 0.6 respectively, corroborating the presence of a bar rotating at 8.9 rad/Gyr. While the more conservative $m = 2$ method indicates a bar length of $l_{\mathrm{m=2}} = 3.8$ kpc, the ellipse fitting technique points to a longer bar with $l_{\mathrm{ell}} = 8.1$ kpc.

In addition to a bar, both galaxies exhibit a two-armed spiral that winds and begins to dissipate $\sim$ 5.5 Gyr after pericenter. As discussed in §2.2.3.3, the presence of both a bar and spiral pattern causes periodic variation in $A_{m=2}$ every $\sim$1 Gyr as the bar and spiral align.

2.3.2 10:1 Prograde

2.3.2.1 Primary

The 10:1 prograde interaction has a subtle impact on the primary (Figure 11). Although a bar is absent following pericenter at 1.13 Gyr, the disk features a both a two-armed spiral ($m = 2$) and a transient three-armed feature ($m = 3$) in its central $\sim$ 4 kpc. When the two patterns align, the stronger two-armed spiral destroys one arm in the three-armed feature. This destruction shifts $m = 3$ power to the bar mode and causes poor ellipse fits intersecting the missing arm. This results in a periodic increase in $A_{m=2}$ that is somewhat echoed in $e_{\max}$ (Figure 11, bottom panel).

While the $A_{m=2}$ parameter peaks and then levels out during the 1:1 prograde interaction, $A_{m=2}$ increases throughout the entire 10:1 interaction to ~ 0.03 ($l_{m=2} = 3.1$ kpc) about 3.3 Gyr after pericenter, half the final value in the 1:1 interaction and below the level signifying a bar. While the spiral arms cause ellipse fits to be erratic during the first part of the simulation, $e_{\max}$ levels out to 0.58 around 3.5 Gyr after pericenter as the two-armed spiral winds and disappears. By ~ 4 Gyr after pericenter, the destruction of the third arm is enough that the ellipse fits identify a $l_{\rm ell} = 5.2$ kpc bar rotating at 9.4 rad/Gyr. However, due to the lack of evidence in $A_{m=2}$, this is not considered a reliable identification.

2.3.2.2 Secondary

Unlike the primary, the 10:1 secondary disk is strongly perturbed (Figure 12). A two-armed spiral forms just 0.2 Gyr after pericenter (at 1.13 Gyr) with $A_{m=2} = 0.12$. As the two galaxies separate, a bar grows to occupy the majority of the disk. The $A_{m=2}$ levels out to 0.06 with a size of $l_{m=2} = 2.4$ kpc and $e_{\max}$ levels out to 0.6 with $l_{\rm ell} = 2.7$ kpc. Both analyses methods intermittently identify a bar from pericenter on. By ~ 4 Gyr after pericenter, the disk is dominated by a bar rotating at 7 rad/Gyr and the spiral arms are weak and transient.

Under-sampling of the surface density introduces noise into the ellipse fits that translates to a large variation in $e_{\max}$. While $A_{m=2}$ is also affected to some degree (responsible for the break at pericenter), the strongest parts of $m = 2$ mode coincide with high density, and thus highly sampled, regions.

2.3.3 1:1 Retrograde

Neither galaxy is strongly perturbed by the 1:1 retrograde interaction (Figure 13) and only a transient three-armed spiral is discernible. However, as this is also seen in isolation, it is likely unrelated to the interaction.

Although $A_{m=2}$ and $e_{\max}$ increase throughout the simulation, $A_{m=2}$ never exceeds 0.02 and this is reflected in the absence of a bar or two-armed spiral. Ellipse fits identify a 5 kpc bar intermittently toward the end of the simulation. However, as in the primary of the 10:1 prograde interaction, this is likely due to fitting of two arms from the inner 3 armed spiral and is not corroborated by the $m = 2$ analysis.

2.4 Discussion and Potential Implications

As mass discrepancy increases, interactions have a smaller impact on the primary and larger impact on the secondary. Because the 1:1 prograde interaction produced a primary bar and the 10:1 did not, the maximum mass ratio to produce a primary bar for these orbital parameters is somewhere in-between and additional simulations are required to pin it down. However, both the 1:1 and 10:1 prograde flybys induced bar formation in the secondary, implying that planar flybys with smaller impact parameters or orbital eccentricities should also form secondary bars as well.

As expected, the retrograde interaction had negligible impact on either galaxy. While planar orbits were selected to maximize the impact, they are cosmologically rare. As inclination angle increases above the plane, an interaction's ability to induce a bar decreases, but the angle beyond which bar formation no longer occurs will depend on other properties

like mass ratio and eccentricity. Quantifying this dependency requires further simulations and is of interest for future studies.

The formation and persistence of flyby-driven stellar bars has important consequences for the observed bar fraction in seemingly isolated galaxies. In our simulations, bars persist several Gyr after the interaction when the galaxies were separated by Mpc. Thus, many bars observed in isolated galaxies may be the result of flyby interactions rather than secular evolution. Like mergers, flybys are more likely in high density environments (Sinha & Holley-Bockelmann 2012) and flyby-induced bars may enhance the bar fraction in the outskirts of these regions.

Surprisingly, Sinha & Holley-Bockelmann (2012) found high mass ratio flybys are as common as mergers at low redshift. Since the secondary, 'intruder' galaxy will be more strongly affected, flyby-triggered bars could also enhance the bar fraction for low mass galaxies at low redshift. Sheth et al. (2008) found that, while bar fraction increases with mass at high redshift ($z = 0.60 - 0.64$), the bar fraction appears to be independent of mass at low redshift ($z = 0.14 - 0.37$) – this may point to an increase of flyby-induced bars in low mass galaxies at the present epoch. At $z = 0.01 - 0.06$, Cheung et al. (2013) found that, while bar likelihood decreases with mass for quiescent galaxies, the trend is reversed for star-forming galaxies where gas suppresses bar formation. As gas would suppress even flyby induced bar formation, flyby enhancement of the bar fraction at the low mass end would be stronger in galaxies with less gas.

Resonant interactions transfer energy and angular momentum from the bar to underlying dark matter halo. This may flatten the inner halo density profile (Holley-Bockelmann et al. 2005, e.g) and even form a bar in the halo itself (Holley-Bockelmann et al. 2005;

Athanassoula 2007). Bar-induced flattening of the central halo may alleviate some of the discrepancy between observations indicating cores and cusps seen in collisionless simulations (de Blok 2010; Weinberg & Katz 2002), but accurately resolving the angular momentum exchange requires fine resolution of the appropriate resonances (Dubinski et al. 2009; Weinberg & Katz 2007a).

Bars and spiral arms enhance radial migration in disks, mixing the stellar populations (e.g. Minchev & Famaey 2010). Given that flyby induced perturbations are long lived, flyby interactions could enhance radial migration after the two galaxies have separated and are essentially evolving in isolation.

$m = 2$ features like bars and two-armed spirals can also transport gas to the centers of galaxies where it may form stars and even fuel SMBH growth (Hernquist & Mihos 1995; Hopkins & Quataert 2010). Gas inflow and star formation has also been tied with the formation of pseudo-bulges with Sersic indices $\lesssim 2$ (Kormendy & Kennicutt 2004; Laurikainen et al. 2007; Scannapieco et al. 2010) which may obey a different $M-\sigma$ relation than classical bulges (Hu 2008; Graham 2008). If flyby-induced $m = 2$ features drive gas inflow, enhanced central star formation, AGN activity, or placement on the $M - \sigma$ relation could signify a recent flyby or evolution history dominated by flybys.

Flybys could also shut-off smooth gas accretion, quenching star formation in the secondary. Combined with tidal stripping, galaxies with massive companions should have higher mass-to-light ratios and redder colors. Since massive halos have more flybys (Sinha & Holley-Bockelmann 2012), this effect would be more prominent in groups and clusters. Such an excess in the red-fraction has been reported (Wang et al. 2009) and Wetzel et al. (2014)

recently speculated that excess in the red-fraction could be attributed to flyby galaxies outside the host virial radius.

2.5 Summary & Future Work

Using N-body simulations, we investigated the ability of galaxy flyby interactions to form bars. We used observationally-based techniques to identify and measure bar properties. We find that:

- *Flybys can induce $m = 2$ perturbations in galaxy disks* reaching 6% of the total potential.
- *Flybys can trigger bar formation* with bar strength decreasing in the primary and increasing in the secondary as mass discrepancy increases.
- *Strong flyby-induced bars can persist long after the interaction.* In the 1:1 and 10:1 prograde interaction, the bars formed persisted ($A_{m=2} > 4\%$) until the end of the simulations at 5 Gyr (~ 4 Gyr after pericenter).
- *Flybys can induce spiral arms.* Two-armed spirals were formed in both the primary and secondary galaxies during both prograde interactions and persisted to the end of the simulations.
- *Planar retrograde flybys do not form bars or spiral arms.*

We have shown that flybys can, in principle, transform galaxy morphology. However, the precise role of flybys in bar formation requires further research to explore the strength of flyby perturbations as a function of orbit eccentricity, inclination and impact parameter,

as well as to characterize any bulk differences between this formation mechanism and one that is more secular. Since these initial simulations were purely collisionless, it is unclear how well flyby-induced bars can drive gas inflow to enhance star formation and/or fuel SMBH growth. Future work will focus on probing the interaction parameter space, including hydrodynamics, and combining results with statistics from cosmological simulations to predict bar formation rates.

We exclude bulges to maximize the effect of the flybys on each galaxy's disk. Because central mass concentrations like a stellar bulge are thought to stabilize disks against bar formation (Shen & Sellwood 2004; Athanassoula et al. 2005), the results presented can be viewed as an upper limit on the ability of flybys to form bars in disk galaxies. For a given interaction, the strength of any $m = 2$ mode can be expected to decrease with increasing bulge mass and concentration (Athanassoula et al. 2005). However, quantifying the exact effect that bulge properties have on $m = 2$ modes induced by flyby interactions will require additional simulations.

K.H-B. acknowledges the support of a National Science Foundation Career Grant AST-0847696, and a National Aeronautics and Space Administration Theory grant NNX08AG74G. Support for M.L. was provided by a National Science Foundation Graduate Research Fellowship. Supercomputing support was provided by Vanderbilt's Advanced Center for Computation Research and Education (ACCRE) and the Stampede system at Texas Advanced Computing Center (TACC) through the Extreme Science and Engineering Discovery Environment (XSEDE), which is supported by National Science Foundation grant number OCI-1053575.

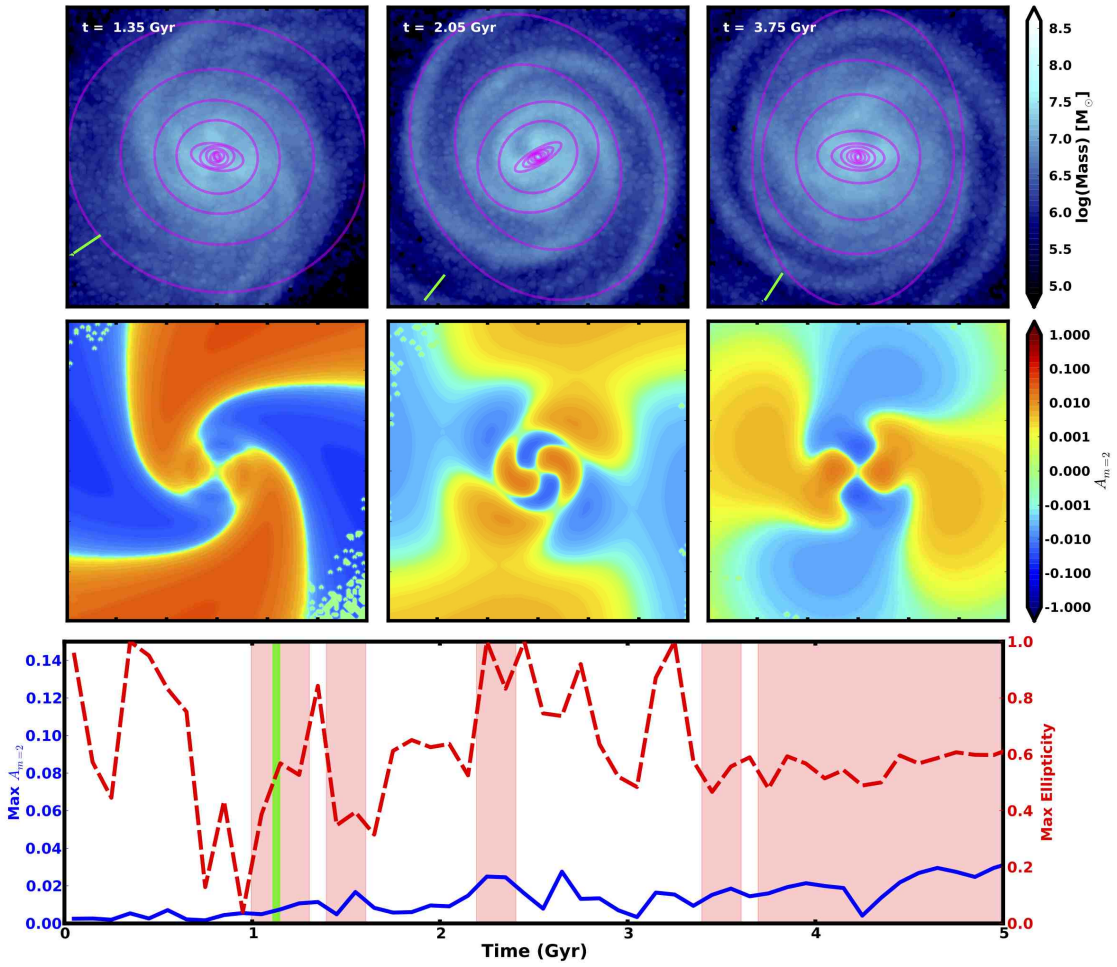

Fig. 11. 10:1 Prograde Primary. Same as Figure 10.

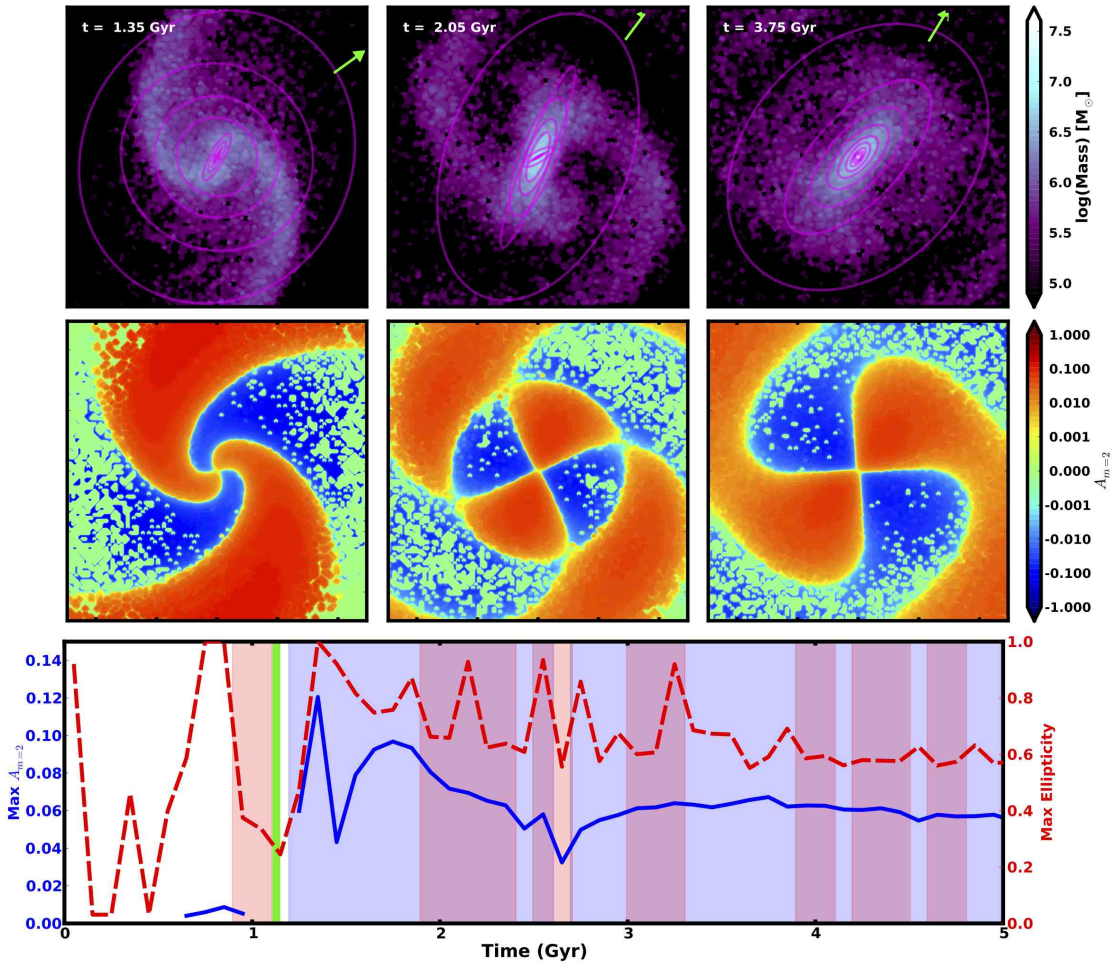

Fig. 12. 10:1 Prograde Secondary. Same as Figure 10, but zoomed in on the central 10 kpc.

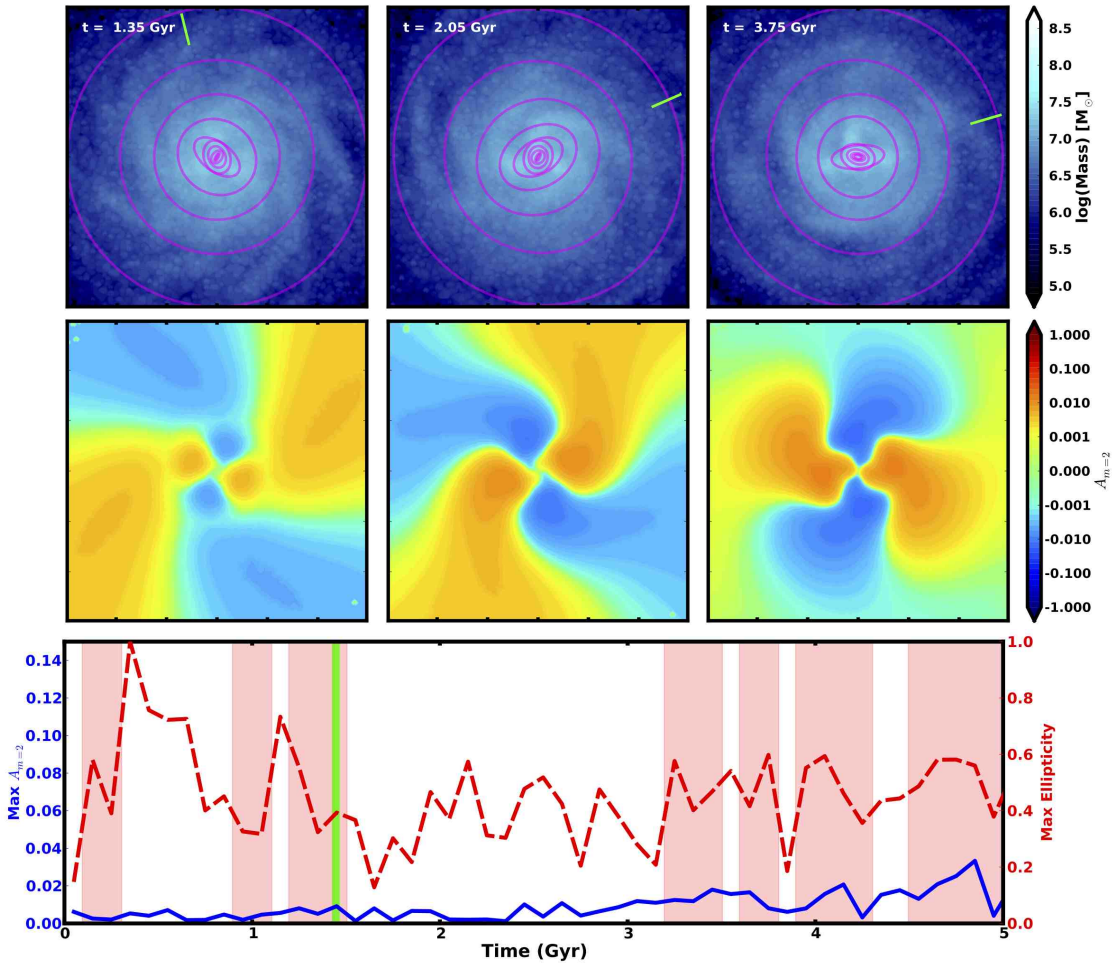

Fig. 13. 1:1 Retrograde Primary. Same as Figure 10.

Chapter III

CAN A SATELLITE GALAXY MERGER EXPLAIN THE ACTIVE PAST OF THE GALACTIC CENTER?

The following work was published in the Monthly Notices of the Royal Astronomical Society (Lang et al. 2013) and is reprinted below in its entirety.

Can a Satellite Galaxy Merger Explain the Active Past of the Galactic Center?

Meagan Lang[1], Kelly Holley-Bockelmann[1,2], Tamara Bogdanović[3,4], Pau Amaro-Seoane[5,6], Alberto Sesana[5] & Manodeep Sinha[1]

[1]Department of Physics and Astronomy, Vanderbilt University, Nashville, TN, email: meagan.lang, manodeep.sinha@vanderbilt.edu

[2]Fisk University, Department of Physics, Nashville, TN, email:k.holley@vanderbilt.edu

[3]Department of Astronomy, University of Maryland, College Park, MD 20742, e-mail: tamarab@astro.umd.edu

[4]Einstein Postdoctoral Fellow

[5]Max Planck Institut für Gravitationsphysik (Albert-Einstein-Institut), D-14476 Potsdam, Germany, email: pau.amaro-seoane, alberto.sesana@aei.mpg.de

[6]Institut de Ciències de l'Espai (CSIC-IEEC), Campus UAB, Torre C-5, parells, 2$^{\rm na}$ planta, ES-08193, Bellaterra, Barcelona, Spain

Abstract

Observations of the Galactic Center (GC) have accumulated a multitude of "forensic" evidence indicating that several million years ago the center of the Milky Way galaxy was

teeming with star formation and accretion-powered activity – this paints a rather different picture from the GC as we understand it today. We examine a possibility that this epoch of activity could have been triggered by the infall of a satellite galaxy into the Milky-Way which began at the redshift of $z = 8$ and ended few million years ago with a merger of the Galactic supermassive black hole with an intermediate mass black hole brought in by the inspiralling satellite.

Key words: galaxies: interactions — Galaxy: center — Galaxy: kinematics and dynamics — Galaxy: nucleus

3.1 Introduction

There is mounting observational evidence that the epoch that ended several million years ago was marked by an unusual level of activity in the Galactic Center (GC). This is remarkable given that at the current epoch, the GC is best characterized by the quiescent and underluminous nature of Sgr A*(Genzel et al. 2010). The picture of the GC as a once powerful nucleus has begun to emerge from circumstantial observational evidence, most recently strengthened by a discovery of the "Fermi bubbles", a pair of giant gamma-ray emitting bubbles that extend nearly 10 kpc north and south of the GC (Dobler et al. 2010; Su et al. 2010). Although there are alternative steady state models for forming the bubbles (Crocker et al. 2011), the well defined shock fronts at their edges suggest an abrupt origin. Current explanations include a past accretion event onto the supermassive black hole (SMBH; Su et al. 2010; Zubovas et al. 2011), AGN jets (Guo & Mathews 2012), a nuclear starburst (Su et al. 2010), and a sequence of star capture events in the last ∼10 Myr (Cheng et al. 2011). The period of increased gamma-ray activity is consistent

with the finding that until several hundred years ago Sgr A* was orders of magnitude more X-ray luminous than it is today, as indicated by the echo in the fluorescent Fe K line emission detected in the direction of the molecular clouds in the vicinity of Sgr A* (Inui et al. 2009; Ponti et al. 2010; Terrier et al. 2010). Although we cannot be certain that the current quiescence of the GC is unusual, it appears clear that the GC experienced an active phase as recently as a few hundred years ago.

The GC is also a hotbed of star formation containing the three most massive young star clusters in the Galaxy: the Central cluster, the Arches cluster, and the Quintuplet cluster (see Figer 2008, for a review). The three clusters are similar in many respects. Each cluster contains $\sim 10^4 M_\odot$ in stars and has central stellar mass density that exceeds those measured in most globular clusters. While our current understanding of massive star and star cluster formation is incomplete, it is plausible that these clusters are all characterized by the star formation event within the past $2-7$ Myr that resulted in the formation of more massive stars (above $100 M_\odot$) than anywhere else in the Galaxy (Krabbe et al. 1995; Paumard et al. 2006). It is possible that the three clusters have a common origin and that they have formed as a consequence of a single event that triggered the flow of the copious amounts of gas into the central ~ 50 pc in the Galaxy (though see Stolte et al. 2008, for a scenario in which the Arches cluster forms at the intersection of X1/X2 gas orbits in the inner Galaxy).

On even smaller scales, the existence of massive and young stars in the Central cluster, well within the central parsec, is especially puzzling. Although a view that the young stellar population formed in situ seems to be prevailing, it is still a mystery how the starforming clouds that gave birth to this population escaped tidal disruption by the

central SMBH (Paumard et al. 2006). A clue in favor of the in-situ formation is that most young, massive stars seem to inhabit one or more disk-like structures, pointing to their birth in a dense accretion disk (Bartko et al. 2010). Star formation in a gaseous disk also provides a natural explanation for the cuspy distribution of the young stars. In order for starforming clumps to withstand tidal forces in the inner parsec of the GC their densities need to be in excess of $10^{11}\,\mathrm{cm}^{-3}$, at least five orders of magnitude higher than the average density of molecular clouds in the GC (Figer et al. 2000). Such densities can only be achieved through highly compressive events (Figer 2008) and it is plausible that both the inflow of large amounts of gas into the GC and its shocking and compression have been caused by a common culprit. Both phenomena are found to arise as consequences of galactic mergers (Noguchi 1988; Barnes & Hernquist 1991, 1992, 1996; Mihos & Hernquist 1996; Hopkins & Quataert 2010) making this a possibility worth examining.

Further evidence that the MW has recently survived a dramatic event comes from the distribution of late-type stars in the GC. While the early-type stellar distribution appears to be cuspy (Genzel et al. 2003; Paumard et al. 2006; Buchholz et al. 2009; Do et al. 2009; Bartko et al. 2010), there seems to be a distinct lack of late-type stars. This evidence is based on number counts of spectroscopically identified late-type stars brighter than magnitude $K = 15.5$ within the sub-parsec region about Sgr A*. The best fits of the inner density profile for the late-type stellar population seem to favor power-laws with slopes of $\gamma < 1$ and even allow the possibility of a core with $\gamma < 0$, with the stellar density decreasing toward the center (Buchholz et al. 2009; Do et al. 2009; Bartko et al. 2010). At this stage, the evidence for a deficit of late-type stars is compelling, however there are still significant uncertainties in the density profile: the population of stars on which this inference

has been made are luminous late-type giants that comprise only a small fraction of the underlying stellar density of the late-type population. Regardless of the precise slope, however, the distribution of the late-type population is contrasted by the steeply rising density distribution of early-type stars.

Possible mechanisms that could create a core in the distribution of late-type stars have been discussed by Merritt (2010) and include 1) stellar collisions that strip red giants of their envelopes such that they are under-luminous, 2) destruction of stars on orbits that pass close to the SMBH in a triaxial nucleus, 3) inhibited star formation near the SMBH at the time when the late-type population was formed, and 4) ejection of stars by a massive black hole binary. In light of the other evidence that points to a discrete event in the recent history of the GC, it is interesting to revisit the latter mechanism.

In giant elliptical galaxies, the existence of cores is often attributed to ejection of stars by an inspiralling binary SMBH (Merritt & Cruz 2001; Faber et al. 1997; Ferrarese et al. 2006; Milosavljević & Merritt 2001) and possibly due to gravitational wave recoil after binary coalescence (Boylan-Kolchin et al. 2004; Gualandris & Merritt 2008). The prediction of these models is that the central stellar mass deficit (traced by the stellar light) is proportional to the mass of the central black hole, $M_{\rm def} \propto M_\bullet$ (Graham 2004; Hopkins & Hernquist 2010). This correlation is interesting in view of the observed dichotomy between ellipticals with cores and those with the extra central light: core light deficit was found to correlate closely with $M_\bullet$ and stellar velocity dispersion σ, in agreement with the theoretical predictions (Milosavljević & Merritt 2001; Gualandris & Merritt 2008), however, the extra light does not (Kormendy & Bender 2009). An explanation of these phenomena offered by Kormendy & Bender (2009) is that the extra light ellipticals were made in wet mergers

with starbursts, where stars formed from gas leftover after the merger, while core ellipticals were created in dry mergers. In galaxies with excess light, the newly formed population of stars fills the core left in the distribution of the older population to form a steep cusp, thus giving rise to characteristic differences in the two stellar populations that may be mirrored in the MW GC.

Because studies of the light excess and deficit in elliptical galaxies focus on major mergers, the scenario seems less relevant for a disk-dominated system like the Milky Way, which may have never experienced a major merger (Gilmore et al. 2002). A minor merger of the SMBH with an intermediate mass black hole (IMBH) however cannot be ruled out. The presence of an IMBH in the Galactic center has been previously considered as a possible vehicle for delivery of young stars into the GC (Hansen & Milosavljevi 2003), a mechanism for creation of hypervelocity stars (Baumgardt et al. 2006), and for the growth of the SMBH (Zwart et al. 2006). Indeed, the possibility that an IMBH with mass $\lesssim 10^4 M_\odot$ is still lurking in the inner parsec of the GC cannot be totally excluded based on observations (Hansen & Milosavljevi 2003; Genzel et al. 2010).

In light of the new observational evidence, which supports the notion that few to 10 Myr ago was a special period in the life of Sgr A*, as indicated by the relatively recent episode of star formation and increased energy output, we revisit the possibility that a minor merger could have triggered this epoch of enhanced activity. We suggest that the cumulative observational evidence favors the minor merger hypothesis relative to the scenarios that propose a steady state evolution or passive relaxation of the GC region. We present a theoretical scenario for one such minor merger in § 2 and discuss the implications in § 3.

3.2 Milky Way – Satellite Merger Scenario

Here we examine the viability of the following scenario: at redshift ∼8, a primordial satellite galaxy with a central IMBH begins to merge with a young Milky Way. As the satellite sinks toward the GC under the influence of dynamical friction it is tidally stripped and its orbit gradually decays toward the Milky Way disk plane (Quinn & Goodman 1986; Callegari et al. 2011). The satellite perturbs previously stable gas clouds in the inner Milky Way disk, driving gas inflow (Noguchi 1988; Barnes & Hernquist 1991, 1996; Hopkins & Quataert 2010) and compressing the gas to densities exceeding those necessary for massive star formation near the GC (Mihos & Hernquist 1996; Hopkins & Quataert 2010). The satellite galaxy is expected to be largely disrupted by the time it reaches the GC, leaving the IMBH spiraling in a dense gaseous and stellar environment. In the context of this scenario we hypothesize that the IMBH reached the central parsec on the order of ∼10 Myr ago. A fraction of perturbed gas that did not form stars accretes onto the Milky Way's SMBH (Hopkins & Quataert 2010), injecting massive amounts of energy into the surrounding medium and giving rise to the Fermi bubbles (Su et al. 2010; Zubovas et al. 2011). Once gravitationally bound, the IMBH-SMBH binary orbit tightens via three-body interactions with surrounding stellar background, scouring the old stellar population to form a central core (Merritt 2010). Finally, the binary coalesces after emitting copious gravitational radiation (Peters & Mathews 1963).

In the context of this hypothetical scenario we use the new GC observations to constrain the initial masses of the satellite and Milky Way galaxies ($M_{\rm sat}$ and $M_{\rm MW}$), the mass deficit in the late-type stellar population ($M_{\rm def}$), the IMBH mass ($M_{\rm IMBH}$), as well as

the amount of gas inflow into the GC triggered by the inspiral of the satellite galaxy. The properties of the satellite bound to reach the inner disk of the Milky Way and deliver its IMBH to the GC must satisfy several criteria: 1. it should be light enough not to disrupt the Galactic disk, 2. it should be sufficiently massive in order for the dynamical friction to operate efficiently and deliver it to the GC within a Hubble time, and 3. its potential well should be sufficiently deep to sustain tidal stripping by the Milky Way. We therefore focus on constraining the most plausible scenario given the current understanding of the processes involved.

3.2.1 Properties of the Progenitor Milky Way

Beginning the merger at high redshift is advantageous in three respects. First, at this early epoch, it is reasonable to assume that the proto-Milky Way was surrounded by primordial satellite galaxies capable of housing a central seed black hole (e.g., Ricotti & Gnedin 2005; Gnedin & Kravtsov 2006; Wise & Abel 2008; Micic et al. 2011). Second, at this stage in its growth, the Milky Way would have been smaller, less massive, and more gas-rich than it is today, thus decreasing the time required for the satellite to sink to the galactic center via dynamical friction. Finally, the orbits of infalling satellites are more radial at high redshift, which further shortens the merger timescale (Wetzel 2011).

To determine the properties of the Milky Way at this epoch, we assume that it grows according to the exponential halo model from McBride et al. (2009):

$$M(z) = M_0(1+z)^{\beta}\exp\left(-\ln 2\frac{z}{z_f}\right), \tag{3.1}$$

where M_0 is the current halo mass and z_f is the formation redshift, defined as the redshift at which the halo has grown to half its current mass. Adopting the properties for the Milky Way at $z_f = 1$ as $M_0 = 2 \times 10^{12} M_\odot$ and $\beta = 0.25$, the Milky Way's mass at $z = 8$ can be estimated to be $M_{\rm MW} = 7 \times 10^9 M_\odot$. Studies of cosmological N-body simulations have found that at the redshift considered, the concentration of dark matter halos is very weakly dependent on mass (Zhao et al. 2003; Gao et al. 2008; Klypin et al. 2011). Following the methods outlined by Prada et al. (2012), we find that at $z = 8$ a halo of this mass will have a concentration of $c(z = 8) \sim 6$. The halo virial radius in a LCDM cosmology is defined as the radius where the mean enclosed density is 96 times the critical density of the universe, $\rho_{\rm crit}$. With the definition of $\rho_{\rm crit}$:

$$\rho_{\rm crit} = \frac{3H_0^2}{8\pi G \left[\Omega_\Lambda + (1+z)^3 + \Omega_m\right]}, \tag{3.2}$$

where $\Omega_\Lambda = 0.73$ is the fraction of energy density in the universe in vacuum energy, while $\Omega_m = 0.27$ is the fraction of energy density in the universe in matter, and z is the redshift. We find that the progenitor MW halo has a virial radius of $\sim$ 6 kpc. This implies the progenitor Milky Way halo will have a density at 10 pc of $30 M_\odot/{\rm pc}^3 \sim 10^6 \rho_{\rm crit}$.

It is important to note that while Eqn. 3.1 assumes a single, smoothly growing Milky Way halo, at these high-redshifts, mergers with other massive halos are very common, and the halo grows in a step-wise fashion. (Diemand et al. 2007). Indeed, the entire picture of a single, virialized progenitor Milky Way halo is not strictly correct, and the 'Milky Way' at this redshift is more likely a set of several halos, many of which have not yet decoupled from the Hubble flow to allow turnaround and collapse into a single virialized structure.

Consequently, our assumption of a virialized NFW halo at the accretion redshift ($z = 8$) must be recognized as an approximation made due to the limits of a semi-analytic approach.

3.2.2 Finding the Culprit Satellite

Broadly, we identify possible culprit satellites by integrating the orbits of infalling halos within an analytic, but evolving Milky Way potential. As both the satellite and Milky Way evolve, we search for the satellites that reach the Inner Lindblad Resonance (ILR) at 150 pc roughly 10 Myr ago after losing over 95% of its initial orbital angular momentum. Of the satellites that survive until they plunge through the ILR, we preferentially select those that retain enough mass to perturb the gas there. The culprit satellite is characterized by the mass, radius and concentration, as well as the energy, angular momentum, infall radius and merger redshift of the orbit. We elaborate on the procedure below.

We adopt a merger redshift of ~ 8. In order to deliver the IMBH to the GC a mere $2-7$ Myr ago, the proposed merger redshift implies that the satellite orbit decayed over a timescale of about 13 Gyr. At such a high redshift, the IMBH and satellite had very little time to evolve before being accreted by the Milky Way, making the pair a "fossil" of the dark ages before reionization (Ricotti & Gnedin 2005; Gnedin & Kravtsov 2006).

We rely on cosmological N-body simulations to constrain the initial conditions of the orbit. These inform us that at the present epoch, satellites are preferentially accreted on very eccentric orbits, with a distribution peak at about $e = 0.85$ (Benson 2005; Wang et al. 2005; Zentner et al. 2005; Khochfar & Burkert 2006; Ghigna et al. 1998; Tormen et al. 1997). At higher redshifts the satellite orbits are characterized by even higher eccentricities, albeit, in both cases the distribution peaks are broad. Seemingly independent of redshift,

a typical satellite is accreted at the virial radius with a total velocity, $|\vec{v}_{\rm sat}| = 1.15 v_{\rm vir}$ ($v_{\rm vir}$ is the circular velocity at the virial radius of the primary galaxy) that marks it as barely bound (Benson 2005; Wetzel 2011). Motivated by these results, we select an orbit that has $|\vec{v}_{\rm sat}| = 1.15 v_{\rm vir}$ at the virial radius of the primary and an eccentricity of 0.9, consistent with expectations for the eccentricity distribution peak at $z = 8$ (Wetzel 2011).

Starting with the above total velocity and eccentricity, we calculate the orbital decay for a range of satellite masses placed at the virial radius of the primary. For a given initial position at the virial radius, the azimuthal and radial components of the satellite's initial velocity within the orbital plane are calculated in terms of the eccentricity (e) and total velocity ($|\vec{v}_{\rm sat}|$) as:

$$v_\phi = \frac{v_{vir}}{|\vec{v}_{\rm sat}|}\sqrt{\frac{G M_{\rm MW}}{r_{\rm vir}}(1-e^2)} \text{ and } v_r = \sqrt{|\vec{v}_{\rm sat}|^2 - v_\phi^2}. \tag{3.3}$$

We adopt an analytic model of the Milky Way that includes a central SMBH, Miyamoto-Nagai thin disk (Miyamoto & Nagai 1975), a spherical Hernquist bulge (Hernquist 1990), and an NFW halo (Navarro et al. 1997). To mimic a young Milky Way, we use Eqn. 3.1 to set the halo mass. We set the virial radius using the mass and the critical density at the starting redshift in Eqn. 3.2, and we initialize the concentration using Prada et al. (2012). We assume that the mass and size of the baryonic components change in the same way as the halo does; this is not true in detail, but allows us to convert the known present-day Milky Way parameters to the starting redshift. Our current Milky Way mass model is similar to analytic models best-fit to rotation curve data (e.g. Widrow & Dubinski 2005; Dehnen & Binney 1998) $z = 0$ disk mass is $5 \times 10^{10} M_\odot$, the disk scale length is 3 kpc

and, and the disk scale height is 300 pc.For the bulge, we set a current epoch bulge mass of $8 \times 10^9 M_\odot$ and scale length of 0.7 kpc.

We integrate the orbits using a fourth-order Runge-Kutta method to step the satellite's position and velocity forward in time. At each timestep, we adjust the analytic Milky Way model using the method described above. We calculate the acceleration of the satellite due to this evolving analytic potential, and we include Chandrasekhar dynamical friction (Chandrasekhar 1943), as well as mass loss from the satellite due to tidal stripping and disk shocks. The acceleration due to dynamical friction is calculated in the uniform density limit as

$$\begin{aligned} \left(\frac{d\vec{v}_{\rm sat}}{dt}\right)_{\rm fric} &= -\frac{4\pi \ln\Lambda G^2 M_{\rm sat}\rho_{\rm MW}}{|\vec{v}_{\rm sat}|^3} \times \cdots \\ &\quad \times \left[\mathrm{erf}(\chi) - \frac{2\chi}{\sqrt{\pi}} e^{-\chi^2}\right] \vec{v}_{\rm sat}, \end{aligned} \tag{3.4}$$

where $M_{\rm sat}$ is the mass of the satellite, $\rho_{\rm MW}$ is the density of the Milky Way at the satellite's position, $\ln\Lambda = \ln\left[1 + (M_{\rm MW}/M_{\rm sat})^2\right]$ is the Coulomb logarithm, $\chi = |\vec{v}_{\rm sat}|/\sqrt{2}\sigma$, and $\sigma = \sqrt{GM_{\rm MW}/2R_{\rm MW}}$ is the average velocity dispersion of the Milky Way halo.

At each step in the orbit, we calculate the local density of the Milky Way and we tidally strip the satellite to the Roche radius, where the density of the satellite is equal to the Milky Way background. We also model mass loss from disk shocking by removing

$$\Delta M_{\rm shock} = \frac{5}{3}\frac{4}{GM_{\rm sat}v^2_{\rm sat,z}}\left(\frac{dv_{\rm sat,z}}{dt}\right)^2_{\rm disk} \tag{3.5}$$

from the satellite's mass each time it passes through the Milky Way disk (Gnedin & Ostriker 1997). We neglect the stellar component of the satellite, since the baryon content of such low mass satellites is relatively uncertain, but likely to be very small (Gnedin 2000; Simon & Geha 2007; Ricotti et al. 2008).

We find that the most likely culprit is a satellite with a mass of $M_{\rm sat} \approx 2 \times 10^8 M_\odot$. Modeling the satellite dark matter profile as an NFW halo, its corresponding concentration parameter at this redshift is about 6 (Prada et al. 2012), making the satellite's central density within the inner 10 pc $\sim 10 M_\odot/{\rm pc}^3 \sim 4 \times 10^5 \, \rho_{crit}$ or $\sim 2 \times 10^4$ times the Milky Way's density at the virial radius. Including an IMBH in our satellite model would deepen its central potential and could aid in delivering the satellite core to the center of the MW intact, although we did not include this effect in our calculations.

By the time the satellite has reached the inner 100 pc, it will have lost most of its mass, with $\sim 2 \times 10^5 M_\odot$ remaining. Without direct hydrodynamic simulations, it is difficult to say how much damage this IMBH-embedded satellite core could do to the gas-rich inner Milky Way. In general, we expect the satellite to perturb the gas in the galactic center, torquing it and transporting angular momentum through narrow resonances (Goldreich & Tremaine 1979); the classical rate of gas inflow from this process is proportional to the strength of the perturbation squared. However, when the system has a significant asymmetric perturbation, the orbits begin to cross one another and gas piles up in shocks (Papaloizou & Pringle 1977). In this case, the radial inflow rate of gas from a global perturbation is linearly proportional to the strength of perturbation (Hopkins & Quataert 2011), and numerical simulations find the shocks induced by even a few % perturbation can destabilize the gas and drive gas inflow (Barnes & Hernquist 1991, 1996; Mihos & Hernquist 1996;

Hopkins & Quataert 2010). To estimate the perturbation a $\sim 2 \times 10^5 M_\odot$ satellite core could exert on the gas accumulated in a ring at the Inner Lindblad Resonance (ILR) of the Milky Way, we refer to Vesperini & Weinberg (2000), which explores the perturbation strength induced by galaxy flyby encounters. Using linear perturbation theory, Vesperini & Weinberg (2000) find that a flyby with a mass ratio of 10 and a pericenter at the half-mass radius will induce a strong perturbation in the density of the primary galaxy of order unity. Since the mass ratio of the inner Milky Way ($\sim 10^8 M_\odot$) to the satellite remnant is 1000 (Lindqvist et al. 1992), we expect a perturbation of the order $|a| \sim 0.01$ in the surface density. The linear relationship between gas inflow and perturbation amplitude derived by Hopkins & Quataert (2011),

$$\frac{dM_{\rm gas}}{dt} = |a|\Sigma_{\rm gas} R^2 \Omega, \tag{3.6}$$

can then be used to gauge the expected amount of gas inflow. Setting the perturbation amplitude to $|a| \sim 0.01$, the radius to $R = 150$ pc (ILR), the rotation frequency to $\Omega(R) = v_{circ}(R)/R = 0.62$ Myr^{-1} (Stark et al. 2004), and the gas surface density to $\Sigma_{\rm gas} = 500 M_\odot/{\rm pc}^2$ based on observations of other barred galaxies (Jogee et al. 2005) and of the molecular ring in the MW GC (Molinari et al. 2011), yields a gas inflow rate of $\sim 7 \times 10^4 M_\odot$/Myr. Assuming this inflow rate over ~ 10 Myr, we find that this satellite should be able to drive a net inflow of $\sim 10^6 M_\odot$ of gas from the ILR.

3.2.3 Late-Type Stellar Mass Deficit and IMBH Mass

If the core in the distribution of late-type stars at the GC (Buchholz et al. 2009; Do et al. 2009) was scoured out by an IMBH-SMBH binary, the amount of stellar mass missing

from the GC can be used to constrain the mass ratio of the black hole binary (Milosavljević & Merritt 2001; Gualandris & Merritt 2008). To determine this mass deficit we compare the stellar distribution inferred from observations with that expected for a dynamically relaxed system without a core. In terms of the number density of the late-type stellar population, the core can be represented by a broken power law

$$n_f(r) = n_0 \left(\frac{r}{r_0}\right)^{-\gamma_i} \left[1 + \left(\frac{r}{r_0}\right)^{\alpha}\right]^{(\gamma_i - \gamma)/\alpha}, \tag{3.7}$$

with $n_0 = 0.21$ pc^{-3}, $r_0 = 0.21$ pc, $\gamma = 1.8$, $\gamma_i = -1.0$, and $\alpha = 4$ (Merritt 2010). We adopt this description in our analysis but note that in presence of strong mass segregation the slopes can be steeper (Alexander & Hopman 2009; Preto & Amaro-Seoane 2010; Amaro-Seoane & Preto 2011). The observed distribution of stars outside of the 0.21 pc core radius is consistent with the Bahcall-Wolf profile ($\propto r^{-1.75}$, Bahcall & Wolf 1976) of a relaxed system as it would have existed prior to scattering by the IMBH-SMBH binary. We model the initial stellar cusp by extending the $r^{-1.8}$ profile to smaller radii:

$$n_i(r) = n_0 \left(\frac{r}{r_0}\right)^{-\gamma}. \tag{3.8}$$

Assuming that the mass density profiles *before* and *after* the creation of the core are proportional to equations (3.8) and (3.7) respectively, we calculate the mass deficit as the integrated difference between the initial and final (observed) profiles. We normalize the profile given by Eqn. 3.7 such that integrating it over the inner parsec yields $1.0 \pm 0.5 \times 10^6 M_\odot$, the mass determined by Schödel et al. (2009), and obtain $M_{\rm def} \approx 2 \times 10^5 M_\odot$.

N-body merger simulations studying the relationship between the ratio of total stellar mass ejected to binary mass, $M_{\rm def}/(M_1 + M_2)$, and binary mass ratio, $q = M_1/M_2$, have not yet been carried out for the mass deficit calculated here. In order to relate the two we use a semi-analytic formalism describing the interaction of massive black hole binaries with their stellar environment (Sesana et al. 2008) to place the upper and lower limits on the mass of the IMBH based on $M_{\rm def}$ inferred from observations.

It has been shown by numerical simulations (Baumgardt et al. 2006; Matsubayashi et al. 2007) and semianalytic models (Sesana et al. 2008), that an IMBH inspiralling in a stellar cusp surrounding a central SMBH starts to efficiently eject stars at a separation a_0, where the stellar mass enclosed in the IMBH orbit is of the order of $2M_2$. The ejection of bound stars causes an IMBH orbital decay of a factor of ≈ 10, excavating a core of radius $r_0 \approx 2a_0$ in the central stellar cusp, resulting in a mass deficit about $3M_2$ (see Sesana et al. 2008, for details). Such orbital decay is in general insufficient to bring the IMBH in the efficient gravitational wave (GW) emission regime, unless its eccentricity grows to > 0.9 during the shrinking process. It is also the case in this picture that the mass of the inspiralling IMBH inferred for a given mass deficit strongly depends on the eccentricity evolution of its orbit. In what follows, we consider both the high and low orbital eccentricity scenario and use them to place a bound on the plausible range of IMBH masses.

If the eccentricity grows efficiently, the IMBH depletes the central cusp, forms a core of a size $\approx 2a_0$, and merges due to GW emission on a time scale of only $1 - 10$ Myr (Sesana et al. 2008). For a stellar distribution described by an isothermal sphere outside of the radius of influence of the SMBH, $a_0 = 2q^{4/5}$pc. Adopting the core radius of $r_0 = 2a_0 = 0.21$ pc, we find $q = 0.02$, and an upper limit on the mass of the IMBH, $M_2 = 8 \times 10^4 M_\odot$. In this

case, the mass evacuated from the stellar cusp by the IMBH is of the order of $3M_2$ (Sesana et al. 2008), i.e., $\approx 2.5 \times 10^5 \mathrm{M}_\odot$, consistent with the stellar mass deficit measurement in the GC.

Alternatively, if the IMBH eccentricity does not grow significantly during the bound cusp erosion, further scattering of stars replenishing the binary loss cone is needed in order to evolve from separation of a_0 to the GW regime. Therefore, a circular orbit regime can be used to establish a lower limit on the mass of the IMBH, for a given mass deficit indicated by observations. We assume that in this case both r_0 and $M_{\rm def}$ created in the cusp erosion phase are small (we justify this assumption below). In this scenario, the final r_0 and $M_{\rm def}$ are reached as a consequence of the diffusion of the stars from the edge of the small core into the loss cone of the binary. The ejections of each star carry away an energy of the order $(3/2)G\mu/a$ (Quinlan 1996), where $\mu = M_1\, M_2/M$. We compute $M_{\rm def}$ by imposing:

$$\frac{3}{2}\frac{G\mu}{a} dM_{\rm def} = \frac{GM_1M_2}{2} d\frac{1}{a} \tag{3.9}$$

to get

$$M_{\rm def} = \frac{M_1 + M_2}{3} \ln\frac{a_i}{a_f}, \tag{3.10}$$

where $a_{\rm i}$ is the hardening radius of the binary (radius at which the scattering of unbound stars becomes effective) and $a_{\rm f}$ is the separation at which the GW emission becomes efficient. Using equations (19) and (20) in Sesana (2010) to express $a_{\rm i}$ and $a_{\rm f}$, it follows that,

$$M_{\rm def} = \frac{M_1 + M_2}{3} \ln\frac{500\, q^{4/5}}{F(e)^{1/5}}, \tag{3.11}$$

where $F(e) = (1-e^2)^{-7/2}(1+73/24\,e^2+37/96\,e^4)$. Assuming for the purpose of this estimate that the binary remains circular throughout its evolution and imposing $M_{\rm def} = 2\times10^5 M_\odot$, we find $q = 5\times10^{-4}$ and a lower limit on the mass of the IMBH is $M_2 = 2\times10^3 M_\odot$ [1]. An IMBH of such mass, would excavate a core of ≈ 0.01 pc, causing a mass deficit of $\sim 3M_2 = 6\times10^3 M_\odot$ in the bound scattering phase and thus, justifying our earlier assumption that the diffusion of stars into the loss cone is the primary process that shapes the properties of the core in this case. Note that in the circular orbit scenario the time scale for the inspiral of the IMBH towards the GW regime is determined by the unknown rate of diffusion of the stars into the loss cone of the binary. Hence, depending on the time scale of relaxation processes this process could in principle lead to the IMBH-SMBH binary "hangup", i.e., a long lived (> 1 Gyr) binary configuration at separation $< r_0$ – tantamount to the classical "final parsec" problem (Begelman et al. 1980). It is however possible that the binary will not stall in our specific case. The galactic center in this phase will be described by a strongly perturbed, non-axisymmetric potential which allows stars to scatter into the loss cone efficiently (Merritt & Poon 2004; Berczik et al. 2006; Perets & Alexander 2008; Khan et al. 2011). Moreover, the orbit will occur in a relatively gas-rich environment, which can further aid the decay of the binary (Escala et al. 2005; Dotti et al. 2007; Cuadra et al. 2009). Finally, any extra stars brought in by the satellite would help the binary decay (see Miller 2002). Even under the assumption of a circular orbit, an efficient coalescence can occur on a timescale of 10 Myr.

[1] Both numerical simulations and semi-analytic models however suggest that the eccentricity in the cusp erosion phase grows to > 0.9, in which case $F(e) > 1000$ and $q > 5\times10^{-3}$, i.e., $M_2 > 2\times10^4 M_\odot$.

This analysis suggests that the observed mass deficit and core size are consistent with the IMBH mass in the range $2\times10^3 M_\odot < M_2 < 8\times10^4 M_\odot$, whereas the efficient eccentricity growth found in N-body simulations and semi-analytic models favor $M_2 \gtrsim 10^4 M_\odot$. Within this range, the time scale for the IMBH to create a core and merge with the SMBH can be as short as few Myr. On the other hand, a possibility that an IMBH may be still be lurking in the GC is not completely ruled out. We discuss the consequences of the latter scenario in the context of the observational constraints on the presence of a second black hole in the Galactic center in § 3.3.

It is useful to consider whether a satellite galaxy with an initial mass of $M_{\rm sat} \sim 2 \times 10^8 M_\odot$ can host a $\gtrsim 10^4 M_\odot$ IMBH. While there are no observational constraints for galaxies or black holes of this mass range, there are three leading theories for IMBH formation at high redshift: 'direct collapse' of metal-free, low angular momentum gas into a $10^3 - 10^6 M_\odot$ black hole (Loeb & Rasio 1994; Begelman et al. 2008), an unstable supermassive star that collapses into a $10^2 - 10^5 M_\odot$ black hole (Colgate 1967; Quinlan & Shapiro 1987; Baumgarte & Shapiro 1999), or a Population III star, which would leave behind seed black holes of $\sim 1 - 10^3 M_\odot$ between redshift 30−12 (Madau & Rees 2001; Bromm et al. 2002; Wise & Abel 2008; Clark et al. 2011). Even if the IMBH in our satellite started as a low mass Pop III seed in a somewhat turbulent environment with a mass of $\sim 5 M_\odot$ (Clark et al. 2011), it is plausible that it would reach the IMBH mass proposed here through a combination of gas accretion and black hole mergers (Holley-Bockelmann et al. 2010). In such a satellite galaxy, it would require less than one percent of the gas to accrete onto a low mass seed to form the IMBH $\gtrsim 10^4 M_\odot$.

Note that the massive seeds produced in a direct collapse typically favor more massive halos than the one we have proposed as our culprit. This is because metal-free gas collapses most efficiently in halos with $T_{\rm vir} > 10^4$ K, corresponding to $M_{\rm vir} > 10^8 M_{\odot}[(1+z)/10]^{3/2}$ (Bromm & Loeb 2003). In the context of the merger hypothesis choosing a slightly more massive satellite would push the accretion redshift closer to the present day, and as long as the resulting satellite merger is still a minor one, this does not significantly affect the outcome of our scenario.

3.2.4 Inflow of Gas and Gamma-ray Bubbles

As noted in § 3.2.1 the inspiral of a satellite galaxy can cause the inflow of a significant amount of gas towards the center of the Galaxy (Noguchi 1988; Barnes & Hernquist 1996; Mihos & Hernquist 1996; Cox et al. 2008). One fraction of this gas could have given rise to the star formation in the Central, Arches, and Quintuplet clusters, which marked the epoch between 2−7 Myr ago in the central 50 pc of the Milky Way. All three clusters contain some of the most massive stars in the Galaxy and have inferred masses of $\sim 10^4 M_{\odot}$ (Figer 2008). Assuming a "standard" star formation efficiency of 10% (Rownd & Young 1999), it follows that the amount of gas necessary to produce the stellar population of the three clusters is a few $\times 10^5 M_{\odot}$. Note that a sequence of strongly compressional events during the satellite-Milky Way merger could have given rise to a higher efficiency of star formation (Di Matteo et al. 2007), in which case the estimated mass of the gas represents an upper limit.

In this merger scenario, the remainder of the perturbed gas that did not form stars would be channeled towards the central parsec (Loose et al. 1982), and the fraction that is accreted into the SMBH could drive the energetic outburst of several Myr ago. The far-IR

and millimeter observations indicate that $\sim 10^4 M_\odot$ of the molecular gas continues to reside in the circumnuclear disk within the central ~ 1.5 pc of the Galaxy (see Genzel et al. 2010, for review and references therein). The maximum amount of the remnant molecular gas that has not been accreted onto the SMBH can also be estimated based on its expected gravitational effect on the orbits of the stars residing within the inner 0.5 pc. In this case, the requirement for stability of the stellar disc over its lifetime of 6 Myr poses a constraint on the mass of the molecular torus of $< 10^6 M_\odot$ (Šubr et al. 2009).

On the other hand, the recent discovery of the two large gamma-raySu2010a bubbles extending from the GC above and below the galactic plane are compelling evidence of a relatively recent period of intense activity in the now quiet GC. The gamma-ray bubbles exhibit several striking properties: they are perpendicular and symmetric with respect to the plane of the Galaxy, have nearly uniform gamma-ray brightness across the bubbles, and well defined sharp edges (Dobler et al. 2010; Su et al. 2010). The gamma-ray emission from the bubbles is characterized by the hard energy spectrum and is most likely to originate from the inverse Compton scattering of the interstellar radiation field on the cosmic ray electrons – the same population of electrons deemed responsible for the diffuse synchrotron microwave radiation detected by the WMAP (Finkbeiner 2004; Dobler & Finkbeiner 2008). The sharp edges of the Fermi bubbles are also traced by the X-ray arcs discovered in the ROSAT maps (Snowden et al. 1997), suggested to be the remnants of shock fronts created by the expanding bubbles (Su et al. 2010; Guo & Mathews 2012).

The morphology, energetics, and emission properties of the Fermi bubbles favor the explanation that bubbles were created in a strong episode of energy injection in the GC in the last ~ 10 Myr that followed an accretion event onto the SMBH (Su et al. 2010). Simulations

by Guo & Mathews (2012) indicate that the bubbles could have been formed by a pair of bipolar jets that released a total energy of $1-8\times10^{57}$ erg over the course of $\sim$0.1$-$0.5 Myr between 1 and 2 Myr ago. This explanation for the Fermi bubbles implies that $\sim 10^4 M_\odot$ of material must have been accreted onto the SMBH at nearly the Eddington rate, assuming the accretion efficiency of 10% (Shakura & Sunyaev 1973; Davis & Laor 2011). Based on the range of models explored by Guo & Mathews (2012) it is possible to estimate that the amount of mass processed in such jets (i.e., the mass of the gas that fills the jet cavities) is as small as $30M_\odot$ and as large as $3\times10^5 M_\odot$.

This estimate, together with the gas that formed stars, the gas accreted onto the SMBH and the gas processed by the jets allows us to put a constraint on the total gas inflow into the central $\sim$ 50 pc of the Galaxy of $\lesssim 10^6 M_\odot$, consistent with the amount expected from the perturbation analysis of the stability of the ILR gas in the Milky Way.

3.3 Discussion

3.3.1 How rare are satellite merger events?

We propose that the timeline began about 13 Gyr ago, when the proto Milky Way accreted a small satellite dark matter halo at the time when their halos were physically closer and less massive. The satellite orbit decayed slowly and only reached the GC a few million years ago, after having been stripped of most its mass. The thinness of the Milky Way disk has often been used as an argument against a recent minor merger (Quinn et al. 1993; Sellwood et al. 1998; Velazquez & White 1999); however, the proposed satellite is so minor, particularly by the time the orbit decays to 10 kpc, that the thin disk could have survived

unscathed (Toth & Ostriker 1992; Walker et al. 1996; Taylor & Babul 2001; Hopkins et al. 2008, 2009). Using the Extended Press-Schechter formalism (Bond et al. 1991; Bower 1991; Lacey & Cole 1993; Parkinson et al. 2007), we estimate that a typical Milky Way mass halo will undergo an average of ~ 1700 satellite accretions in the $M_{\rm sat} = 10^7 - 10^9 M_\odot$ range from $z = 8 - 0$. However, about half of these accretions occur after $z = 1$ — and are unlikely to have made it to the GC by $z = 0$.

Figure 14 illustrates a realization of the current distribution of accreted satellites in the mass range $M_{\rm sat} = 10^7 - 10^9 M_\odot$. We used Sinha & Holley-Bockelmann (2012) to define the number of accreted halos from $z = 10 - 0$ for this mass range and set the energy and angular momentum distributions at each redshift using the expressions $7 - 9$ in (Wetzel 2011). As in section 2, we integrated orbits of the satellites from the accretion epoch to the present day, scaling the Milky Way mass and size to the redshift of accretion using Eqn. 3.1. Figure 14 shows the inner 40 kpc of the current-day Milky Way; approximately 85% of the accreted satellites are at separations larger than 40 kpc, and only 5 reached the GC and merged with the SMBH. We estimate the surface brightness of the satellites assuming that the baryons are confined to a radius within the dark matter halo ten times smaller than the satellite virial radius. We infer the initial star fraction from Ricotti & Gnedin (2005) and assume a total mass-to-light ratio of ~ 300 (Strigari et al. 2008) for the bound stars that remain after tidal stripping.

While it is very clear that not all of the small satellites can reach the GC, what fraction does is a question of some subtlety. Galaxy merger timescales cited in the literature, particularly for the small mass ratios considered here, span a wide range. The key

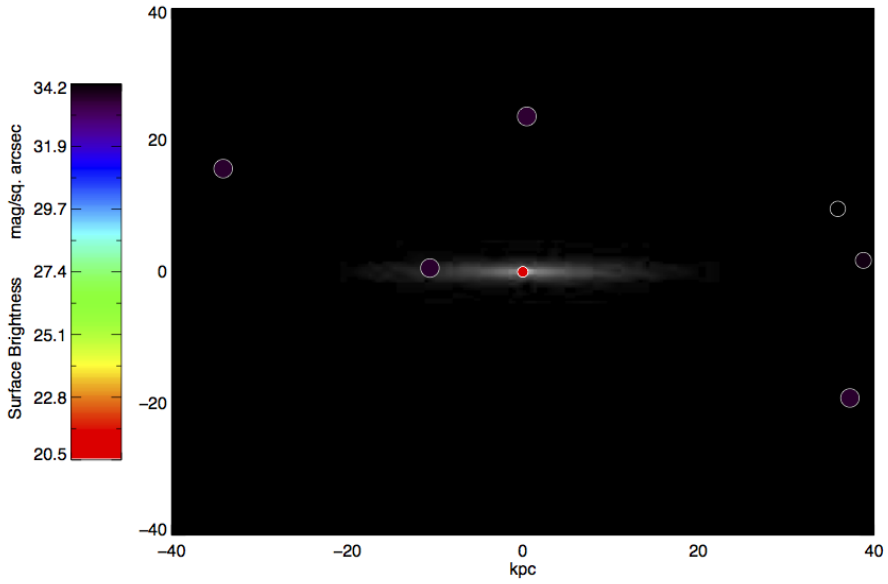

Fig. 14. Distribution of accreted low mass satellites at the present day. The inner 40 kpc region of the Milky Way disk is shown in greyscale with current accreted satellite positions overplotted. The color maps to the surface brightness, and the relative size corresponds to the tidal radius of the satellite. Note that the circle size is not to scale and that none of these satellites would be observable above the background. Also note that satellites that have merged with SMBH or completely disrupted are not plotted.

to the uncertainties is the treatment of dynamical friction: most semi-analytic works, including this one, rely on the dynamical friction formalism as described by Chandrasekhar (1943) but change the Coulomb logarithm to account for inhomogeneous or anisotropic systems (Peñarrubia et al. 2004; Just & Pearrubia 2005), or to include mass loss (Taylor & Babul 2001; Velazquez & White 1999). This approach has been shown to underestimate the decay time in pure dark matter simulations (Colpi et al. 1999; Boylan-Kolchin et al. 2008). On the other hand, the presence of gas can dramatically decrease the orbital decay time of a satellite by efficiently dissipating its orbital energy throughout the system (Ostriker 1999; Sánchez-Salcedo & Brandenburg 1999) – thus, making the Chandrasekhar formula a significant overestimate. Compounding the issue, linear perturbation theory and limited N-body experiments indicate that resonant heating caused by orbits in the satellite galaxy that are commensurate with the orbit of the satellite about the GC can enhance mass loss and can change the angular momentum of the orbit in non-trivial ways (Weinberg 1997; Choi et al. 2009). Although the Milky Way has likely accreted over a thousand of these small satellites, it is uncertain how often they reached the galactic center. It is however plausible that the GC has experienced a handful of these accretion events spread over its lifespan. Despite the uncertainty that arises in the mass of our culprit satellite due to the imprecise dynamical friction timescale, the scenario itself remains viable, because other constraints on satellite mass (satellite evaporation, disk disruption) are flexible so long as the merger timescale remains less than the age of the universe.

3.3.2 Hypervelocity stars and stellar core

While the properties of the newly formed stars and perturbed gas were dictated by the accreted satellite, the IMBH was responsible for carving out the old stellar population. As a gravitationally bound binary IMBH-SMBH formed and decayed, it scoured out $2 \times 10^5 M_\odot$ of the relaxed old and initially cuspy stellar population. Many of these stars could have been ejected from the GC as hypervelocity stars (HVSs; Brown et al. 2005; Baumgardt et al. 2006), though most may simply have received enough energy to traverse the inner parsec. Simulations of IMBH-SMBH binaries in stellar environments indicate that HVSs are created in a short burst which lasts only a few Myr in case of a $\sim 10^4 M_\odot$ IMBH (Baumgardt et al. 2006; Sesana et al. 2008). In the context of our picture we predict that this event created $\sim 10^3$ hypervelocity stars that, if they were ejected at about 1000 $\mathrm{km\,s^{-1}}$ (Baumgardt et al. 2006), ought to lie $\sim$ 10 kpc from the GC today. It is worth noting that about a dozen of HVSs observed in the Galactic halo thus far have travel times that span $60-240$ Myr and appear to be consistent with a continuous ejection model (Brown 2008; Brown et al. 2009; Tillich et al. 2009; Irrgang et al. 2010) and not with the IMBH-SMBH binary picture (Brown 2008; Sesana et al. 2008). Along similar lines, the spatial and velocity distribution of the current observed HVSs seem to be inconsistent with a IMBH-SMBH slingshot origin (Sesana et al. 2007).

The large size of the observed GC core, $r_0 = 0.21$ pc, could be seen as a challenge to any scenario involving 3-body scattering, since state of the art high resolution direct N-body simulations that modeled the ejection of hypervelocity stars from a SMBH-IMBH binary in the galactic center never generated a core larger than 0.02 parsecs (Baumgardt et al. 2006).

However, there are several effects that could conspire to cause the simulated core size to be a lower limit. First, the mass of the simulated SMBH in Baumgardt et al. (2006) is $3 \times 10^6 M_\odot$, which would eject fewer stars than somewhat more massive Milky Way SMBH. Second, the density profile was sharply curtailed by a factor of $(1 + r^5)$ in order to minimize the number of stars far from the SMBH; this makes the spatial distribution of stars in the simulated nuclear star cluster more centrally peaked relative to that in the GC, which can also result in a smaller core. In general, though, it is important to note that the size of the scoured core is a property that sensitively depends on the density, the eccentricity, and kinematic structure of the GC or on assumptions in the model used to represent it.

3.3.3 Has IMBH-SMBH binary merged?

We now return to the question whether the IMBH-SMBH binary has already merged or whether the IMBH could still be lurking in the GC. As discussed in § 3.2.3, the N-body and semi-analytic modeling of the GC favor the evolutionary scenarios in which the inspiral and coalescence of the SMBH with a $M_2 \gtrsim 10^4 M_\odot$ IMBH is relatively efficient. Moreover, there is currently no empirical evidence for a second black hole in the central parsec. In order to be consistent with the observations, the IMBH present in the GC would have to have a mass $\sim 10^3 - 10^{4.5} M_\odot$ and be either very close ($\leq 10^{-3}$ pc) or at > 0.1 pc from the SMBH (see Genzel et al. 2010, for a review of observational constraints). An IMBH in this mass range that reaches a separation of 10^{-4} pc would merge with the SMBH in less than 10 Myr due to the emission of GWs, thus severely restricting the amount of parameter space where the IMBH and SMBH can exist in a long lived binary configuration. Nevertheless,

given the uncertainties in the binary mass ratio, eccentricity, and the structure of the initial stellar cusp, the presence of an IMBH in the GC cannot be entirely ruled out at this point.

If on the other hand, the IMBH and SMBH coalesced several million years ago, one possible signature of this event could be a SMBH recoil caused by the asymmetric emission of GWs (Peres 1962; Bekenstein 1973). Current astrometric observations of the reflex motion of the SMBH put strong constraints on the allowed recoil velocity; the SMBH cannot have velocity with respect to the Central cluster larger than 3.5 km/s (within 1σ error), at the distance of the GC (Yelda et al. 2010). Similarly, Reid & Brunthaler (2004) constrain the peculiar motion of Sgr A* in the plane of the Galaxy to -18 ± 7 km/s and perpendicular to the Galactic plane to -0.4 ± 0.9 km/s, where quoted uncertainties are 1σ errors. There is however a caveat with respect to the interpretation of the SMBH reflex motion: if the reference frame in which the reflex motion is measured is based on the nearby gas and stars bound to the SMBH, the resulting relative velocity of the SMBH will be zero because in this case, the stars and the gas move together with the SMBH as long as their orbital velocity is higher than the that of the reflex motion. The radio and near-infrared reference frames in Yelda et al. (2010) are defined based on the nearby stars orbiting around the SMBH and are thus a subject to this caveat. The measurement of Reid & Brunthaler (2004) is however carried out in the reference frame defined by the extragalactic radio sources and can be used to test the recoil hypothesis.

For $10^4 M_\odot$ IMBH the black hole merger can give rise to a modest recoil velocity of about 80 m/s, assuming that the IMBH is not spinning rapidly. The recoil velocity magnitude in this case scales as $\propto q^2$ (Campanelli et al. 2007; Baker et al. 2008), thus implying that the coalescence of the SMBH with a slowly spinning IMBH more massive

than $1.5 \times 10^5 M_\odot$ can be ruled out based on larger of the observational constraints, as long as damping of the recoil motion of a remnant SMBH is inefficient on the time scale of several million years. More stringent constraints on the mass of the IMBH, based on the motion of the SMBH perpendicular to the Galactic plane, can be placed given the (unknown) orientation of the orbital plane of the binary before the merger in addition to the binary mass ratio and the spin vector of the IMBH.

3.3.4 Orientation of the SMBH spin axis

The nearly perpendicular orientation of the spin axis of the SMBH to the Galactic disk plane, indicated by the orientation of the observed gamma-ray bubbles and jets in simulations of Guo & Mathews (2012), implies that the evolution of the SMBH spin has been determined by accretion from the Galactic gas disk rather than random accretion events with isotropic spatial distribution. Such events would include tidal disruptions of stars and giant molecular clouds triggered by the satellite inspiral and a merger with the satellite IMBH which orbital plane in principle may not be aligned with the plane of the Galaxy. It is thus interesting to consider whether a sequence of such accretion events can exhibit a cumulative torque on the SMBH sufficient to re-orient its spin axis, assuming that before the merger with a satellite galaxy it was perpendicular to the Galactic plane.

Consider first the effect of episodic gas accretion resulting from multiple tidal disruption events. Chen et al. (2009, 2011) show that three-body interactions between bound stars in a stellar cusp and a massive binary with properties similar to the IMBH-SMBH considered here can produce a burst of tidal disruptions, which for a short period of time

(~ 0.1 Myr) can exceed the tidal disruption rate for a single massive black hole by two orders of magnitude, reaching $\dot{N} \sim 10^{-2}\,\mathrm{yr}^{-1}$. This implies that in the process of the IMBH inspiral the SMBH could have disrupted $\sim 10^3$ stars. A key element in this consideration follows from the finding by Natarajan & Pringle (1998) and Natarajan & Armitage (1999) that the orientation of the spin axis of a SMBH is very sensitive to the angular momentum of the accreted gas: namely, accretion of a mere few % in mass of a SMBH can exert torques that change the direction but not the magnitude of the spin of a black hole. Because each in a sequence of random accretion events imposes an infinitesimal change in the orientation of the SMBH spin axis, collectively they can cause the spin axis to perform a random walk about its initial orientation. Thus, the magnitude of the effect scales with the number of disrupted stars and their mass as $\sim \sqrt{N}\, m_*$. Since this is much less than few percent of M_1, the cumulative effect of tidal disruption events on the orientation of the spin axis of the SMBH will be negligible.

This conclusion is reinforced by an additional property of post-tidal disruption accretion disks: they are compact in size and usually confined to the region of a size few $\times\, r_t$, where $r_t \approx r_* \left(M_1/m_*\right)^{1/3}$ is the tidal disruption radius of a star and r_* is the stellar radius (Rees 1988). Such small accretion disks effectively act as very short lever arms for torques acting on the spin axis of the SMBH, thus further reducing the efficiency of this process (Natarajan & Pringle 1998).

Similar conclusions can be reached about the tidally disrupted molecular clouds and gas flows that plunge towards the SMBH on nearly radial orbits as a consequence of perturbations excited by the satellite galaxy. In section § 3.2.4 we estimated that the amount of mass accreted by the SMBH is $\sim 10^4 M_\odot$. A modest mass, combined with

the small circularization radius of the gas accretion disk is insufficient to cause a significant change in the SMBH spin orientation. Even "accretion" of a spinning IMBH is not expected to noticeably influence the spin orientation of the remnant SMBH. The large mass ratio of the binary ensures that the final contribution of the IMBH's spin and orbital angular momentum to the final spin of the SMBH is small, as long as the pre-merger SMBH has a moderate initial spin, $>$ few $\times 0.1$, in terms of the dimensionless spin parameter (Barausse & Rezzolla 2009). Hence, coalescence with the IMBH would not have had a significant effect on the SMBH spin axis orientation.

In summary, the torques from the accretion of tidally disrupted stars, gas, and the IMBH in the aftermath of the satellite inspiral will be insufficient to change the orientation of the SMBH spin axis as long as the SMBH spin is $>$ few $\times$ 0.1. It follows that the perpendicular orientation of the spin axis has been set by the physical processes before the merger with the satellite, and most likely by the accretion of gas from the Galactic disk.

3.4 Conclusions

A range of theoretical arguments and observational evidence could indicate a satellite infall event within our GC which triggered a brief epoch of strong star formation and AGN activity millions of years ago. When coupling the newest data – on the Fermi bubble and the dearth of late-type stars – to the well-established features of the GC such as the cuspy early-type stellar population, a timeline of the recent dynamical events in the galactic center emerges.

While the case for a merger of the Milky Way with a satellite galaxy is not beyond reproach, it is a plausible explanation that naturally accounts for both the late- and early-type stellar distributions and the recent violent past of Sgr A*. This event may not be unique in the evolution of the Milky Way; indeed N-body simulations of the growth of Milky Way-mass galaxies suggest that the present epoch is rife with mergers of relic satellite galaxies with the galactic center, occurring at a rate of one per few Gyr (Diemand et al. 2007; Sinha & Holley-Bockelmann 2012). This implies that there may have been other bursts of hypervelocity star ejections, which can seed a population of "intragroup stars" farther out in the halo of the Galaxy. Interestingly, we see tentative evidence in the SDSS archive for a potential set of very late M giants at $\sim 300\,\mathrm{kpc}$, outside the virial radius of our galaxy (Palladino et al. 2012). Although a followup observation is needed to ensure that these intragroup candidates are not L dwarfs, if these do prove to be very distant giants, they may be provide supporting evidence of a previous minor-merger induced burst of ejected stars $\sim 10^8$ years ago.

Along similar lines, if satellite infall induced activity is common, then there may be a subset of spiral galaxies which exhibits the signs of the recent onset of the accretion-powered jets. While the longer term X- and γ-ray signatures of jets expanding into the intragalactic medium may be too faint to observe in galaxies other than the Milky Way, relatively bright and short lived radio-jets ($\sim 0.1\,\mathrm{Myr}$; Guo & Mathews 2012) may be present in a fraction of up to $\sim 10^{-4}$ Milky-Way-like spirals, assuming the minor merger rate cited above. Some of these galaxies may be observed serendipitously, during the transient phase associated with the onset of a powerful jet, similar to the case of the previously inactive galaxy J164449.3+573451 that was recently detected by the Swift observatory as a powerful

source of beamed emission (Burrows et al. 2011). If it can be shown that such a sequence of events occurred in the not so distant past in our Galaxy, it would forever change the paradigm of the Milky Way as an inactive galaxy with an underluminous central SMBH.

We thank Cole Miller, Melvyn Davies, Jorge Cuadra and Rainer Schödel for insightful discussions. K.H-B., T.B., P.A-S. and A.S. also acknowledge the hospitality of the Aspen Center for Physics, where the work was conceived and carried out. K.H-B. acknowledges the support of a National Science Foundation Career Grant AST-0847696, and a National Aeronautics and Space Administration Theory grant NNX08AG74G as well as the supercomputing sup- port of Vanderbilt's Advanced Center for Computation Research and Education, and NASA's Pleiades and Columbia clusters. Support for T.B. was provided by the National Aeronautics and Space Administration through Einstein Postdoctoral Fellowship Award Number PF9-00061 issued by the Chandra X-ray Observatory Center, which is operated by the Smithsonian Astrophysical Observatory for and on behalf of the National Aeronautics Space Administration under contract NAS8-03060. Support for M.L. was provided by a National Science Foundation Graduate Research Fellowship.

Chapter IV

VORONOI TESSELLATION AND NON-PARAMETRIC HALO CONCENTRATION

The following work was submitted to the Astrophysical Journal (Lang et al. 2015) and is reprinted below in its entirety.

Voronoi Tessellation and Non-parametric Halo Concentration

Meagan Lang[1], Kelly Holley-Bockelmann[1,2], & Manodeep Sinha[1]
[1]Department of Physics and Astronomy, Vanderbilt University, Nashville, TN, USA; meagan.lang@vanderbilt.edu
[2]Fisk University, Department of Physics, Nashville, TN, USA; k.holley@vanderbilt.edu

Abstract

We present and test TesseRACt, a non-parametric technique for recovering the concentration of simulated dark matter halos using Voronoi tessellation. TesseRACt is tested on idealized N-body halos that are axisymmetric, triaxial, and contain substructure and compared to traditional least-squares fitting as well as two non-parametric techniques that assume spherical symmetry. TesseRACt recovers halo concentrations within 3% of the true value regardless of whether the halo is spherical, axisymmetric, or triaxial. Traditional fitting and non-parametric techniques that assume spherical symmetry can return concentrations that are systematically off by as much as 10% from the true value for non-spherical halos. TesseRACt also performs significantly better when there is substructure present outside $0.5R_{200}$. Given that cosmological halos are rarely spherical and often contain substructure, we discuss implications for studies of halo concentration in cosmological

N-body simulations including how choice of technique for measuring concentration might bias scaling relations.

Key words: galaxies: fundamental parameters — galaxies: halos — methods: numerical

4.1 Introduction

There has long been a disconnect between the way we describe a dark matter halo and the reality of that dark matter structure. In theoretical terms, we think of a halo as a smooth, isotropic, virialized, usually spherical, typically uniformly rotating, distribution of mass that obeys a distinct radial distribution. However, while halos in cosmological simulations and observations may conform to these in a statistical sense, any one halo is not really any of these things. Halos are triaxial, anisotropic, and contain significant substructure (e.g. Jing & Suto 2002; Gao et al. 2004; Despali et al. 2014; Groener & Goldberg 2014). Despite this well known fact, many analysis techniques try to extract halo properties by imposing one or more of these assumptions. For example, any procedure which fits a radial profile, be it Hernquist (Hernquist 1990), NFW (Navarro et al. 1996), or Einasto (Einasto & Haud 1989), to a halos mass distribution assumes the halo is both spherical and smooth. In an era of simulations quickly surpassing 10^9 particles, there is a need for physically motivated analysis techniques that do not impose constraints on what a halo should look like.

Halo concentration is a particularly useful statistic for characterizing halos. Since halos that gain the majority of their mass at earlier times (when the mean density of the universe was higher) should be more compact, concentration is believed to encode a great deal of information about halo formation and growth. There have been numerous studies

on the relationships between halo concentration in cosmological simulations and halo mass (Navarro et al. 1996; Neto et al. 2007), redshift (Bullock et al. 2001a; Gao et al. 2008; Klypin et al. 2011; Prada et al. 2012; Bhattacharya et al. 2013; Dutton & Maccio 2014; Ludlow et al. 2014; Diemer & Kravtsov 2015), environment (Bullock et al. 2001a; Maccio et al. 2007), assembly history (Wechsler et al. 2002; Zhao et al. 2009; Ludlow et al. 2013), and cosmology (Colin et al. 2000; Eke et al. 2001; Macciò et al. 2008; Dooley et al. 2014). However, claims are often conflicting and the majority of techniques used to measure concentration fall victim to the above assumptions.

We propose a non-parametric method for estimating halo concentration using Voronoi tessellation that we dub Tessellation based Recovery of Amorphous halo Concentrations (TesseRACt). Section §4.2 briefly describes Voronoi tessellation and outlines TesseRACt, §4.3 summarizes several tests, and §4.4 summarizes our findings and describes studies that can benefit from TesseRACt.

4.2 Theory/Background

4.2.1 Measuring Concentration

The concentration parameter is traditionally defined in an NFW halo as

$$c_{\rm nfw} = \frac{R_{200}}{R_{\rm s}} \tag{4.1}$$

where R_{200} is the radius enclosing a mean density that is 200 times the critical density of the universe and $R_{\rm s}$ is the scale radius. Since R_{200} can be easily found, concentration is

typically obtained by fitting Eqn. 4.2 to the radially enclosed mass profile to find $R_{\rm s}$.

$$M_{\rm enc}(r) \;=\; 4\pi\rho_0 R_{\rm s}^3 \left[\ln\left(\frac{R_{\rm s}+r}{R_{\rm s}}\right) - \frac{r}{R_{\rm s}+r}\right] \tag{4.2}$$

Although this is simple in theory, fitting even spherical halos without substructure can be difficult. Fits can be highly sensitive to resolution at the center, deviation from the expected NFW power laws, and choice of binning (See Prada et al. 2012). These effects can be alleviated in practice by avoiding fitting altogether. Instead, the unknown profile parameters are related to other halo properties that can be robustly measured. For example, if $R_{\rm half}$ (the radius enclosing half the mass) and R_{200} of a halo are known, it is possible to numerically solve

$$\frac{1}{2} = \frac{\ln\left[(R_{\rm s}+R_{\rm half})/R_{\rm s}\right] - R_{\rm half}/(R_{\rm s}+R_{\rm half})}{\ln\left[(R_{\rm s}+R_{200})/R_{\rm s}\right] - R_{200}/(R_{\rm s}+R_{200})} \tag{4.3}$$

for $R_{\rm s}$.

This can be done for any two independent halo properties, typically characteristic radii or velocities (Avila-Reese et al. 1999; Thomas et al. 2001; Alam et al. 2002; Gao et al. 2004; Klypin et al. 2011; Prada et al. 2012). While such techniques are more robust against deviations from NFW and yield more accurate results than fitting for dense halos with under sampled central regions, even these techniques still assume that halos are spherical and do not contain substructure.

In principle, more accurate concentrations for non-spherical halos could be obtained by fitting to triaxial or ellipsoidal bins. Such techniques have been found to provide more accurate mass estimates in both simulations and observations, but generally assume that the axis ratio and alignment remains constant throughout the halo (Warren et al. 1992; Jing

& Suto 2002; Allgood et al. 2006; Despali et al. 2013, 2014). In reality, simulations show that halo shape is highly dependent on radius, becoming less and less spherical as you look deeper in the halo (Allgood et al. 2006; Vera-Ciro et al. 2011). This makes measurements assuming a constant shape dependent upon the location within the halo at which shape is measured. In addition, despite allowing for more freedom in halo shape, non-spherical fitting is still victim to the same caveats as spherical fitting and relies on the additional measurement of halo shape.

While both non-spheroidal binning and non-parametric spherical techniques have advantages, neither is completely free of assumptions or can handle substructure. However, using Voronoi tessellation, we can construct a technique that does not rely on fitting, does not make any assumptions of spherical symmetry, and allows for substructure.

4.2.2 Tessellation Based Concentration

Given a set of seed points $\{p_1, \ldots, p_n\}$ in some space, Voronoi tessellation divides the space between the seeds such that each seed is the closest seed to its Voronoi region. In this way, each seed (p_i) has a corresponding Voronoi region of volume V_i encompassing all points in space which are closest to that seed. Voronoi tessellation has been used to non-parametrically identify galaxy clusters in galaxy surveys (Soares-Santos et al. 2011), identify dark matter halos (Neyrinck et al. 2004) and voids (Neyrinck 2008) in cosmological simulations, and improve the treatment of hydrodynamics in simulations (Mocz et al. 2013; Hopkins 2014). We take this one step further. Once halos are identified in cosmological

simulations (either by friends-of-friends, spherical over-density, or tessellation), the additional information provided by the particles' associated volumes can be used to derive halo properties (like concentration) without imposing any additional functional form.

To determine concentration from the particle volumes, a profile is constructed that describes how mass scales with volume rather than radius. For a particle p_i with mass m_i and a Voronoi volume V_i, the volume $V_{\mathrm{enc},i}$ 'enclosed' by that particle is taken to be the sum of all particle volumes which are smaller than V_i or

$$V_{\mathrm{enc},i} = \sum_{j=0}^{n} V_j [V_j \leq V_i]. \tag{4.4}$$

Similarly, the mass $M_{\mathrm{enc},i}$ 'enclosed' by a particle p_i is

$$M_{\mathrm{enc},i} = \sum_{j=0}^{n} m_j [V_j \leq V_i]. \tag{4.5}$$

Each particle can then be assigned a theoretical 'radius' $R'_i = (3V_{\mathrm{enc},i}/4\pi)^{1/3}$ that is defined as the radius the particle would be at if $V_{\mathrm{enc},i}$ were spherical. The result is a volume based mass profile $M_{\mathrm{enc}}(R')$. Naively, the volume based concentration could then be defined as

$$c_{\mathrm{vol}} = \left(\frac{V_{200}}{V_{\mathrm{s}}}\right)^{1/3} \tag{4.6}$$

where V_{200} is the densest volume containing an average density that is 200 times the critical density of the universe and V_{s} is some scale volume. If the theoretical radii (R'_{200} and R'_{s}) associated with these volumes converged to the corresponding physical radii (R_{200} and R_{s})

in the case of a spherical halo, $c_{\rm vol}$ would equal $c_{\rm nfw}$ and this would be sufficient. However, this is not strictly true.

For even a spherical halo, the relationship between a particle's physical radius R_i and theoretical radius R'_i is not 1:1. Due to the intrinsic scatter in the inter-particle spacing at a given physical radius, particles with slightly larger/smaller volumes will be scattered to larger/smaller theoretical radii. Because the density of particles is always greater toward smaller physical radii, it is more likely for particles inside R_i to be scattered to larger theoretical radii. As a result, there will then be systematically fewer particles considered 'enclosed' by particle p_i and R'_i will be systematically lower.

In order to correct for this and preserve the same numerical values for $c_{\rm vol}$ and $c_{\rm nfw}$ in the case of spherical halos, the volume based concentration is defined as

$$c_{\rm vol} = \beta \left(\frac{V_{200}}{V_{\rm s}} \right)^{\alpha/3}. \tag{4.7}$$

$\beta = 0.8062$ and $\alpha = 1.0417$ were obtained by fitting to measurements of V_{200} and $V_{\rm s}$ for 10 spherical halos with known concentrations between 5 and 70. While this treatment is simplistic, tests performed in §4.3.1 indicate that it should be sufficient for most studies.

Eqn. 4.7 can then be simplified in terms of the radii a halo would have if it were spherical.

$$c_{\rm vol} = \beta \left(\frac{R'_{200}}{R'_{\rm s}} \right)^{\alpha}. \tag{4.8}$$

Note that since V_{200} is defined as the densest volume containing an average density that is 200 times the critical density of the universe, R'_{200} can be found directly from the Voronoi volumes. However, V_s and R'_s are somewhat arbitrary in the absence of fitting. Instead, we choose to define the scale radius and volume in terms of a quantity we can measure. We adopt $V_{\rm half} = 4\pi R'^3_{\rm half}/3$, the densest volume enclosing half the mass.

Once $R'_{\rm half}$ is known, the corresponding R'_s for a spherical halo can be found by numerically solving Eqn. 4.3. This relationship yields unique concentrations for each $R_{\rm half}$ when $1 < c < 100$. Above $c = 100$, $R_{\rm half}/R_{200}$ becomes somewhat degenerate about 0.1.

The TesseRACt procedure for finding $c_{\rm vol}$ is then:

1. Run Voronoi tessellation to determine the volumes and densities at each particle.
2. Rank particles in order of decreasing density (increasing volume).
3. Calculate enclosed mass ($M_{\rm enc}$) and volume ($V_{\rm enc}$) at each particle by summing the masses and volumes of 'denser' particles.
4. Calculate mean enclosed density at each particle ($\langle \rho_{\rm enc} \rangle = M_{\rm enc}/V_{\rm enc}$)
5. Find V_{200} and M_{200} (the volume and mass enclosed by the particle at which the mean enclosed density reaches 200 times the critical density of the universe)
6. Find $V_{\rm half}$ (the volume enclosed by the particle at which the enclosed mass reaches $M_{200}/2$)
7. Calculate R'_{200} and $R'_{\rm half}$ from V_{200} and $V_{\rm half}$
8. Numerically solve Eqn. 4.3 for R'_s
9. Calculate $c_{\rm vol}$ from Eqn. 4.8

4.3 Tests

For the tests that follow, we compare our volume-based non-parametric technique TesseRACt to both least-squares NFW fitting, as well as two non-parametric techniques that assume spherical symmetry. The first infers the scale radius from the $R_{\rm half}$ and R_{200} in the same fashion as Eqn. 4.3, but using the physical particle radii. The second uses the relationship between the peak circular velocity and circular velocity at R_{200} from Prada et al. (2012),

$$\frac{v_{\rm max}}{v_{200}} = \left[\frac{0.216c}{\ln(1+c) - c/(1+c)}\right]^{1/2}. \tag{4.9}$$

For each test, we run all four techniques on isolated N-body halos generated by sampling spherical NFW profiles of known concentration. Unless otherwise stated, each halo has $N_{\rm part} = 1 \times 10^6$ particles, $M_{200} = 1 \times 10^{12} {\rm M}_\odot$, and $R_{200} = 200\,{\rm kpc}$. The halos only differ in ρ_0 and $R_{\rm s}$.

To ensure that insufficient sampling of the profile does not affect the accuracy of the least squares fitting, fits are bounded on the lower end at $0.05R_{200}$ and R_{200} on the upper end.

Errors on concentration measurements were determined by running each technique on 10 different realizations of each test halo generated by using a different random number seed. In the tests below, the mean concentration returned by each technique is plotted with the standard deviation across the different realizations.

4.3.1 Concentration

We first tested the performance of each method on halos with concentrations of 5, 10, 25, and 50. Results are shown in Figure 15.

As these are idealized halos, all of the tested techniques return accurate measures of concentration as expected. For the idealized halos, TesseRACt is the most accurate for all but the $c = 5$ halo for which the measured concentration is still within 2% of the correct value. Of the techniques which assume spherical symmetry, all three perform similarly with the maximum circular velocity and fitting techniques returning marginally more accurate concentrations at the low and high ends respectively. The accuracy of the techniques which assume spherical symmetry does not appear to be overly concentration dependent. However, as the modified concentration definition used for TesseRACt in Eqn. 4.8 was fit to measurements across a range of concentrations, TesseRACt is slightly more accurate for halos with intermediate concentrations. All of the techniques tested were consistent across the 10 halo realizations with standard deviations of $< 0.6\%$.

4.3.2 Halo Shape

4.3.2.1 Oblateness

To test how each method performed on oblate halos, the $c = 10$ halo from above was squeezed along the z axis using the volume preserving transformation

$$\begin{bmatrix} x' \\ y' \\ z' \end{bmatrix} = \left(\frac{a}{b}\right)^{1/3} \begin{bmatrix} a & 0 & 0 \\ 0 & a & 0 \\ 0 & 0 & b \end{bmatrix} \begin{bmatrix} x \\ y \\ z \end{bmatrix}, \tag{4.10}$$

for 7 different values of ellipticity where $e_{\text{oblate}} = b/a$ and $a = 1$. Results are shown in Figure 16.

For all but the least spherical halos, TesseRACt consistently recovers concentrations within 0.5% of the correct value, with a minor dependence on halo shape (overestimated by 0.4% for $e_{\text{oblate}} = 0.3$ vs. underestimate by 0.02% for spherical halos). However, the performance of the techniques which assume spherical symmetry is highly dependent on halo shape. Fitting performs the worst overall, with increasingly underestimated values for the least spherical halos (10% for $e_{\text{oblate}} = 0.3$). The performance of the two non-parametric spherical techniques is dependent on halo shape in a more complicated manner.

For decreasing values of e_{oblate} (decreasing spherical symmetry), both non-parametric spherical techniques have moderately increasing positive residuals until around $e_{\text{oblate}} = 0.6$ to 0.7 where the residuals begin to rapidly decrease resulting in underestimates of 6 and 8% for the half-mass and peak-velocity techniques respectively. These dependencies arise because the deformation of the halo flattens the radial mass profile. As fitting uses the entire profile, the concentration is underestimated for all non-spherical halos. However, non-parametric techniques use only two points in the profile (R_{200} and some inner radius) and their performance will depend up how these parts of the profile are affected by the transformation. R_{200} continually increases as compression of the halo edge decreases the density at the edge of the profile. The inner radius will increase as well, but at a slower rate resulting in an overestimation of the concentration until the edge of the halo is compressed to a size comparable to the inner radius. Once this occurs, the inner radius increases more rapidly than R_{200} resulting in underestimates. The precise value of e_{oblate} at which this occurs will depend on the radius that a particular non-parametric technique utilizes. Since

the velocity peaks at a smaller radius than the half-mass radius for an NFW profile, the technique which uses the peak velocity is less sensitive to this effect.

The test halos here have the same ellipticity at all radii by design. However, real halos are found to be decreasingly spherical at their centers (Allgood et al. 2006; Vera-Ciro et al. 2011). While TesseRACt would not be affected, it is likely that the spherical techniques would produce less accurate concentrations. This would be particularly pronounced for fitting due to sensitivity to the inner profile slope.

4.3.2.2 Prolateness

To test how each method performed on prolate halos, the $c = 10$ halo from above was squeezed along it's z and y axes using the volume preserving transformation

$$\begin{bmatrix} x' \\ y' \\ z' \end{bmatrix} = \left(\frac{a^2}{b^2}\right)^{1/3} \begin{bmatrix} a & 0 & 0 \\ 0 & b & 0 \\ 0 & 0 & b \end{bmatrix} \begin{bmatrix} x \\ y \\ z \end{bmatrix}, \tag{4.11}$$

for 7 different values of ellipticity where $e_{\text{prolate}} = b/a = c/a$ and $a = 1$. Results are shown in Figure 17.

The performance across all techniques is similar to the above tests for oblate halos. However, there does appear to be a stronger dependence on ellipticity at intermediate values for prolate halos than for oblate halos for techniques which assume spherical symmetry. This is because the prolate transformation flattens the radial mass profile to a greater degree than the oblate transformation.

4.3.2.3 Triaxiality

We then tested the performance of each method on triaxial halos (See Figure 18). For 9 different values of triaxiallity ($T = \frac{c^2-b^2}{c^2-a^2}$, for $c \leq b \leq a$, Franx et al. 1991), the $c = 10$ halo from above was squeezed along the z and y axes using the volume preserving transformation

$$\begin{bmatrix} x' \\ y' \\ z' \end{bmatrix} = \left(\frac{a}{bc}^2\right)^{1/3} \begin{bmatrix} a & 0 & 0 \\ 0 & b & 0 \\ 0 & 0 & c \end{bmatrix} \begin{bmatrix} x \\ y \\ z \end{bmatrix}, \tag{4.12}$$

where $a = 1$, $c/a = 0.3$, and $b = \sqrt{c^2 - T(c^2 - a^2)}$.

TesseRACt out performs all spherical techniques at $< 0.2\%$ for all triaxialities. The spherical techniques return concentrations that are only slightly less accurate overall ($<4\%$) than in the case where $T = 1$. While TesseRACt's performance does not depend on triaxiality, the accuracy of the techniques which assume spherical symmetry does to a small degree. The two non-parametric techniques become less accurate for lower values of T, while fitting only exhibits this behavior until $T \sim 0.3$, where this trend is reversed. However, since the residuals never exceed 4%, it is reasonable to conclude that only the ratio between the largest and smallest halo axes appears to have a significant impact on the accuracy of the concentration estimate.

4.3.3 Halos with Substructure

To test the ability of TesseRACt to recover concentrations in the presence of substructure, idealized subhalos of varying mass and concentration were added to the $c = 10$ halo at varying radii. In each case the mass of the subhalo was set by downsampling the test halo from the previous section with the desired concentration. The size of the subhalo was then scaled such that the mean density within $0.2R_{200}$ was half that of the parent halo.

4.3.3.1 Substructure Mass

Figure 19 shows the results from varying the mass of the subhalo across 1-20% of the parent halo's M_{200}. The subhalos had a concentration of 50 and were placed $0.5R_{200}$ from the center of the parent halo. Since subhalos were scaled to have a constant central density, increasing the mass of the subhalo also increases its size.

As expected, all techniques become less accurate as the subhalo increases in mass and size, but TesseRACt performs significantly better. For the most massive subhalo, 20% the mass of the parent, TesseRACt overestimates the concentration by 8%, while techniques assuming spherical symmetry underestimate concentrations by up to 30% of the true value. TesseRACt overestimates concentrations because particles in the subhalo have small enough volumes that they are assumed to be within the inner parts of the parent halo and thus result in a smaller half-mass volume. The techniques assuming spherical symmetry underestimate concentrations in the presence of substructure because the subhalo contributes mass to the outer profile.

4.3.3.2 Substructure Radius

Figure 20 shows the results from varying the distance of the subhalo from the center of the parent halo from 0.05 to $0.5R_{200}$. The subhalos each had a concentration of 50 and 1% the mass of the parent halo.

At small radii, the subhalo almost coincides with the center of the parent halo, causing all techniques to return higher concentrations than they would had there been no substructure present. As the subhalo is placed at larger radii, the concentrations returned by all techniques become lower. However, while concentrations returned by techniques assuming spherical symmetry continue to drop past the true value as additional mass is added to the outer profile resulting in underestimates by up to 20%, TesseRACt becomes more accurate, underestimating the concentration by only 0.7% at $0.75R_{200}$. This occurs because, when the subhalo is placed at larger radii where the density of the parent is lower, the densities assigned to the subhalo particles using tessellation become lower and contribute less to the half-mass volume. The radius at which the spherical techniques change from overestimating to underestimating depends upon which part of the mass profile is used to calculate concentration.

4.3.3.3 Substructure Concentration

Figure 21 shows the results from varying the concentration of the subhalo from 5 to 50. The subhalos were placed $0.5R_{200}$ from the center of the parent halo and had 1% the mass of the parent.

For subhalos of equal or greater concentration than the parent ($c_{\rm sub} \geq 10$), TesseRACt is more accurate than the spherical techniques ($< 3\%$ vs. $<20\%$). While the accuracy

of the spherical techniques shows little dependence on concentration in this regime, TesseRACt's accuracy changes with concentration. Since TesseRACt places no constraints on where the center of the halo is, the measured concentration is essentially an average of the concentrations of the two halos present, the parent and the subhalo. As a result, the same dependence on halo concentration that was seen in §4.3.1 is also present for subhalo concentration.

The case of a subhalo that is less concentrated than the parent halo ($c_{\rm sub} = 5$) is less physical. In order to maintain a central density half that of the $c = 10$ parent halo with 1% of the mass, the $c = 5$ halo must be scaled to less than half of its original size. This means that the substructure contributes to a narrower region of the radial mass profile, resulting in lower estimates for R_{200} and M_{200} that are closer to those for the parent halo alone. For fitting, which uses the entire profile, the result is a significantly underestimated concentration (20%). However, the non-parametric techniques, which are not dependent on the whole profile, are significantly more accurate in this case. The half-mass technique is slightly more accurate (2%) than the peak velocity technique (3%) because while $R_{\rm half}$ changes with R_{200}, the peak velocity occurs well within the radius at which the substructure was placed.

4.3.4 Dependence on Particle Number

Finally, we tested the performance of each technique for different resolutions (See Figure 22). Beginning with the $c = 10$ halo containing 10^6 particles, transformed to be prolate with an $e_{\rm prolate} = 0.3$, random subsets of the particles were selected to create halos of the same size and shape, but lower resolution.

Above 2×10^3 particles, all of the tested techniques are reasonably convergent (<10%) around the fiducial concentration for $N = 1 \times 10^6$. For fewer particles, the residuals for the peak velocity technique climb quickly to $> 80\%$ of the fiducial value for 100 particles. TesseRACt and the half-mass non-parametric technique perform similarly on average, returning concentrations within 20% of the fiducial value at the lowest resolution. However, TesseRACt was more precise than the half-mass technique. Across the 10 halo realizations, the standard deviation in the concentrations returned by TesseRACt and the half-mass technique were 40% and 50% respectively at $N = 100$. Fitting was surprisingly accurate at low resolutions with residuals $< 10\%$ and standard deviations similar to TesseRACt.

4.4 Summary & Discussion

For idealized spherical halos, TesseRACt is slightly more accurate at recovering intermediate concentrations for N-body halos than techniques that assume spherical symmetry ($\sim$0.5% vs. $\sim$1%). However, TesseRACt truly shines for non-spherical halos. For the most oblate or triaxial galaxies, even the most accurate spherical technique using the peak circular velocity returned concentrations that underestimated the true value by up to $\sim$10%, while TesseRACt had residuals of only $\sim$0.5%. This is troubling given that halos in simulations are not often spherical.

Studies of halos in cosmological simulations indicate that halos tend to be prolate overall, halos become increasingly triaxial at higher redshifts, and the most massive halos at all redshifts are the least spherical (Allgood et al. 2006; Bett et al. 2007; Vera-Ciro et al. 2011; Despali et al. 2014). Therefore, concentrations resulting from techniques that assume spherical symmetry would result in median concentrations that are biased overall

to be lower than the true value and especially biased for halos that are massive or at high redshift. This bias could be expressed in the scaling relations between concentration and other intrinsic halo properties like mass, formation redshift, and environment.

The concentration of a halo is believed to reflect the state of the universe at its collapse (Navarro et al. 1996). Therefore, on average, more massive halos should have lower concentrations, halos at higher redshift should have lower concentrations than those of the same mass at lower redshift, and halos in denser environments should have higher concentrations. However, the exact relationship between halo concentration, mass, redshift, and environment is still under debate (Bullock et al. 2001a; Eke et al. 2001; Neto et al. 2007; Gao et al. 2008; Klypin et al. 2011; Prada et al. 2012; Bhattacharya et al. 2013; Dutton & Maccio 2014; Ludlow et al. 2014; Diemer & Kravtsov 2015). Since halo shape also varies systematically with mass and redshift, it is possible that imposing the assumption of spherical symmetry could systematically bias such studies. Use of a non-parametric technique that is independent of halo shape like TesseRACt could be instrumental in eliminating this bias and pinning down these relations.

In addition to biasing the median measured concentration for halos in a given mass and redshift bin, the error introduced by assuming spherical symmetry would also increase scatter in the distribution of concentration for these halos due to scatter in halo shape. Intrinsic scatter in this relationship is expected to result from differences between any two halos' mass assembly histories that result in slightly different concentrations. However, if scatter is also being introduced by the technique used to measure concentration, measurement of this scatter becomes less informative. Since scatter in the concentration-mass relationship is greatest for those halos which are the least virialized and have the poorest

NFW fits (Jing 2000; Neto et al. 2007), removing these halos can help to remove some of this bias. However, even virialized halos can be non-spherical and it is likely that the assumption of spherical symmetry would still contribute to the remaining scatter. TesseRACt could help to identify what the true intrinsic scatter in the concentration-mass relationship is for both virialized and un-virialized halos.

TesseRACt could be improved for future studies in a number of ways. One possibility is using tessellation in the full six dimensional phase space to place better constraints on how deep a particle resides within the host galaxy's potential. This would be particularly useful for correcting for substructure. While substructure particles may be confused with parent halo particles on the basis of spatial volumes alone, the two would be more easily differentiated in velocity space. It may also be possible to improve TesseRACt's performance by more accurately parameterizing the relationship between traditional concentration and that calculated using tessellation based volumes as in Eqn. 4.8. Fitting over a wider range of concentrations and allowing a more complex relationship should improve the slight dependence of TesseRACt's performance on concentration. However, since this dependence only affects concentrations by $< 3\%$, the parameterization presented here should be sufficient for most studies.

Although only spatial information was used here, tessellation can also be used to glean information non-parametrically from simulations by tessellating over other parameters. In simulations which include gas, tessellation over parameters like star formation rate, temperature, and metallicity in addition to position and velocity can help to identify structure and explore formation scenarios.

K.H-B. acknowledges the support of a National Science Foundation Career Grant AST-0847696 as well as the supercomputing support of Vanderbilt's Advanced Center for Computation Research and Education. Support for M.L. was provided by a National Science Foundation Graduate Research Fellowship.

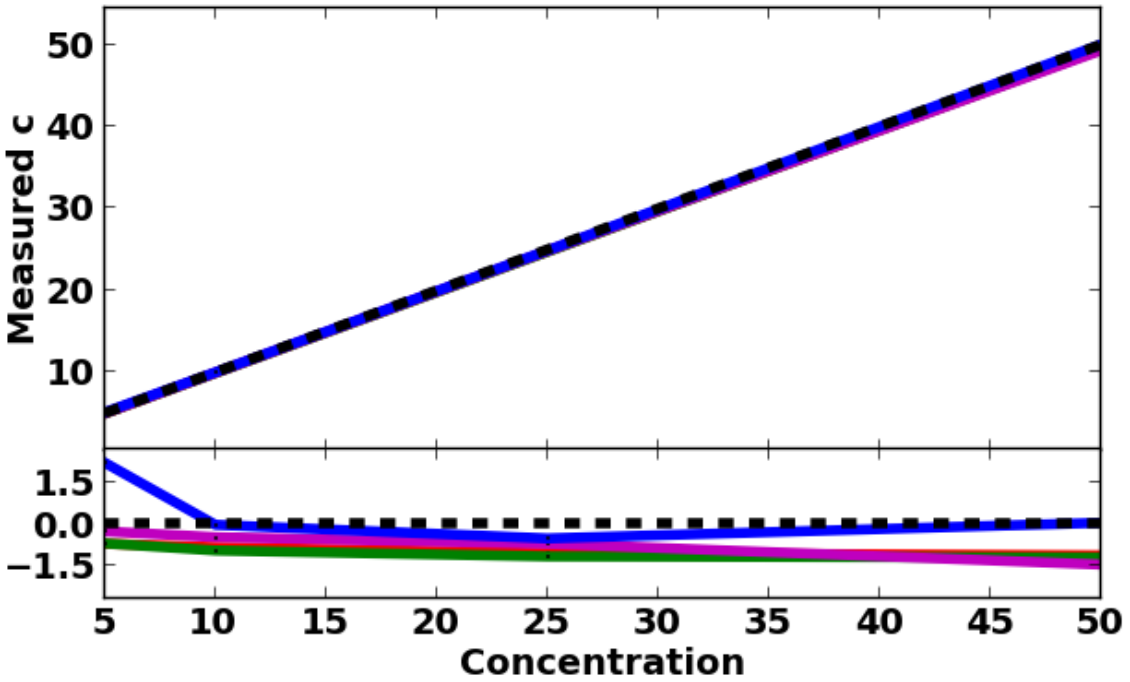

Fig. 15. Top: Concentration measured by TesseRACt and different spherical techniques as a function of known halo concentration. Bottom: % relative residuals, 100*(measured-true)/true. The black line is the known concentration, blue is TesseRACt, red is least-squares fitting to Eqn. 4.2, green is the half mass technique from Eqn. 4.3 assuming spherical symmetry, and magenta is the maximum circular velocity technique from Prada et al. (2012). All of the techniques recover the correct value to within 2%, regardless of concentration.

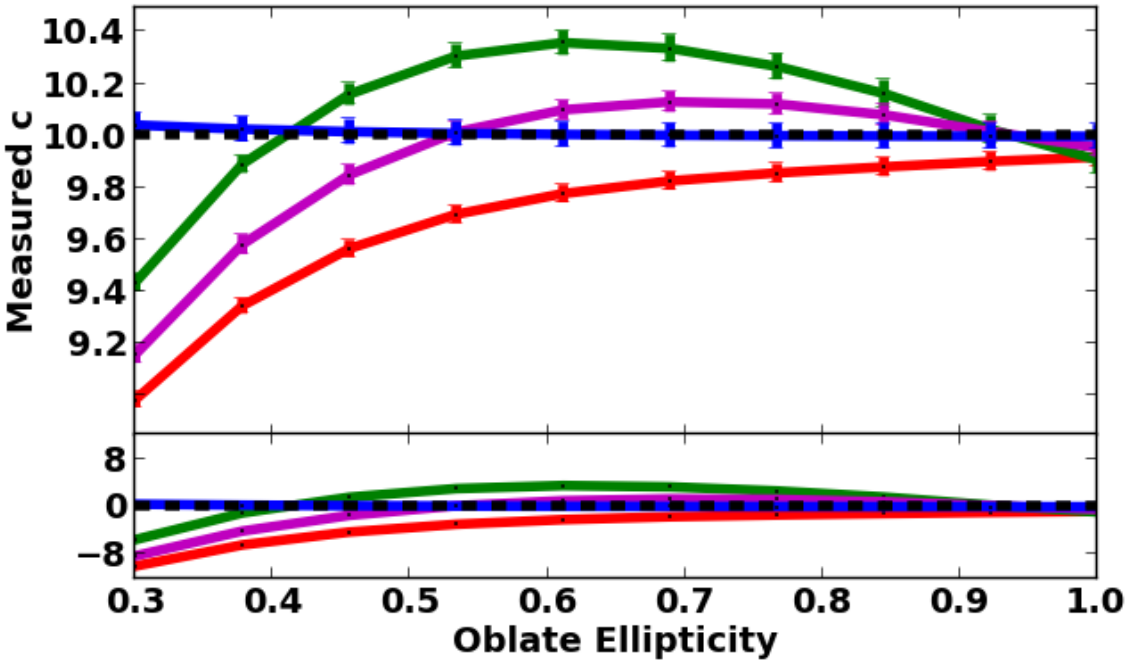

Fig. 16. Performance of TesseRACt vs. spherical techniques as a function of oblate halo ellipticity. While TesseRACt recovers concentration with 0.5% of the correct value for all halo shapes, techniques assuming spherical symmetry do not and underestimate the concentration of the least spherical halos by up to 10%.

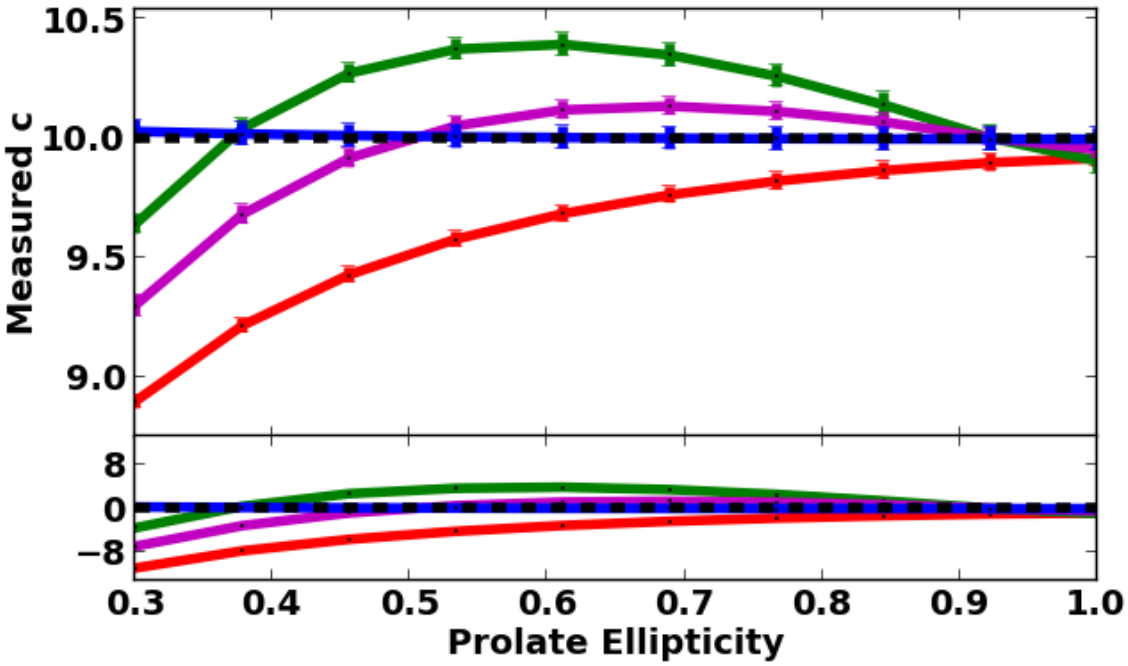

Fig. 17. Performance of TesseRACt vs. spherical techniques as a function of prolate halo ellipticity. TesseRACt recovers concentrations to within 0.3% regardless of halo shape. The performance of techniques assuming spherical symmetry are highly dependent on halo shape and return less accurate halo concentrations by over 10%. Overall, the spherical techniques are less accurate at recovering concentrations for prolate halos than oblate halos.

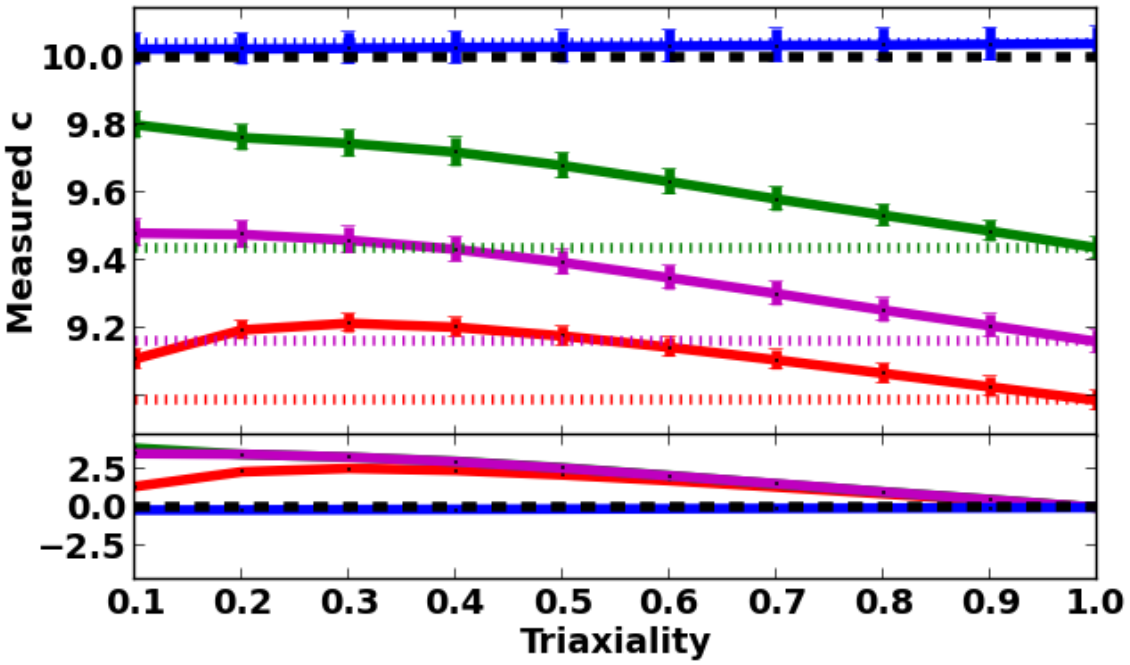

Fig. 18. Performance of TesseRACt vs. spherical techniques as a function of halo triaxiality. The dotted colored lines denote the fiducial value returned by each technique in the case where $T = 1$ (an oblate halo with $e_{\rm oblate} = 0.3$) and the residuals plotted here are with respect to this value. TesseRACt recovers concentrations within 0.2% of the fiducial value for all triaxialities. The techniques which assume spherical symmetry display moderate dependence on triaxiality, but do not return concentrations that deviate from the fiducial value by more than 4%.

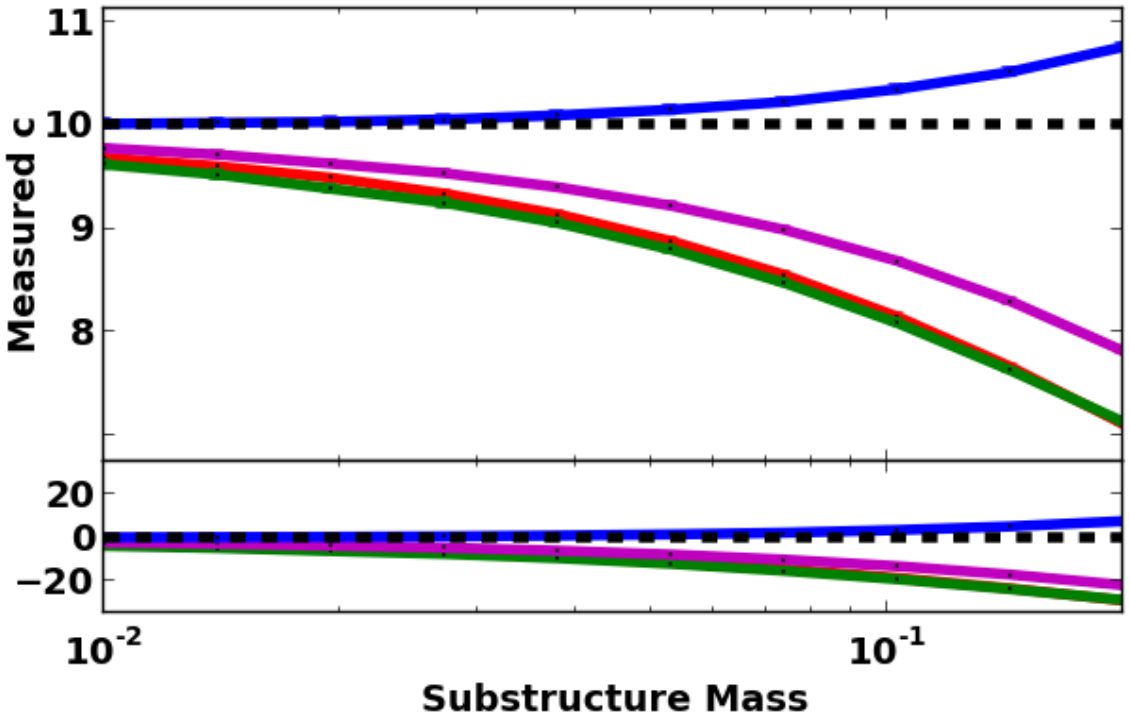

Fig. 19. Performance of TesseRACt vs. spherical techniques as a function of subhalo mass. The concentrations returned by all techniques become less accurate as the mass of the subhalo increases. However, at the most massive end, TesseRACt is three times as accurate as techniques assuming spherical symmetry.

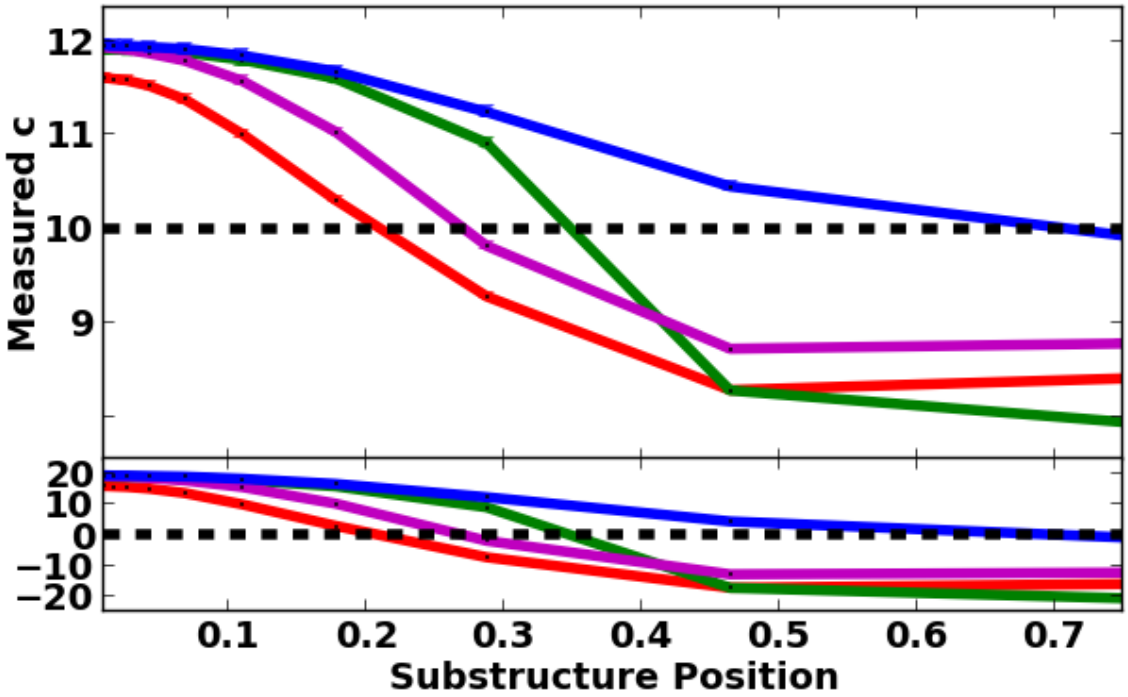

Fig. 20. Performance of TesseRACt vs. spherical techniques as a function of subhalo location in the parent halo. All techniques perform poorly when the subhalo is close to the center of the parent halo. However, while TesseRACt becomes more accurate as the subhalo is placed further out, spherical techniques do not.

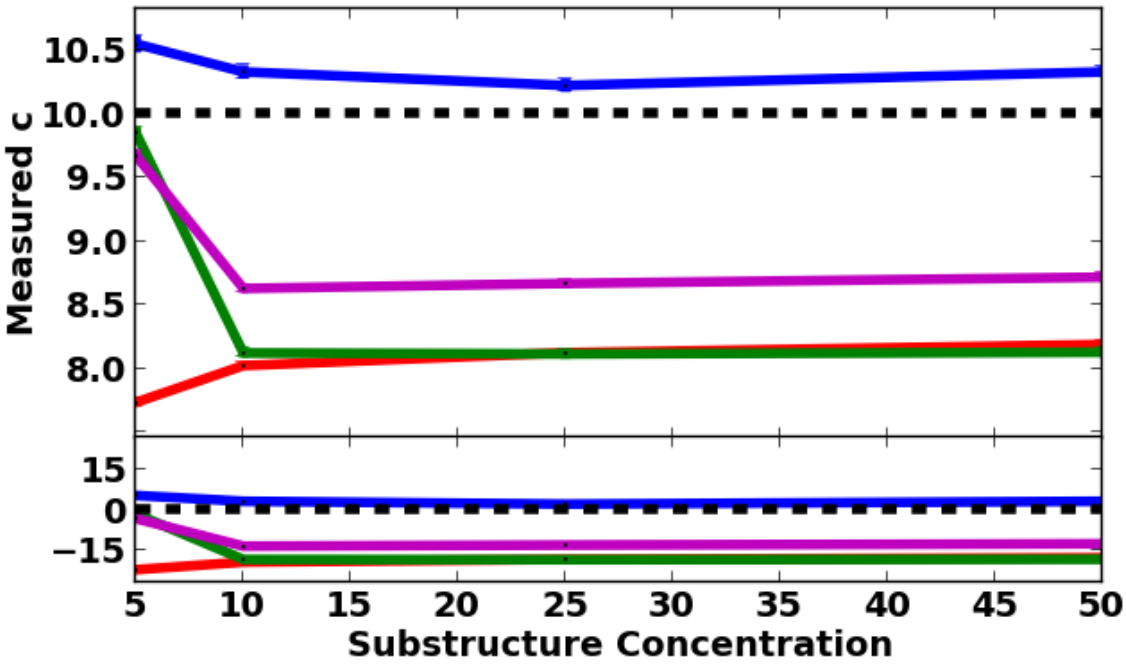

Fig. 21. Performance of TesseRACt vs. spherical techniques as a function of subhalo concentration. TesseRACt is more accurate than the spherical techniques overall, but exhibits some dependence on the concentration of the subhalo. The spherical techniques only exhibit a slight dependence for the subhalo that is less concentrated than the parent, where the non-parametric spherical techniques become more accurate.

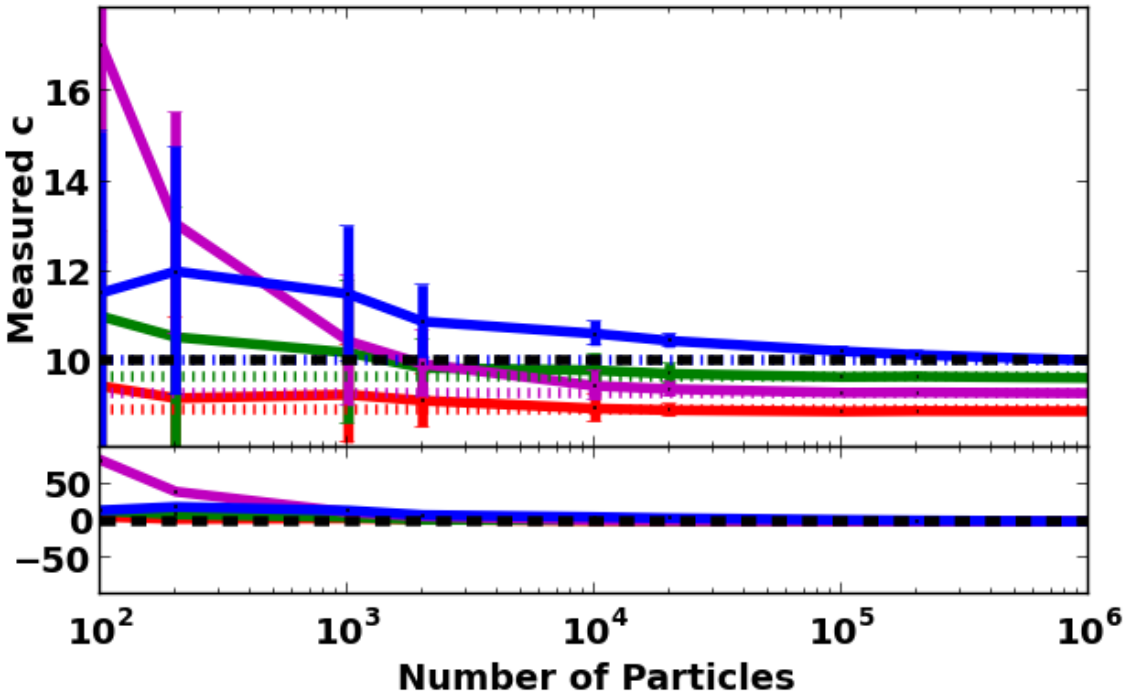

Fig. 22. Performance of TesseRACt vs. spherical techniques as a function of particle number. Dotted colored lines denote the fiducial value returned by each technique in the case of the full resolution, prolate halo. Residuals were computed with respect to this value. TesseRACt , fitting, and the half-mass technique are much less dependent on particle number than the technique which uses the peak velocity.

Chapter V

CONCLUSION

The work presented aimed to further our understanding of the role interactions play in galaxy evolution by assessing the ability of flyby interactions to trigger bar formation, compiling evidence of a recent minor merger from observations of the Milky Way Galactic Center, and developing a new technique for characterizing halos disturbed by interactions.

5.1 Flybys and Bar Formation

There has been a dearth of research on the effects of flyby interactions between galaxies despite indications that they can be as common as mergers (Sinha & Holley-Bockelmann 2012). The work presented in Chapter II indicates this is a significant gap in the current understanding of galaxy evolution. In fact, flybys can induce long lived bars that have the potential to dramatically shape their host galaxies through gas inflow (Hernquist & Mihos 1995), nuclear star formation (Barnes & Hernquist 1996), and AGN fueling (Hopkins & Quataert 2010).

This result also implies that there should exist an over-abundance of barred galaxies in regions where flybys are common (groups and clusters). While there are hints that this may be expressed in observations (Skibba et al. 2012), this trend can also be explained by a deficit of bar surpressing gas (Athanassoula et al. 2013) in these regions. Disentangling the two effects is not feasible from observations as the bars formed by flybys would persist long after the interacting galaxies are no longer associated spatially. However, cosmological

simulations that include gas are now probing scales such that it may be possible to observe bars formed by flybys in the cosmological context (Scannapieco & Athanassoula 2012; Kim et al. 2014; Vogelsberger et al. 2014; Dubois et al. 2014). Future work will include identifying flybys in such simulations and characterizing the competing effects of gas content and flyby rate in determining the environmental preference of bars, as well as simulations of isolated galaxy flybys that include gas.

In addition to the formation of bars, preliminary results also indicate that flybys can change the spin of the dark matter halo by imparting angular momentum aligned with that of the interaction. Such an effect would be temporary given that subsequent interactions are not guaranteed to have the same angular momentum alignment. However, even a temporary mis-alignment between the halo and disk can impact disk formation and growth (Bett & Frenk 2012; Padilla et al. 2014). While major mergers are found to have a larger impact on the spin of a dark matter halo, minor mergers have a larger impact on halo spin cosmologically speaking since they are more common (Bett & Frenk 2012). The same may be true of flyby induced spin changes. Future work examining the spin of halos in cosmological simulations following flybys will help determine if flybys play an important role in changing halo spin.

5.2 A Milky Way Minor Merger

The Milky Way has typically been viewed as a relatively quiescent galaxy with an under-luminous supermassive black hole (Dobler et al. 2010) and quiet merger history (Quinn et al. 1993; Sellwood et al. 1998; Velazquez & White 1999). However, even quiet galaxies will experience $\mathcal{O}(10^2)$ minor mergers that should leave an imprint on the galaxy.

Individual phenomena observed at the Milky Way Galactic Center, including the Fermi bubbles (Su et al. 2010; Zubovas et al. 2011; Guo & Mathews 2012) and young star clusters (Paumard et al. 2006; Figer 2008; Bartko et al. 2010), have been attributed to past interactions. However, they had not been tied together in a coherent picture. The work presented in Chapter III demonstrates that all of these phenomena can be explained by a single minor merger in the Milky Way's recent past and used to place constraints on the relevant masses and timescales involved. This work highlights the need for the Milky Way to be treated as an actively evolving galaxy that, while not currently in the throws of a major merger, is still subject to the influences of recent and on-going minor mergers.

5.3 Characterizing Interacting Halos

Interactions between halos in cosmological simulations can cause halos to deviate significantly from the idealized shapes and profiles typically assumed by analysis techniques (Jing 2000; Neto et al. 2007; Maccio et al. 2007). This can lead to systematically biased measurements and halo scaling relations. The TesseRACt technique described in Chapter IV can recover concentrations that are accurate to within 3% for even the least spherical halo and will allow scientists to measure the concentrations of dark matter halos consistently regardless of how disturbed they are by interactions. This work has important implications for future studies of halo scaling relations.

Reports on scaling relations in the literature can vary dramatically and even conflict due to differences in the criteria used to select halos and the techniques used to measure halo properties. In particular, the scatter in the measured relationship between halo concentration, mass, and redshift is believed to reflect a diversity of mass assembly histories.

However, much of this scatter could result from errors introduced by the assumption of spherical symmetry when concentration is measured. TesseRACt will be used to measured halo concentrations in cosmological simulations and determine how much scatter the assumption of spherical symmetry introduces.

"Nothing is impossible. Not if you can imagine it.

That's what being is a scientist is all about."

- Professor Hubert J. Farnsworth

References

Aarseth, S. J. & Fall, S. M. 1980, The Astrophysical Journal, 236, 43

Alam, S. M. K., Bullock, J. S., & Weinberg, D. H. 2002, The Astrophysical Journal, 572, 34

Alexander, T. & Hopman, C. 2009, The Astrophysical Journal, 697, 1861

Allgood, B., Flores, R. A., Primack, J. R., Kravtsov, A. V., Wechsler, R. H., Faltenbacher, A., & Bullock, J. S. 2006, Monthly Notices of the Royal Astronomical Society, 367, 1781

Amaro-Seoane, P. & Preto, M. 2011, Classical and Quantum Gravity, 28, 094017

Athanassoula, E. 1996, Barred galaxies. Astronomical Society of the Pacific Conference Series, 91

—. 2000, Stars, 221

—. 2002, The Astrophysical Journal, 569, L83

—. 2007, Monthly Notices of the Royal Astronomical Society, 377, 1569

Athanassoula, E., Lambert, J. C., & Dehnen, W. 2005, Monthly Notices of the Royal Astronomical Society, 363, 496

Athanassoula, E., Machado, R. E. G., & Rodionov, S. A. 2013, Monthly Notices of the Royal Astronomical Society, 429, 1949

Athanassoula, E. & Sellwood, J. A. 1986, Monthly Notices of the Royal Astronomical Society (ISSN 0035-8711), 221, 213

Avila-Reese, V., Firmani, C., Klypin, A., & Kravtsov, A. V. 1999, Monthly Notices of the Royal Astronomical Society, 310, 527

Bahcall, J. N. & Wolf, R. A. 1976, The Astrophysical Journal, 209, 214

Baker, J. G., Boggs, W. D., Centrella, J., Kelly, B. J., McWilliams, S. T., Miller, M. C., & van Meter, J. R. 2008, The Astrophysical Journal, 682, L29

Balcells, M. & Quinn, P. J. 1990, The Astrophysical Journal, 361, 381

Barausse, E. & Rezzolla, L. 2009, The Astrophysical Journal, 704, L40

Barnes, J. E. 1988, The Astrophysical Journal, 331, 699

Barnes, J. E. & Hernquist, L. E. 1991, The Astrophysical Journal, 370, L65

—. 1992, Annual Review of Astronomy and Astrophysics, 30, 705

—. 1996, The Astrophysical Journal, 471, 115

Barnes, J. E. & Hut, P. 1986, Nature, 324, 446

Bartko, H., Martins, F., Trippe, S., Fritz, T. K., Genzel, R., Ott, T., Eisenhauer, F., Gillessen, S., Paumard, T., Alexander, T., Dodds-Eden, K., Gerhard, O., Levin, Y., Mascetti, L., Nayakshin, S., Perets, H. B., Perrin, G., Pfuhl, O., Reid, M. J., Rouan, D., Zilka, M., & Sternberg, A. 2010, The Astrophysical Journal, 708, 834

Baumgardt, H., Gualandris, A., & Portegies Zwart, S. 2006, Monthly Notices of the Royal Astronomical Society, 372, 174

Baumgarte, T. W. & Shapiro, S. L. 1999, The Astrophysical Journal, 526, 941

Begelman, M. C., Blandford, R. D., & Rees, M. J. 1980, Nature, 287, 307

Begelman, M. C., Rossi, E. M., & Armitage, P. J. 2008, Monthly Notices of the Royal Astronomical Society, 387, 1649

Behroozi, P. S., Conroy, C., & Wechsler, R. H. 2010, The Astrophysical Journal, 717, 379

Bekenstein, J. D. 1973, The Astrophysical Journal, 183, 657

Bekki, K. 1995, Monthly Notices of the Royal Astronomical Society, 276, 9

Bekki, K. & Couch, W. J. 2011, Monthly Notices of the Royal Astronomical Society, 415, 1783

Bell, E. F., Phleps, S., Somerville, R. S., Wolf, C., Borch, A., & Meisenheimer, K. 2006, The Astrophysical Journal, 652, 270

Bender, R. & Surma, P. 1992, Astronomy and Astrophysics (ISSN 0004-6361), 258, 250

Benson, A. J. 2005, Monthly Notices of the Royal Astronomical Society, 358, 551

Berczik, P., Merritt, D., Spurzem, R., & Bischof, H.-P. 2006, The Astrophysical Journal, 642, L21

Berentzen, I., Athanassoula, E., Heller, C. H., & Fricke, K. J. 2004, Monthly Notices of the Royal Astronomical Society, 347, 220

Berentzen, I., Shlosman, I., & Jogee, S. 2006, The Astrophysical Journal, 637, 582

Berrier, J. C., Bullock, J. S., Barton, E. J., Guenther, H. D., Zentner, A. R., & Wechsler, R. H. 2006, The Astrophysical Journal, 652, 56

Bertola, F. & Corsini, E. M. 1999, Galaxy Interactions at Low and High Redshift

Bett, P., Eke, V., Frenk, C. S., Jenkins, A., Helly, J., & Navarro, J. 2007, Monthly Notices of the Royal Astronomical Society, 376, 215

Bett, P. E. & Frenk, C. S. 2012, Monthly Notices of the Royal Astronomical Society, 420, no

Bhattacharya, S., Habib, S., Heitmann, K., & Vikhlinin, A. 2013, The Astrophysical Journal, 766, 32

Bond, J. R., Cole, S., Efstathiou, G., & Kaiser, N. 1991, The Astrophysical Journal, 379, 440

Bower, . 1991, Monthly Notices of the Royal Astronomical Society (ISSN 0035-8711), 248, 332

Boylan-Kolchin, M., Ma, C.-P., & Quataert, E. 2004, The Astrophysical Journal, 613, L37

—. 2008, Monthly Notices of the Royal Astronomical Society, 383, 93

Boylan-Kolchin, M., Springel, V., White, S. D. M., Jenkins, A., & Lemson, G. 2009, Monthly Notices of the Royal Astronomical Society, 398, 1150

Bromm, V., Coppi, P. S., & Larson, R. B. 2002, The Astrophysical Journal, 564, 23

Bromm, V. & Loeb, A. 2003, The Astrophysical Journal, 596, 34

Brown, W. R. 2008, arXiv e-print, 10

Brown, W. R., Geller, M. J., & Kenyon, S. J. 2009, The Astrophysical Journal, 690, 1639

Brown, W. R., Geller, M. J., Kenyon, S. J., & Kurtz, M. J. 2005, The Astrophysical Journal, 622, L33

Buchholz, R. M., Schödel, R., & Eckart, A. 2009, Astronomy and Astrophysics, 499, 483

Bullock, J. S. & Johnston, K. V. 2005, The Astrophysical Journal, 635, 22

Bullock, J. S., Kolatt, T. S., Sigad, Y., Somerville, R. S., Kravtsov, A. V., Klypin, A. A., Primack, J. R., & Dekel, A. 2001a, Monthly Notices of the Royal Astronomical Society, 321, 559

Bullock, J. S., Kravtsov, A. V., & Weinberg, D. 2001b, The Astrophysical Journal, 548, 33

Burrows, D. N., Kennea, J. A., Ghisellini, G., Mangano, V., Zhang, B., Page, K. L., Eracleous, M., Romano, P., Sakamoto, T., Falcone, A. D., Osborne, J. P., Campana, S., Beardmore, A. P., Breeveld, A. A., Chester, M. M., Corbet, R., Covino, S., Cummings, J. R., D'Avanzo, P., D'Elia, V., Esposito, P., Evans, P. A., Fugazza, D., Gelbord, J. M., Hiroi, K., Holland, S. T., Huang, K. Y., Im, M., Israel, G., Jeon, Y., Jeon, Y.-B., Jun, H. D., Kawai, N., Kim, J. H., Krimm, H. A., Marshall, F. E., P Mészáros, Negoro, H., Omodei, N., Park, W.-K., Perkins, J. S., Sugizaki, M., Sung, H.-I., Tagliaferri, G., Troja, E., Ueda, Y., Urata, Y., Usui, R., Antonelli, L. A., Barthelmy, S. D., Cusumano, G., Giommi, P., Melandri, A., Perri, M., Racusin, J. L., Sbarufatti, B., Siegel, M. H., & Gehrels, N. 2011, Nature, 476, 421

Callegari, S., Kazantzidis, S., Mayer, L., Colpi, M., Bellovary, J. M., Quinn, T., & Wadsley, J. 2011, The Astrophysical Journal, 729, 85

Campanelli, M., Lousto, C., Zlochower, Y., & Merritt, D. 2007, The Astrophysical Journal, 659, L5

Cassata, P., Cimatti, A., Franceschini, A., Daddi, E., Pignatelli, E., Fasano, G., Rodighiero, G., Pozzetti, L., Mignoli, M., & Renzini, A. 2005, Monthly Notices of the Royal Astronomical Society, 357, 903

Chandrasekhar, S. 1943, The Astrophysical Journal, 97, 255

Chen, X., Madau, P., Sesana, A., & Liu, F. K. 2009, The Astrophysical Journal, 697, L149

Chen, X., Sesana, A., Madau, P., & Liu, F. K. 2011, The Astrophysical Journal, 729, 13

Cheng, K.-S., Chernyshov, D. O., Dogiel, V. a., Ko, C.-M., & Ip, W.-H. 2011, The Astrophysical Journal, 731, L17

Cheung, E., Athanassoula, E., Masters, K. L., Nichol, R. C., Bosma, A., Bell, E. F., Faber, S. M., Koo, D. C., Lintott, C., Melvin, T., Schawinski, K., Skibba, R. A., & Willett, K. W. 2013, The Astrophysical Journal, 779, 162

Choi, J.-H., Weinberg, M. D., & Katz, N. 2009, Monthly Notices of the Royal Astronomical Society, 400, 1247

Clark, P. C., Glover, S. C. O., Klessen, R. S., & Bromm, V. 2011, The Astrophysical Journal, 727, 110

Colgate, S. A. 1967, The Astrophysical Journal, 150, 163

Colin, P., AvilaReese, V., & Valenzuela, O. 2000, The Astrophysical Journal, 542, 622

Colpi, M., Mayer, L., & Governato, F. 1999, The Astrophysical Journal, 525, 720

Conselice, C. J., Rajgor, S., & Myers, R. 2008, Monthly Notices of the Royal Astronomical Society, 386, 909

Conselice, C. J., Yang, C., & Bluck, A. F. L. 2009, Monthly Notices of the Royal Astronomical Society, 394, 1956

Cox, T. J., Jonsson, P., Somerville, R. S., Primack, J. R., & Dekel, A. 2008, Monthly Notices of the Royal Astronomical Society, 384, 386

Crocker, R. M., Jones, D. I., Aharonian, F., Law, C. J., Melia, F., Oka, T., & Ott, J. 2011, Monthly Notices of the Royal Astronomical Society, 413, 763

Cuadra, J., Armitage, P. J., Alexander, R. D., & Begelman, M. C. 2009, Monthly Notices of the Royal Astronomical Society, 393, 1423

Davies, R. L., Kuntschner, H., Emsellem, E., Bacon, R., Bureau, M., Carollo, C. M., Copin, Y., Miller, B. W., Monnet, G., Peletier, R. F., Verolme, E. K., & de Zeeuw, P. T. 2001, The Astrophysical Journal, 548, L33

Davis, M., Efstathiou, G., Frenk, C. S., & White, S. D. M. 1985, The Astrophysical Journal, 292, 371

Davis, S. W. & Laor, A. 2011, The Astrophysical Journal, 728, 98

de Blok, W. J. G. 2010, Advances in Astronomy, 2010, 1

de Ravel, L., Le Fèvre, O., Tresse, L., Bottini, D., Garilli, B., Le Brun, V., Maccagni, D., Scaramella, R., Scodeggio, M., Vettolani, G., Zanichelli, A., Adami, C., Arnouts, S., Bardelli, S., Bolzonella, M., Cappi, A., Charlot, S., Ciliegi, P., Contini, T., Foucaud, S., Franzetti, P., Gavignaud, I., Guzzo, L., Ilbert, O., Iovino, A., Lamareille, F., McCracken, H. J., Marano, B., Marinoni, C., Mazure, A., Meneux, B., Merighi, R., Paltani, S., Pellò, R., Pollo, A., Pozzetti, L., Radovich, M., Vergani, D., Zamorani, G., Zucca, E., Bondi, M., Bongiorno, A., Brinchmann, J., Cucciati, O., de la Torre, S., Gregorini, L., Memeo, P., Perez-Montero, E., Mellier, Y., Merluzzi, P., & Temporin, S. 2009, Astronomy and Astrophysics, 498, 379

De Rijcke, S., Dejonghe, H., Zeilinger, W. W., & Hau, G. K. T. 2004, Astronomy and Astrophysics, 426, 53

Dehnen, W. & Binney, J. 1998, Monthly Notices of the Royal Astronomical Society, 294, 429

Despali, G., Giocoli, C., & Tormen, G. 2014, Monthly Notices of the Royal Astronomical Society, 443, 3208

Despali, G., Tormen, G., & Sheth, R. K. 2013, Monthly Notices of the Royal Astronomical Society, 431, 1143

Di Matteo, P., Combes, F., Melchior, A.-L., & Semelin, B. 2007, Astronomy and Astrophysics, 468, 61

Di Matteo, T., Springel, V., & Hernquist, L. E. 2005, Nature, 433, 604

Diemand, J., Kuhlen, M., & Madau, P. 2007, The Astrophysical Journal, 667, 859

Diemand, J. & Moore, B. 2011, Advanced Science Letters, 4, 297

Diemer, B. & Kravtsov, A. V. 2015, The Astrophysical Journal, 799, 108

Do, T., Ghez, A. M., Morris, M. R., Lu, J. R., Matthews, K., Yelda, S., & Larkin, J. 2009, The Astrophysical Journal, 703, 1323

Dobler, G. & Finkbeiner, D. P. 2008, The Astrophysical Journal, 680, 1222

Dobler, G., Finkbeiner, D. P., Cholis, I., Slatyer, T. R., & Weiner, N. 2010, The Astrophysical Journal, 717, 825

D'Onghia, E., Vogelsberger, M., Faucher-Giguere, C.-A., & Hernquist, L. 2010, The Astrophysical Journal, 725, 353

Dooley, G. A., Griffen, B. F., Zukin, P., Ji, A. P., Vogelsberger, M., Hernquist, L. E., & Frebel, A. 2014, The Astrophysical Journal, 786, 50

Dotti, M., Colpi, M., Haardt, F., & Mayer, L. 2007, Monthly Notices of the Royal Astronomical Society, 379, 956

Dubinski, J., Berentzen, I., & Shlosman, I. 2009, The Astrophysical Journal, 697, 293

Dubinski, J. & Chakrabarty, D. 2009, The Astrophysical Journal, 703, 2068

Dubinski, J., Gauthier, J.-R., Widrow, L., & Nickerson, S. 2008, Formation and Evolution of Galaxy Disks ASP Conference Series, 396

Dubinski, J., Mihos, J. C., & Hernquist, L. 1999, The Astrophysical Journal, 526, 607

Dubois, Y., Pichon, C., Welker, C., Le Borgne, D., Devriendt, J., Laigle, C., Codis, S., Pogosyan, D., Arnouts, S., Benabed, K., Bertin, E., Blaizot, J., Bouchet, F., Cardoso, J.-F., Colombi, S., de Lapparent, V., Desjacques, V., Gavazzi, R., Kassin, S., Kimm, T., McCracken, H., Milliard, B., Peirani, S., Prunet, S., Rouberol, S., Silk, J., Slyz, A., Sousbie, T., Teyssier, R., Tresse, L., Treyer, M., Vibert, D., & Volonteri, M. 2014, Monthly Notices of the Royal Astronomical Society, 444, 1453

Dutton, A. A. & Maccio, A. V. 2014, Monthly Notices of the Royal Astronomical Society, 441, 3359

Efstathiou, G., Ellis, R. S., & Carter, D. 1982, Monthly Notices of the Royal Astronomical Society, 201, 975

Einasto, . & Haud, . 1989, Astronomy and Astrophysics (ISSN 0004-6361), 223, 89

Eke, V. R., Navarro, J. F., & Steinmetz, M. 2001, The Astrophysical Journal, 554, 114

Eliche-Moral, M. C., Balcells, M., Aguerri, J. A. L., & González-García, A. C. 2006, Astronomy and Astrophysics, 457, 91

Escala, A., Larson, R. B., Coppi, P. S., & Mardones, D. 2005, The Astrophysical Journal, 630, 152

Faber, S. M., Tremaine, S., Ajhar, E. A., Byun, Y.-I., Dressler, A., Gebhardt, K., Grillmair, C., Kormendy, J., Lauer, T. R., & Richstone, D. 1997, The Astronomical Journal, 114, 1771

Fakhouri, O. & Ma, C.-P. 2008, Monthly Notices of the Royal Astronomical Society, 386, 577

Fakhouri, O., Ma, C.-P., & Boylan-Kolchin, M. 2010, Monthly Notices of the Royal Astronomical Society, 406, 2267

Ferrarese, L., Côté, P., Dalla Bontà, E., Peng, E. W., Merritt, D., Jordán, A., Blakeslee, J. P., Haegan, M., Mei, S., Piatek, S., Tonry, J. L., & West, M. J. 2006, The Astrophysical Journal, 644

Ferrarese, L. & Merritt, D. 2000, The Astrophysical Journal, 539, L9

Figer, D. F. 2008, Proceedings of the International Astronomical Union, 3, 247

Figer, D. F., Becklin, E. E., McLean, I. S., Gilbert, A. M., Graham, J. R., Larkin, J. E., Levenson, N. A., Teplitz, H. I., Wilcox, M. K., & Morris, M. 2000, The Astrophysical Journal, 533, L49

Finkbeiner, D. P. 2004, The Astrophysical Journal, 614, 186

Fisher, D. B. & Drory, N. 2010, The Astrophysical Journal, 716, 942

Franx, M., Illingworth, G., & de Zeeuw, T. 1991, The Astrophysical Journal, 383, 112

Franx, M. & Illingworth, G. D. 1988, The Astrophysical Journal, 327, L55

Gao, L., Navarro, J. F., Cole, S., Frenk, C. S., White, S. D. M., Springel, V., Jenkins, A., & Neto, A. F. 2008, Monthly Notices of the Royal Astronomical Society, 387, 536

Gao, L., White, S. D. M., Jenkins, A., Stoehr, F., & Springel, V. 2004, Monthly Notices of the Royal Astronomical Society, 355, 819

Garcia-Ruiz, I., Kuijken, K., & Dubinski, J. 2002, Monthly Notices of the Royal Astronomical Society, 337, 459

Gebhardt, K., Bender, R., Bower, G., Dressler, A., Faber, S. M., Filippenko, A. V., Green, R., Grillmair, C., Ho, L. C., Kormendy, J., Lauer, T. R., Magorrian, J., Pinkney, J., Richstone, D. O., & Tremaine, S. 2000, The Astrophysical Journal, 539, L13

Geha, M., Guhathakurta, P., & van der Marel, R. P. 2005, The Astronomical Journal, 129, 2617

Genel, S., Genzel, R., Bouché, N., Naab, T., & Sternberg, A. 2009, The Astrophysical Journal, 701, 2002

Genzel, R., Eisenhauer, F., & Gillessen, S. 2010, Reviews of Modern Physics, 82, 3121

Genzel, R., Schödel, R., Ott, T., Eisenhauer, F., Hofmann, R., Lehnert, M., Eckart, A., Alexander, T., Sternberg, A., Lenzen, R., Clenet, Y., Lacombe, F., Rouan, D., Renzini, A., & TacconiGarman, L. E. 2003, The Astrophysical Journal, 594, 812

Georgakakis, A., Forbes, D. A., & Norris, R. P. 2000, Monthly Notices of the Royal Astronomical Society, 318, 124

Gerin, M., Combes, F., & Athanassoula, E. 1990, Astronomy and Astrophysics (ISSN 0004-6361), 230, 37

Ghigna, S., Moore, B., Governato, F., Lake, G., Quinn, T., & Stadel, J. 1998, Monthly Notices of the Royal Astronomical Society, 300, 146

Gilmore, G., Wyse, R. F. G., & Norris, J. E. 2002, The Astrophysical Journal, 574, L39

Giocoli, C., Meneghetti, M., Metcalf, R. B., Ettori, S., & Moscardini, L. 2014, Monthly Notices of the Royal Astronomical Society, 440, 1899

Gnedin, N. Y. 2000, The Astrophysical Journal, 542, 535

Gnedin, N. Y. & Kravtsov, A. V. 2006, The Astrophysical Journal, 645, 1054

Gnedin, O. Y. & Ostriker, J. P. 1997, Astrophysical Journal v.474

Gold, T. & Hoyle, F. 1959, Paris Symposium on Radio Astronomy

Goldreich, P. & Tremaine, S. 1979, The Astrophysical Journal, 233, 857

González-García, A. C., Aguerri, J. A. L., & Balcells, M. 2005, Astronomy and Astrophysics, 444, 803

Gottlober, S., Klypin, A., & Kravtsov, A. V. 2001, The Astrophysical Journal, 546, 223

Graham, A. W. 2004, The Astrophysical Journal, 613, L33

—. 2008, The Astrophysical Journal, 680, 143

Groener, A. M. & Goldberg, D. M. 2014, The Astrophysical Journal, 795, 153

Gualandris, A. & Merritt, D. 2008, The Astrophysical Journal, 678, 780

Guo, F. & Mathews, W. G. 2012, The Astrophysical Journal, 756, 181

Guo, Q. & White, S. D. M. 2008, Monthly Notices of the Royal Astronomical Society, 384, 2

Hansen, B. M. S. & Milosavljevi, M. 2003, The Astrophysical Journal, 593, L77

Harding, P., Morrison, H. L., Olszewski, E. W., Arabadjis, J., Mateo, M., Dohm-Palmer, R. C., Freeman, K. C., & Norris, J. E. 2001, The Astronomical Journal, 122, 1397

Häring, N. & Rix, H.-W. R. 2004, The Astrophysical Journal, 604, L89

Hasan, H. & Norman, C. 1990, The Astrophysical Journal, 361, 69

Hau, G. K. T. & Thomson, R. C. 1994, Monthly Notices of the Royal Astronomical Society, 270

Hearin, A. P., Behroozi, P. S., & van den Bosch, F. C. 2015, arXiv e-print

Hernquist, L. E. 1990, The Astrophysical Journal, 356, 359

—. 1992, The Astrophysical Journal, 400, 460

Hernquist, L. E. & Barnes, J. E. 1991, Nature, 354, 210

Hernquist, L. E. & Mihos, J. C. 1995, The Astrophysical Journal, 448, 41

Hernquist, L. E., Sigurdsson, S., & Bryan, G. L. 1995, The Astrophysical Journal, 446, 717

Hernquist, L. E. & Weinberg, M. D. 1989, Monthly Notices of the Royal Astronomical Society, 238, 407

Hibbard, J. E. & Mihos, J. C. 1995, The Astronomical Journal, 110, 140

Holley-Bockelmann, K., Micic, M., Sigurdsson, S., & Rubbo, L. J. 2010, The Astrophysical Journal, 713, 1016

Holley-Bockelmann, K., Weinberg, M. D., & Katz, N. 2005, Monthly Notices of the Royal Astronomical Society, 363, 991

HolleyBockelmann, K. & Richstone, D. 1999, The Astrophysical Journal, 517, 92

Holmberg, E. 1941, The Astrophysical Journal, 94, 385

Hopkins, P. F. 2014, arXiv e-print, 56

Hopkins, P. F., Bundy, K., Croton, D., Hernquist, L. E., Kereš, D., Khochfar, S., Stewart, K. R., Wetzel, A. R., & Younger, J. D. 2010a, The Astrophysical Journal, 715, 202

Hopkins, P. F., Cox, T. J., Younger, J. D., & Hernquist, L. E. 2009, The Astrophysical Journal, 691, 1168

Hopkins, P. F., Croton, D., Bundy, K., Khochfar, S., van den Bosch, F., Somerville, R. S., Wetzel, A., Keres, D., Hernquist, L., Stewart, K., Younger, J. D., Genel, S., & Ma, C.-P. 2010b, The Astrophysical Journal, 724, 915

Hopkins, P. F. & Hernquist, L. 2010, Monthly Notices of the Royal Astronomical Society, 407, 447

Hopkins, P. F., Hernquist, L. E., Cox, T. J., Di Matteo, T., Robertson, B. E., & Springel, V. 2006, The Astrophysical Journal Supplement Series, 163, 1

Hopkins, P. F., Hernquist, L. E., Cox, T. J., Robertson, B. E., & Krause, E. 2007, The Astrophysical Journal, 669, 45

Hopkins, P. F., Hernquist, L. E., Cox, T. J., Younger, J. D., & Besla, G. 2008, The Astrophysical Journal, 688, 757

Hopkins, P. F. & Quataert, E. 2010, Monthly Notices of the Royal Astronomical Society, 407, 1529

—. 2011, Monthly Notices of the Royal Astronomical Society, 415, no

Hu, J. 2008, Monthly Notices of the Royal Astronomical Society, 386, 2242

Inui, T., Koyama, K., Matsumoto, H., & Tsuru, T. G. 2009, Publications of the Astronomical Society of Japan

Irrgang, A., Przybilla, N., Heber, U., Fernanda Nieva, M., & Schuh, S. 2010, The Astrophysical Journal, 711, 138

Jedrzejewski, R. I. 1987, Monthly Notices of the Royal Astronomical Society (ISSN 0035-8711), 226, 747

Jing, Y. P. 2000, The Astrophysical Journal, 535, 30

Jing, Y. P. & Suto, Y. 2002, The Astrophysical Journal, 574, 538

Jogee, S. 2006, Physics of Active Galactic Nuclei at all Scales, 693

Jogee, S., Miller, S. H., Penner, K., Skelton, R. E., Conselice, C. J., Somerville, R. S., Bell, E. F., Zheng, X. Z., Rix, H.-W., Robaina, A. R., Barazza, F. D., Barden, M., Borch, A., Beckwith, S. V. W., Caldwell, J. A. R., Peng, C. Y., Heymans, C., McIntosh, D. H., Häuß ler, B., Jahnke, K., Meisenheimer, K., Sanchez, S. F., Wisotzki, L., Wolf, C., & Papovich, C. 2009, The Astrophysical Journal, 697, 1971

Jogee, S., Scoville, N., & Kenney, J. D. P. 2005, The Astrophysical Journal, 630, 837

Johansson, P. H., Naab, T., & Burkert, A. 2009, The Astrophysical Journal, 690, 802

Johnston, K. V., Spergel, D. N., & Hernquist, L. 1995, The Astrophysical Journal, 451, 598

Just, A. & Pearrubia, J. 2005, Astronomy and Astrophysics, 431, 861

Kalirai, J. S., Guhathakurta, P., Gilbert, K. M., Reitzel, D. B., Majewski, S. R., Rich, R. M., & Cooper, M. C. 2006, The Astrophysical Journal, 641, 268

Kaviraj, S. 2013, Monthly Notices of the Royal Astronomical Society: Letters, 437, L41

—. 2014, Monthly Notices of the Royal Astronomical Society, 440, 2944

Kazantzidis, S., Bullock, J. S., Zentner, A. R., Kravtsov, A. V., & Moustakas, L. A. 2008, The Astrophysical Journal, 688, 254

Khan, F. M., Just, A., & Merritt, D. 2011, The Astrophysical Journal, 732, 89

Khochfar, S. & Burkert, A. 2006, Astronomy and Astrophysics, 445, 403

Kim, J.-h., Abel, T., Agertz, O., Bryan, G. L., Ceverino, D., Christensen, C., Conroy, C., Dekel, A., Gnedin, N. Y., Goldbaum, N. J., Guedes, J., Hahn, O., Hobbs, A., Hopkins, P. F., Hummels, C. B., Iannuzzi, F., Keres, D., Klypin, A., Kravtsov, A. V., Krumholz, M. R., Kuhlen, M., Leitner, S. N., Madau, P., Mayer, L., Moody, C. E., Nagamine, K., Norman, M. L., Onorbe, J., O'Shea, B. W., Pillepich, A., Primack, J. R., Quinn, T., Read, J. I., Robertson, B. E., Rocha, M., Rudd, D. H., Shen, S., Smith, B. D., Szalay, A. S., Teyssier, R., Thompson, R., Todoroki, K., Turk, M. J., Wadsley, J. W., Wise, J. H., & Zolotov, A. 2014, The Astrophysical Journal Supplement Series, 210, 14

Kleineberg, K., Sánchez-Blázquez, P., & Vazdekis, A. 2011, The Astrophysical Journal, 732, L33

Klypin, A., Gottlober, S., Kravtsov, A. V., & Khokhlov, A. M. 1999, The Astrophysical Journal, 516, 530

Klypin, A., Valenzuela, O., Colín, P., & Quinn, T. 2009, Monthly Notices of the Royal Astronomical Society, 398, 1027

Klypin, A. A., Trujillo-Gomez, S., & Primack, J. R. 2011, The Astrophysical Journal, 740, 102

Knebe, A., Pearce, F. R., Lux, H., Ascasibar, Y., Behroozi, P., Casado, J., Moran, C. C., Diemand, J., Dolag, K., Dominguez-Tenreiro, R., Elahi, P., Falck, B., Gottlober, S., Han, J., Klypin, A., Lukic, Z., Maciejewski, M., McBride, C. K., Merchan, M. E., Muldrew, S. I., Neyrinck, M., Onions, J., Planelles, S., Potter, D., Quilis, V., Rasera, Y., Ricker, P. M., Roy, F., Ruiz, A. N., Sgro, M. A., Springel, V., Stadel, J., Sutter, P. M., Tweed, D., & Zemp, M. 2013, Monthly Notices of the Royal Astronomical Society, 435, 1618

Knebe, A., Power, C., Gill, S. P. D., & Gibson, B. K. 2006, Monthly Notices of the Royal Astronomical Society, 368, 741

Knollmann, S. R. & Knebe, A. 2009, The Astrophysical Journal Supplement Series, 182, 608

Kormendy, J. 1984, The Astrophysical Journal, 287, 577

Kormendy, J. & Bender, R. 2009, The Astrophysical Journal, 691, L142

Kormendy, J. & Ho, L. C. 2013, Annual Review of Astronomy and Astrophysics, 51, 511

Kormendy, J. & Kennicutt, R. C. 2004, Annual Review of Astronomy and Astrophysics, 42, 603

Kormendy, J. & Richstone, D. O. 1995, Annual Review of Astronomy and Astrophysics, 33, 581

Krabbe, A., Genzel, R., Eckart, A., Najarro, F., Lutz, D., Cameron, M., Kroker, H., Tacconi-Garman, L. E., Thatte, N., Weitzel, L., Drapatz, S., Geballe, T., Sternberg, A., & Kudritzki, R. 1995, The Astrophysical Journal, 447

Kuhlen, M., Diemand, J., & Madau, P. 2007, The Astrophysical Journal, 671, 1135

Lacey, C. & Cole, S. 1993, Monthly Notices of the Royal Astronomical Society (ISSN 0035-8711), 262, 627

Lang, M., Holley-Bockelmann, K., Bogdanovic, T., Amaro-Seoane, P., Sesana, A., & Sinha, M. 2013, Monthly Notices of the Royal Astronomical Society, 430, 2574

Lang, M., Holley-Bockelmann, K., & Sinha, M. 2014, The Astrophysical Journal, 790, L33

Lang, M., Sinha, M., & HolleyBockelmann, K. 2015, arXiv e-print, 8

Laurikainen, E., Salo, H., Buta, R., & Knapen, J. H. 2007, Monthly Notices of the Royal Astronomical Society, 381, 401

Le Fevre, O., Abraham, R., Lilly, S. J., Ellis, R. S., Brinchmann, J., Schade, D., Tresse, L., Colless, M., Crampton, D., Glazebrook, K., Hammer, F., & Broadhurst, T. 2000, Monthly Notices of the Royal Astronomical Society, 311, 565

Lindqvist, ., Habing, ., & Winnberg, . 1992, Astronomy and Astrophysics (ISSN 0004-6361), 259, 118

Loeb, A. & Rasio, F. A. 1994, The Astrophysical Journal, 432, 52

Loebman, S. R., Ivezić, v., Quinn, T. R., Bovy, J., Christensen, C. R., Jurić, M., Roškar, R., Brooks, A. M., & Governato, F. 2014, The Astrophysical Journal, 794, 151

Lokas, E. L., Athanassoula, E., Debattista, V. P., Valluri, M., del Pino, A., Semczuk, M., Gajda, G., & Kowalczyk, K. 2014, Monthly Notices of the Royal Astronomical Society, 445, 1339

Loose, ., Kruegel, ., & Tutukov, . 1982, Astronomy and Astrophysics, 105, 342

Lotz, J. M., Davis, M., Faber, S. M., Guhathakurta, P., Gwyn, S., Huang, J., Koo, D. C., Le Floch, E., Lin, L., Newman, J., Noeske, K., Papovich, C., Willmer, C. N. A., Coil, A., Conselice, C. J., Cooper, M., Hopkins, A. M., Metevier, A., Primack, J., Rieke, G., & Weiner, B. J. 2008, The Astrophysical Journal, 672, 177

Lotz, J. M., Jonsson, P., Cox, T. J., Croton, D., Primack, J. R., Somerville, R. S., & Stewart, K. 2011, The Astrophysical Journal, 742, 103

Ludlow, A. D., Navarro, J. F., Angulo, R. E., Boylan-Kolchin, M., Springel, V., Frenk, C., & White, S. D. M. 2014, Monthly Notices of the Royal Astronomical Society, 441, 378

Ludlow, A. D., Navarro, J. F., Boylan-Kolchin, M., Bett, P. E., Angulo, R. E., Li, M., White, S. D. M., Frenk, C., & Springel, V. 2013, Monthly Notices of the Royal Astronomical Society, 432, 1103

Lynden-Bell, D. & Kalnajs, A. J. 1972, Monthly Notices of the Royal Astronomical Society, 157

Lynds, R. & Toomre, A. 1976, The Astrophysical Journal, 209, 382

Macciò, A. V., Dutton, A. A., & van den Bosch, F. C. 2008, Monthly Notices of the Royal Astronomical Society, 391, 1940

Maccio, A. V., Dutton, A. A., Van Den Bosch, F. C., Moore, B., Potter, D., & Stadel, J. 2007, Monthly Notices of the Royal Astronomical Society, 378, 55

Madau, P. & Rees, M. J. 2001, The Astrophysical Journal, 551, L27

Magorrian, J., Tremaine, S., Richstone, D. O., Bender, R., Bower, G., Dressler, A., Faber, S. M., Gebhardt, K., Green, R., Grillmair, C., Kormendy, J., & Lauer, T. R. 1998, The Astronomical Journal, 115, 2285

Maller, A. H., Katz, N., Kereš, D., Dave, R., & Weinberg, D. H. 2006, The Astrophysical Journal, 647, 763

Marconi, A. & Hunt, L. K. 2003, The Astrophysical Journal, 589, L21

Marinova, I. & Jogee, S. 2007, The Astrophysical Journal, 659, 1176

Matsubayashi, T., Makino, J., & Ebisuzaki, T. 2007, The Astrophysical Journal, 656, 879

Mayer, L., Kazantzidis, S., Madau, P., Colpi, M., Quinn, T., & Wadsley, J. 2007, Science (New York, N.Y.), 316, 1874

Mayer, L., Moore, B., Quinn, T., Governato, F., & Stadel, J. 2002, Monthly Notices of the Royal Astronomical Society, 336, 119

McBride, J., Fakhouri, O., & Ma, C.-P. 2009, Monthly Notices of the Royal Astronomical Society, 398, 1858

McLure, R. J. & Dunlop, J. S. 2002, Monthly Notices of the Royal Astronomical Society, 331, 795

Meneghetti, M., Rasia, E., Merten, J., Bellagamba, F., Ettori, S., Mazzotta, P., Dolag, K., & Marri, S. 2010, Astronomy and Astrophysics, 514, A93

Merritt, D. 2010, The Astrophysical Journal, 718, 739

Merritt, D. & Cruz, F. 2001, The Astrophysical Journal, 551

Merritt, D. & Poon, M. Y. 2004, The Astrophysical Journal, 606, 788

Micic, M., Holley-Bockelmann, K., & Sigurdsson, S. 2011, Monthly Notices of the Royal Astronomical Society, 414, 1127

Mihos, J. C. & Hernquist, L. E. 1996, The Astrophysical Journal, 464, 641

Miller, M. C. 2002, The Astrophysical Journal, 581, 438

Milosavljević, M. & Merritt, D. 2001, The Astrophysical Journal, 563, 34

Minchev, I. & Famaey, B. 2010, The Astrophysical Journal, 722, 112

Mirabel, I. F., Lutz, D., & Maza, J. 1991, Astronomy and Astrophysics, 243, 367

Miwa, T. & Noguchi, M. 1998, The Astrophysical Journal, 499, 149

Miyamoto, . & Nagai, . 1975, Astronomical Society of Japan, 27, 533

Mocz, P., Vogelsberger, M., Sijacki, D., Pakmor, R., & Hernquist, L. 2013, Monthly Notices of the Royal Astronomical Society, 437, 397

Molinari, S., Bally, J., Noriega-Crespo, A., Compiègne, M., Bernard, J. P., Paradis, D., Martin, P., Testi, L., Barlow, M., Moore, T., Plume, R., Swinyard, B., Zavagno, A., Calzoletti, L., Di Giorgio, A. M., Elia, D., Faustini, F., Natoli, P., Pestalozzi, M., Pezzuto,

S., Piacentini, F., Polenta, G., Polychroni, D., Schisano, E., Traficante, A., Veneziani, M., Battersby, C., Burton, M., Carey, S., Fukui, Y., Li, J. Z., Lord, S. D., Morgan, L., Motte, F., Schuller, F., Stringfellow, G. S., Tan, J. C., Thompson, M. A., Ward-Thompson, D., White, G., & Umana, G. 2011, The Astrophysical Journal, 735, L33

Moore, B., Katz, N., Lake, G., Dressler, A., & Oemler, A. 1996, Nature, 379, 613

Moore, B., Lake, G., & Katz, N. 1998, The Astrophysical Journal, 495, 139

Mundell, C. G. & Shone, D. L. 1999, Monthly Notices of the Royal Astronomical Society, 304, 475

Naab, T. & Burkert, A. 2001, in Galaxy Disks and Disk Galaxies, 230, 451

Natarajan, P. & Armitage, P. J. 1999, Monthly Notices of the Royal Astronomical Society, 309, 961

Natarajan, P. & Pringle, J. E. 1998, The Astrophysical Journal, 506, L97

Navarro, J. F., Frenk, C. S., & White, S. D. M. 1996, The Astrophysical Journal, 462, 563

Navarro, ., Frenk, ., & White, . 1997, The Astrophysical Journal, 490, 493

Negroponte, J. 1982, Ph.D. Thesis California Univ.

Neistein, E. & Dekel, A. 2008, Monthly Notices of the Royal Astronomical Society, 388, 1792

Neto, A. F., Gao, L., Bett, P., Cole, S., Navarro, J. F., Frenk, C. S., White, S. D. M., Springel, V., & Jenkins, A. 2007, Monthly Notices of the Royal Astronomical Society, 381, 1450

Neyrinck, M. C. 2008, Monthly Notices of the Royal Astronomical Society, 386, 2101

Neyrinck, M. C., Gnedin, N. Y., & Hamilton, A. J. S. 2004, American Astronomical Society Meeting 204, 36

Noguchi, M. 1987, Monthly Notices of the Royal Astronomical Society, 228, 635

Noguchi, M. & Ishibashi, S. 1986, Monthly Notices of the Royal Astronomical Society (ISSN 0035-8711), 219, 305

Noguchi, . 1988, Astronomy and Astrophysics (ISSN 0004-6361), 203, 259

Ostriker, E. C. 1999, The Astrophysical Journal, 513, 252

Ostriker, J. P. & Peebles, P. J. E. 1973, The Astrophysical Journal, 186, 467

Padilla, N. D., Salazar-Albornoz, S., Contreras, S., Cora, S. A., & Ruiz, A. N. 2014, Monthly Notices of the Royal Astronomical Society, 443, 2801

Palladino, L. E., Holley-Bockelmann, K., Morrison, H., Durrell, P. R., Ciardullo, R., Feldmeier, J., Wade, R. A., Davy Kirkpatrick, J., & Lowrance, P. 2012, The Astronomical Journal, 143, 128

Papaloizou, . & Pringle, . 1977, Monthly Notices of the Royal Astronomical Society, 181, 441

Parkinson, H., Cole, S., & Helly, J. 2007, Monthly Notices of the Royal Astronomical Society, 383, 557

Patton, D. R. & Atfield, J. E. 2008, The Astrophysical Journal, 685, 235

Paumard, T., Genzel, R., Martins, F., Nayakshin, S., Beloborodov, A. M., Levin, Y., Trippe, S., Eisenhauer, F., Ott, T., Gillessen, S., Abuter, R., Cuadra, J., Alexander, T., & Sternberg, A. 2006, The Astrophysical Journal, 643, 1011

Peñarrubia, J., Just, A., & Kroupa, P. 2004, Monthly Notices of the Royal Astronomical Society, 349, 747

Peres, A. 1962, Phys. Rev., 128

Perets, H. B. & Alexander, T. 2008, The Astrophysical Journal, 677, 146

Peters, P. C. & Mathews, J. 1963, Phys. Rev., 131

Pfleiderer, J. 1963, Zeitschrift für Astrophysik, 58

Pfleiderer, J. & Siedentopf, H. 1961, Zeitschrift für Astrophysik, 51

Pikel'ner, S. B. 1968, Annual Review of Astronomy and Astrophysics, 6, 165

Planelles, S. & Quilis, V. 2010, Astronomy and Astrophysics, 519, A94

Ponti, G., Terrier, R., Goldwurm, A., Belanger, G., & Trap, G. 2010, The Astrophysical Journal, 714, 732

Power, C., Knebe, A., & Knollmann, S. R. 2012, Monthly Notices of the Royal Astronomical Society, 419, 1576

Prada, F., Klypin, A. A., Cuesta, A. J., Betancort-Rijo, J. E., & Primack, J. 2012, Monthly Notices of the Royal Astronomical Society, 423, 3018

Press, W. H. & Schechter, P. 1974, The Astrophysical Journal, 187, 425

Preto, M. & Amaro-Seoane, P. 2010, The Astrophysical Journal, 708, L42

Prodanović, T., Bogdanović, T., & Urošević, D. 2012, Memorie della Societa Astronomica Italiana Supplement, 22, 207

Quinlan, G. D. 1996, New Astronomy, 1, 35

Quinlan, G. D. & Shapiro, S. L. 1987, The Astrophysical Journal, 321, 199

Quinn, P. J. & Goodman, J. 1986, The Astrophysical Journal, 309, 472

Quinn, P. J., Hernquist, L. E., & Fullagar, D. P. 1993, The Astrophysical Journal, 403, 74

Rees, M. J. 1988, Nature, 333, 523

Reid, M. J. & Brunthaler, A. 2004, The Astrophysical Journal, 616, 872

Ricotti, M. & Gnedin, N. Y. 2005, The Astrophysical Journal, 629, 259

Ricotti, M., Gnedin, N. Y., & Shull, J. M. 2008, The Astrophysical Journal, 685, 21

Robertson, B. E., Hernquist, L. E., Cox, T. J., Di Matteo, T., Hopkins, P. F., Martini, P., & Springel, V. 2006, The Astrophysical Journal, 641, 90

Romano-Díaz, E., Shlosman, I., Heller, C., & Hoffman, Y. 2008, The Astrophysical Journal, 687, L13

Rownd, B. K. & Young, J. S. 1999, The Astronomical Journal, 118, 670

Rubin, V. C., Thonnard, N., & Ford, W. K. 1980, The Astrophysical Journal, 238, 471

Sánchez-Salcedo, F. J. & Brandenburg, A. 1999, The Astrophysical Journal, 522, L35

Sarzi, M., Corsini, E. M., Pizzella, A., Vega Beltrán, J. C., Cappellari, M., Funes, J. G., & Bertola, F. 2000, Astronomy and Astrophysics, 360

Scannapieco, C. & Athanassoula, E. 2012, Monthly Notices of the Royal Astronomical Society: Letters, 425, L10

Scannapieco, C., Gadotti, D. A., Jonsson, P., & White, S. D. M. 2010, Monthly Notices of the Royal Astronomical Society: Letters, 407, L41

Schödel, R., Merritt, D., & Eckart, a. 2009, Astronomy and Astrophysics, 502, 91

Scudder, J. M., Ellison, S. L., Momjian, E., Rosenberg, J. L., Torrey, P., Patton, D. R., Fertig, D., & Mendel, J. T. 2015, Monthly Notices of the Royal Astronomical Society, 449, 3719

Sellwood, J. A. 1981, Astronomy and Astrophysics, 99, 362

—. 2000, Dynamics of Galaxies: from the Early Universe to the Present, 197

—. 2008, The Astrophysical Journal, 679, 379

Sellwood, J. A., Nelson, R. W., & Tremaine, S. 1998, The Astrophysical Journal, 506, 590

Sesana, A. 2010, The Astrophysical Journal, 719, 851

Sesana, A., Haardt, F., & Madau, P. 2007, Monthly Notices of the Royal Astronomical Society: Letters, 379, L45

—. 2008, The Astrophysical Journal, 686, 432

Shakura, . & Sunyaev, . 1973, Astronomy and Astrophysics, 24

Shen, J. & Sellwood, J. A. 2004, The Astrophysical Journal, 604, 614

Sheth, K., Elmegreen, D. M., Elmegreen, B. G., Capak, P., Abraham, R. G., Athanassoula, E., Ellis, R. S., Mobasher, B., Salvato, M., Schinnerer, E., Scoville, N. Z., Spalsbury, L., Strubbe, L., Carollo, M., Rich, R. M., & West, A. A. 2008, The Astrophysical Journal, 675, 1141

Shlosman, I., Frank, J., & Begelman, M. C. 1989, Nature, 338, 45

Simon, J. D. & Geha, M. 2007, The Astrophysical Journal, 670, 313

Sinha, M. & Holley-Bockelmann, K. 2012, The Astrophysical Journal, 751, 17

Skibba, R. A., Masters, K. L., Nichol, R. C., Zehavi, I., Hoyle, B., Edmondson, E. M., Bamford, S. P., Cardamone, C. N., Keel, W. C., Lintott, C., & Schawinski, K. 2012, Monthly Notices of the Royal Astronomical Society, 423, 1485

Snowden, S. L., Egger, R., Freyberg, M. J., McCammon, D., Plucinsky, P. P., Sanders, W. T., Schmitt, J. H. M. M., Trumper, J., & Voges, W. 1997, The Astrophysical Journal, 485, 125

Soares-Santos, M., de Carvalho, R. R., Annis, J., Gal, R. R., La Barbera, F., Lopes, P. A. A., Wechsler, R. H., Busha, M. T., & Gerke, B. F. 2011, The Astrophysical Journal, 727, 45

Sparke, L. S. & Sellwood, J. A. 1987, Monthly Notices of the Royal Astronomical Society (ISSN 0035-8711), 225, 653

Spitzer, L. & Baade, W. 1951, The Astrophysical Journal, 113, 413

Springel, V. 2005, Monthly Notices of the Royal Astronomical Society, 364, 1105

Springel, V. & White, S. D. M. 1999, Monthly Notices of the Royal Astronomical Society, 307, 162

Springel, V., White, S. D. M., Tormen, G., & Kauffmann, G. 2001a, Monthly Notices of the Royal Astronomical Society, 328, 726

Springel, V., Yoshida, N., & White, S. D. M. 2001b, New Astronomy, 6, 79

Stark, A. A., Martin, C. L., Walsh, W. M., Xiao, K., Lane, A. P., & Walker, C. K. 2004, The Astrophysical Journal, 614, L41

Steinmetz, M. & Navarro, J. F. 2002, New Astronomy, 7, 155

Stewart, K. R., Bullock, J. S., Barton, E. J., & Wechsler, R. H. 2009, The Astrophysical Journal, 702, 1005

Stolte, A., Ghez, A. M., Morris, M., Lu, J. R., Brandner, W., & Matthews, K. 2008, The Astrophysical Journal, 675, 1278

Strigari, L. E., Bullock, J. S., Kaplinghat, M., Simon, J. D., Geha, M., Willman, B., & Walker, M. G. 2008, Nature, 454, 1096

Su, M., Slatyer, T. R., & Finkbeiner, D. P. 2010, The Astrophysical Journal, 724, 1044

Taylor, J. E. & Babul, A. 2001, The Astrophysical Journal, 559, 716

Terrier, R., Ponti, G., Bélanger, G., Decourchelle, A., Tatischeff, V., Goldwurm, A., Trap, G., Morris, M. R., & Warwick, R. 2010, The Astrophysical Journal, 719, 143

Theys, J. C. & Spiegel, E. A. 1977, The Astrophysical Journal, 212, 616

Thomas, P. A., Muanwong, O., Pearce, F. R., Couchman, H. M. P., Edge, A. C., Jenkins, A., & Onuora, L. 2001, Monthly Notices of the Royal Astronomical Society, 324, 450

Tillich, A., Przybilla, N., Scholz, R.-D., & Heber, U. 2009, Astronomy and Astrophysics, 507, L37

Toomre, A. 1964, The Astrophysical Journal, 139, 1217

Toomre, A. & Toomre, J. 1972, The Astrophysical Journal, 178, 623

Tormen, ., Bouchet, ., & White, . 1997, Monthly Notices of the Royal Astronomical Society, 286, 865

Toth, G. & Ostriker, J. P. 1992, The Astrophysical Journal, 389, 5

Tremaine, S., Gebhardt, K., Bender, R., Bower, G., Dressler, A., Faber, S. M., Filippenko, A. V., Green, R., Grillmair, C., Ho, L. C., Kormendy, J., Lauer, T. R., Magorrian, J., Pinkney, J., & Richstone, D. O. 2002, The Astrophysical Journal, 574, 740

Tremaine, S. & Weinberg, M. D. 1984, Monthly Notices of the Royal Astronomical Society (ISSN 0035-8711), 209, 729

Tutukov, A. V. & Fedorova, A. V. 2006, Astronomy Reports, 50, 785

Tweed, D., Devriendt, J., Blaizot, J., Colombi, S., & Slyz, A. 2009, Astronomy and Astrophysics, 506, 647

van der Hulst, J. M. 1979, Astronomy and Astrophysics, 75, 97

Velazquez, H. & White, S. D. M. 1999, Monthly Notices of the Royal Astronomical Society, 304, 254

Vera-Ciro, C. A., Sales, L. V., Helmi, A., Frenk, C. S., Navarro, J. F., Springel, V., Vogelsberger, M., & White, S. D. M. 2011, Monthly Notices of the Royal Astronomical Society, 416, 1377

Vesperini, E. & Weinberg, M. D. 2000, The Astrophysical Journal, 534, 598

Vogelsberger, M., Genel, S., Springel, V., Torrey, P., Sijacki, D., Xu, D., Snyder, G., Bird, S., Nelson, D., & Hernquist, L. 2014, Nature, 509, 177

Šubr, L., Schovancová, J., & Kroupa, P. 2009, Astronomy and Astrophysics, 496, 695

Walker, I. R., Mihos, J. C., & Hernquist, L. E. 1996, The Astrophysical Journal, 460, 121

Wang, H. Y., Jing, Y. P., Mao, S., & Kang, X. 2005, Monthly Notices of the Royal Astronomical Society, 364, 424

Wang, Y., Yang, X., Mo, H. J., van den Bosch, F. C., Katz, N., Pasquali, A., McIntosh, D. H., & Weinmann, S. M. 2009, The Astrophysical Journal, 697, 247

Warnick, K., Knebe, A., & Power, C. 2008, Monthly Notices of the Royal Astronomical Society, 385, 1859

Warren, M. S., Quinn, P. J., Salmon, J. K., & Zurek, W. H. 1992, The Astrophysical Journal, 399, 405

Wechsler, R. H., Bullock, J. S., Primack, J. R., Kravtsov, A. V., & Dekel, A. 2002, The Astrophysical Journal, 568, 52

Weinberg, M. D. 1985, Monthly Notices of the Royal Astronomical Society (ISSN 0035-8711), 213, 451

—. 1998, Monthly Notices of the Royal Astronomical Society, 299, 499

Weinberg, M. D. & Blitz, L. 2006, The Astrophysical Journal, 641, L33

Weinberg, M. D. & Katz, N. 2002, The Astrophysical Journal, 580, 627

—. 2007a, Monthly Notices of the Royal Astronomical Society, 375, 460

—. 2007b, Monthly Notices of the Royal Astronomical Society, 375, 425

Weinberg, . 1997, The Astrophysical Journal, 478, 435

Wetzel, A. R. 2011, Monthly Notices of the Royal Astronomical Society, 412, 49

Wetzel, A. R., Cohn, J. D., & White, M. 2009, Monthly Notices of the Royal Astronomical Society, 395, 1376

Wetzel, A. R., Tinker, J. L., Conroy, C., & Bosch, F. C. v. d. 2014, Monthly Notices of the Royal Astronomical Society, 439, 2687

Whitaker, K. E., Rigby, J. R., Brammer, G. B., Gladders, M. D., Sharon, K., Teng, S. H., & Wuyts, E. 2014, The Astrophysical Journal, 790, 143

White, S. D. M. 1978, Monthly Notices of the Royal Astronomical Society, 184, 185

Widrow, L. M. & Dubinski, J. 2005, The Astrophysical Journal, 631, 838

Wise, J. H. & Abel, T. 2008, The Astrophysical Journal, 684, 1

Yelda, S., Lu, J. R., Ghez, A. M., Clarkson, W., Anderson, J., Do, T., & Matthews, K. 2010, The Astrophysical Journal, 725, 331

Younger, J. D., Hopkins, P. F., Cox, T. J., & Hernquist, L. E. 2008, The Astrophysical Journal, 686, 815

Zentner, A. R., Kravtsov, A. V., Gnedin, O. Y., & Klypin, A. A. 2005, The Astrophysical Journal, 629, 219

Zhang, J., Fakhouri, O., & Ma, C.-P. 2008, Monthly Notices of the Royal Astronomical Society, 389, 1521

Zhao, D. H., Jing, Y. P., Mo, H. J., & Börner, G. 2003, The Astrophysical Journal, 597

—. 2009, The Astrophysical Journal, 707, 354

Zubovas, K., King, A. R., & Nayakshin, S. 2011, Monthly Notices of the Royal Astronomical Society: Letters, 415, L21

Zwart, S. F. P., Baumgardt, H., McMillan, S. L. W., Makino, J., Hut, P., & Ebisuzaki, T. 2006, The Astrophysical Journal, 641, 319

Zwicky, F. 1956, Ergebnisse der exakten Naturwissenschaften, 29, 344

—. 1959, Handbuch der Physik, 53